

**ON CRACK IDENTIFICATION USING
NEURAL NETWORKS**

CENTRE FOR NEWFOUNDLAND STUDIES

**TOTAL OF 10 PAGES ONLY
MAY BE XEROXED**

(Without Author's Permission)

BOBBY WELIYANTO



National Library
of Canada

Bibliothèque nationale
du Canada

Acquisitions and
Bibliographic Services

Acquisitions et
services bibliographiques

395 Wellington Street
Ottawa ON K1A 0N4
Canada

395, rue Wellington
Ottawa ON K1A 0N4
Canada

Your file *Votre référence*

ISBN: 0-612-84048-4

Our file *Notre référence*

ISBN: 0-612-84048-4

The author has granted a non-exclusive licence allowing the National Library of Canada to reproduce, loan, distribute or sell copies of this thesis in microform, paper or electronic formats.

L'auteur a accordé une licence non exclusive permettant à la Bibliothèque nationale du Canada de reproduire, prêter, distribuer ou vendre des copies de cette thèse sous la forme de microfiche/film, de reproduction sur papier ou sur format électronique.

The author retains ownership of the copyright in this thesis. Neither the thesis nor substantial extracts from it may be printed or otherwise reproduced without the author's permission.

L'auteur conserve la propriété du droit d'auteur qui protège cette thèse. Ni la thèse ni des extraits substantiels de celle-ci ne doivent être imprimés ou autrement reproduits sans son autorisation.

Canada

**ON CRACK IDENTIFICATION
USING NEURAL NETWORKS**

by

© Bobby Weliyanto, B. Eng.

A thesis submitted to the
School of Graduate Studies
in partial fulfillment of the
requirements for the degree of
Master of Engineering

Faculty of Engineering and Applied Science
Memorial University of Newfoundland

June 2002

St. John's

Newfoundland

Canada

Abstract

Most structures suffer fatigue damage at some point during their operational life. This damage may lead to a structural failure. An early damage identification is needed to prevent such a structural failure. A technique which depends on the measurement of the changes in the vibration characteristics of the structure can be effective, since inspection can be performed while the structure is in normal operation. This work presents a methodology for using neural networks in identifying structural damage employing the vibration signature data.

An experimental study was carried out to measure the random response of undamaged and damaged beam models. The damage was simulated by introducing a hand-made saw cut at different points along the length of the beam. The depth of crack was also varied. Two beam models were used: one was simply supported, and the other was a fixed-fixed beam. The beam was excited using random excitation. The auto-correlation function was calculated and used as an approximation for the free vibration of the model. A neural network technique was performed to identify the crack occurrence and its extent. The results show that this technique is able to detect the occurrence of the crack.

Acknowledgements

All the glory, honor and praise are given to beloved Heavenly Father, God Almighty. Without His grace and love, I would never have the opportunity to study in Canada and finish it till the end.

I am very thankful to my family, important persons in my life, my loving dad, dear mom and my brothers (Ivan, Stephanus and Christian) for their continuous encouragements, prayers and moral support. Also to my cousin, Karen, for being a lovely cousin and good friend during my stay in Canada. Many thanks to Herry, Ria, Cindy and Gomgom for the encouragements and moral support. Special thanks to Daniel Alexander, for the prayers, teachings and being another loving dad.

I would like to express my sincere gratitude to my supervisor, Dr. M. Haddara, for his continuous support and guidance during the course of the program. I respect and admire his patience and commitment to help me working out this study. I also want to thank to Craig Monahan for the financial support and computer. All the academic contributions during the course of the study made by Dr. L. Lye, Dr. A.S.J. Swamidas, Dr. S.M.R. Adluri and Dr. G. Sabin are also highly appreciated.

Many thanks to A. Burse for the technical supports given during the experimentation in Structural Laboratory. Also, to Achmad Zubaydi, Moses Owolabi Agung, Gatot and to all the people who have helped me through out the duration of this study and experiment.

Table of Content

| | |
|---|-----|
| ABSTRACT | i |
| ACKNOWLEDGEMENTS | ii |
| TABLE OF CONTENT | iii |
| LIST OF FIGURES..... | vi |
| LIST OF TABLES | ix |
| | |
| 1. INTRODUCTION..... | 1 |
| 1.1 SCOPE OF WORK | 4 |
| 1.2 METHODOLOGY | 4 |
| 1.3 ORGANISATION OF THE THESIS | 6 |
| | |
| 2. LITERATURE REVIEW..... | 8 |
| 2.1 DAMAGE IDENTIFICATION | 9 |
| 2.2 AUTO-CORRELATION FUNCTION..... | 15 |
| 2.3 SUMMARY | 16 |
| | |
| 3. MATHEMATICAL FORMULATION | 18 |
| 3.1 EQUATION OF MOTION | 18 |
| 3.2 RANDOM DECREMENT SIGNATURE | 21 |
| 3.2.1 <i>Random Decrement Technique</i> | 21 |
| 3.2.2 <i>Auto-correlation Function</i> | 23 |
| 3.3 NEURAL NETWORK TECHNIQUE..... | 25 |
| 3.3.1 <i>Artificial Neural Networks Computing</i> | 25 |
| 3.3.2 <i>The Neural Network Algorithm</i> | 26 |
| 3.4 SUMMARY | 28 |
| | |
| 4. EXPERIMENTAL STUDY | 30 |

| | |
|--|-----|
| 4.1 MODEL DESCRIPTION | 31 |
| 4.2 INSTRUMENTATION | 34 |
| 4.2.1 <i>Signal Generator</i> | 34 |
| 4.2.2 <i>Vibration Exciter</i> | 35 |
| 4.2.3 <i>Load Cell</i> | 35 |
| 4.2.4 <i>Power Amplifiers</i> | 35 |
| 4.2.5 <i>Transducers</i> | 36 |
| 4.2.6 <i>Oscilloscope</i> | 39 |
| 4.3 EXPERIMENTAL SETUP | 39 |
| 4.4 EXPERIMENTAL PROCEDURE | 42 |
| 4.4.1 <i>Auto-correlation Calculation</i> | 46 |
| 4.5 SUMMARY | 50 |
| | |
| 5. RESULTS AND DISCUSSION | 51 |
| 5.1 NATURAL FREQUENCY PREDICTION | 52 |
| 5.1.1 <i>Filtering</i> | 52 |
| 5.1.2 <i>Experimental Results</i> | 54 |
| 5.1.3 <i>Exact and Finite Element Solution</i> | 64 |
| 5.1.4 <i>Discussion</i> | 66 |
| 5.2 IDENTIFICATION OF G FUNCTION..... | 67 |
| 5.2.1 <i>Results</i> | 67 |
| 5.2.2 <i>Discussions</i> | 77 |
| 5.2.3 <i>Multivariate Linear Regression</i> | 81 |
| | |
| 6. CONCLUSIONS AND RECOMMENDATIONS | 86 |
| 6.1 CONCLUSIONS | 86 |
| 6.2 RECOMMENDATIONS | 88 |
| | |
| REFERENCES..... | 90 |
| | |
| APPENDIX A | 97 |
| | |
| APPENDIX B | 106 |

APPENDIX C 119

List of Figures

| | | |
|---------------|--|----|
| Figure 3.1: | Block diagram for the Neural Network used in crack identification.... | 29 |
| Figure 4.1: | The aluminum beam model and the dimensions..... | 31 |
| Figure 4.2: | The idealization and dimensions for the simply-supported beam..... | 32 |
| Figure 4.3: | The fixed-fixed beam..... | 33 |
| Figure 4.4: | The simply-supported beam..... | 33 |
| Figure 4.5: | Vibration Exciter B&K 4809, Load Cell and Accelerometers..... | 37 |
| Figure 4.6: | Detailed vibration testing instrumentation scheme..... | 40 |
| Figure 4.7: | Instrumentation setup..... | 41 |
| Figure 4.8: | Experimental setup..... | 41 |
| Figure 4.9: | Locations of accelerometers..... | 43 |
| Figure 4.10: | A fixed beam with a crack at $1/16 L$ | 45 |
| Figure 4.11: | A simply-supported beam with a crack at $1/16 L$ | 45 |
| Figure 4.12: | Random response data taken from accelerometer No.3. (after calibration)..... | 47 |
| Figure 4.13: | Procedure for obtaining the Auto-correlation function..... | 48 |
| Figure 4.14a: | Random response from an accelerometer, before Filtering..... | 49 |
| Figure 4.14b: | Random response from an accelerometer, after Filtering..... | 49 |
| Figure 4.14c: | The auto-correlation function (half side, only circled part is used in the analysis)..... | 49 |
| Figure 4.14d: | The free vibration decay (the first 3 cycles)..... | 50 |
| Figure 5.1: | Comparison of the auto-correlation function before and after filtering. | 53 |
| Figure 5.2: | Estimated free vibration (auto-correlation function) of fixed-fixed beam with a 2.54mm crack depth at the center of the beam..... | 55 |
| Figure 5.3: | Estimated free vibration (auto-correlation function) of fixed-fixed beam with a 5.08mm crack depth at the center of the beam..... | 55 |

| | | |
|--------------|---|----|
| Figure 5.4: | Estimated free vibration (auto-correlation function) of fixed-fixed beam with a 7.62mm crack depth at the center of the beam..... | 56 |
| Figure 5.5: | Estimated free vibration (auto-correlation function) of fixed-fixed beam with a 10.16mm crack depth at the center of the beam..... | 56 |
| Figure 5.6: | Estimated free vibration (auto-correlation function) of fixed-fixed beam with a 12.70mm crack depth at the center of the beam..... | 57 |
| Figure 5.7: | Estimated free vibration (auto-correlation function) of fixed-fixed beam with a 15.24mm crack depth at the center of the beam..... | 57 |
| Figure 5.8: | Estimated free vibration (auto-correlation function) of fixed-fixed beam with a 17.78mm crack depth at the center of the beam..... | 58 |
| Figure 5.9: | Auto-correlation functions for simply supported beam crack at 8/16L. | 60 |
| Figure 5.10: | Fundamental frequency ratio as a function of crack depth and location on the simply supported beam..... | 61 |
| Figure 5.11: | Fundamental frequency ratio as a function of crack depth and location on the fixed-fixed beam..... | 62 |
| Figure 5.12: | 3D plots of the natural frequencies for different crack locations and depths..... | 63 |
| Figure 5.13: | Comparison between original Auto-correlation function and the neural network prediction for fixed-fixed beam (2.54mm crack depth) | 68 |
| Figure 5.14: | Comparison between original Auto-correlation function and the neural network prediction for fixed-fixed beam (5.08mm crack depth) | 69 |
| Figure 5.15: | Comparison between original Auto-correlation function and the neural network prediction for fixed-fixed beam (7.62mm crack depth) | 69 |
| Figure 5.16: | Comparison between original Auto-correlation function and the neural network prediction for fixed-fixed beam (10.16mm crack depth)..... | 70 |
| Figure 5.17: | Comparison between original Auto-correlation function and the neural network prediction for fixed-fixed beam (12.70mm crack | 70 |

| | | |
|--------------|---|----|
| | depth)..... | |
| Figure 5.18: | Comparison between original Auto-correlation function and the neural network prediction for fixed-fixed beam (15.24mm crack depth)..... | 71 |
| Figure 5.19: | Comparison between original Auto-correlation function and the neural network prediction for fixed-fixed beam (17.78mm crack depth)..... | 71 |
| Figure 5.20: | Plot of G function as a function of time (2.54mm crack depth)..... | 72 |
| Figure 5.21: | Plot of G function as a function of time (5.08mm crack depth)..... | 72 |
| Figure 5.22: | Plot of G function as a function of time (7.62mm crack depth)..... | 73 |
| Figure 5.23: | Plot of G function as a function of time (10.16mm crack depth)..... | 73 |
| Figure 5.24: | Plot of G function as a function of time (12.70mm crack depth)..... | 74 |
| Figure 5.25: | Plot of G function as a function of time (15.24mm crack depth)..... | 74 |
| Figure 5.26: | Plot of G function as a function of time (17.78mm crack depth)..... | 75 |
| Figure 5.27: | Plot of normalized G amplitude for fixed-fixed beam..... | 78 |
| Figure 5.28: | Plot of normalized G amplitude for simply supported beam..... | 79 |
| Figure 5.29: | 3D Plot of normalized G amplitude for fixed-fixed beam..... | 80 |
| Figure 5.30: | 3D Plot of normalized G amplitude for simply supported beam..... | 80 |
| Figure 5.31: | Plot of amplitude G and the predicted value versus crack depth for fixed-fixed beam..... | 84 |
| Figure 5.32: | Plot of amplitude G and the predicted value versus crack location for fixed-fixed beam..... | 84 |
| Figure 5.33: | Plot of amplitude G and the predicted value versus crack depth for simply supported beam..... | 85 |
| Figure 5.34: | Plot of amplitude G and the predicted value versus crack location for simply supported beam..... | 85 |

List of Tables

| | | |
|------------|---|----|
| Table 4.1: | Material properties of the beam model..... | 32 |
| Table 4.2: | Characteristics of accelerometers..... | 38 |
| Table 4.3: | Sensitivities of calibrated accelerometers..... | 38 |
| Table 4.4: | Crack location..... | 44 |
| Table 4.5: | Crack depth..... | 44 |
| Table 5.1: | Predicted fundamental frequency for different crack depths and locations on simply supported beam..... | 58 |
| Table 5.2: | Predicted fundamental frequency for different crack depths and locations on fixed-fixed beam..... | 59 |
| Table 5.3: | Reduction of natural frequencies due to a presence of a 1/10d crack (2.54mm) for simply supported and fixed-fixed beam model..... | 59 |
| Table 5.4: | Comparison of the natural frequencies obtained from the experiment, the exact solution and the finite element solution..... | 64 |
| Table 5.5: | Amplitude of G for different crack depths and locations on simply supported beam..... | 76 |
| Table 5.6: | Amplitude of G for different crack depths and locations on fixed-fixed beam..... | 76 |
| Table 5.7: | Reduction in the amplitude of G in presence of a 1/10d crack (2.54mm) for simply supported and fixed-fixed beam..... | 77 |
| Table 5.8: | Summary output for fixed-fixed beam..... | 82 |
| Table 5.9: | Summary output for simply supported beam..... | 82 |

CHAPTER 1

INTRODUCTION

Structural condition monitoring has received great attention from many researchers and industrial experts in recent years. Condition monitoring can be used to detect the occurrence of structural damage. This is very important since early detection of a crack may save the structure from catastrophic failure. Nondestructive evaluation techniques (NDE), such as magnetic particle inspection, ultrasonic inspection, radiography, alternating current field measurement, eddy current, and acoustic emission, are some of the techniques used for structural damage identification. However, the use of the above NDE techniques may not be feasible when the structure is in operation. As well, the NDE techniques are complicated and very costly when the structure is located

underwater, as in the case of an offshore platform or a ship structure. In the case of underwater structures, sophisticated equipment and intelligent remote operated vehicles or NDE divers may be needed to assess the structure condition.

Vibration monitoring has a great potential since it can be carried out without shutting down the operation of the structure. It is ideally suited for developing an on-line crack detection and monitoring system. The approach also requires very simple and commercially available instrumentation. This technique may be able to detect cracks which are far away from the measuring sensors. This eliminates the need of costly remotely operated vehicles and other sophisticated equipment needed for inspection. Moreover, vibration monitoring can identify the occurrence of the crack, as well as its location and extent. Vibration monitoring can be an inexpensive and sophisticated technique in damage identification of structure when compared to other NDE techniques.

In the past few years, many concepts have been developed for vibration monitoring to get a better identification of damage occurrence, extent and location. The basic idea behind this technology is to identify modal parameters (natural frequencies, mode shapes, and modal damping) which are functions of the physical properties of the structure (mass, damping and stiffness). When there are changes in the physical properties, such as reductions in the stiffness resulting from the presence of a crack, it can be detected by observing the changes in the modal parameters. Estimates for modal parameters were obtained using the measured response of the structure. The change in

the natural (fundamental) frequency is the indicator that most researchers have used to identify the presence of a crack. Other indicators used by the researchers to identify the cracks on a structure are mode shapes, damping ratio and modal flexibilities. The information of the fundamental frequency of a structure could be easily known by vibrating the structure with a low frequency excitation. However, the main disadvantage of this indicator is the fact that for large structures, the fundamental frequency will only change slightly as a result of a crack. On the other hand, in practice it is difficult to excite the higher frequency of a structure. As well, the environmental conditions may not allow this type of excitation. The literature review in Chapter 2 will discuss further about the indicators and methods that have been used in crack identification using vibration analysis.

Recently, many researchers have been trying to develop non-parametric identification approaches to predict the occurrence of a crack or damage. One of the well-known techniques is using a new computing architecture called artificial neural networks. Artificial neural networks are biologically inspired and analogous to the most elementary functions of the biological neuron. The ability of learning from experience, generalising from previous examples to new ones, and performing abstract essential characteristics from inputs make neural networks a powerful tool to recognise a given system and detect the changes.

In this study a neural network technique is performed to determine the change in the modal parameters in the equation of motion due to the presence of a crack. A sensitive indicator is developed to predict the occurrence of cracks.

1.1 Scope of Work

The main purpose of this work is to develop a technique for the prediction of crack development in structures. The technique is based on the use of the concept of random decrement and neural networks techniques to identify the parameters in the equation describing the free vibration of the structure. The work is primarily based on experimental study. The experiment included performing vibration testing on beams with different boundary conditions, different crack depths and locations. The scope of the work is developing and employing the neural network technique on the experimental measurements to obtain a sensitive indicator to the presence of cracks as well as utilizing the random decrement concept in predicting free vibration response of the structure.

1.2 Methodology

A simple structure was used to develop a technique for the identification of the development of cracks in a structure. An approximation of the free vibration response of the beam was obtained from its stationary random response which later will be used in

predicting the beam's natural frequency. Then, the estimated free vibration response is employed on the equation of motion of the beam in order to determine a crack identification indicator. This indicator is a function of the natural frequency, damping ratio and the restoring parameters of the beam. A neural networks algorithm is utilized to determine the magnitude of the indicator for a number of cracks of different depths and locations.

The procedural steps for this experiment are given as follows:

- a. Measuring the experimental steady state random vibratory response of the beam models.
- b. Determining an analogous representation for the free vibration response of the models using their auto-correlation functions.
- c. Predicting natural frequency of the beam using the estimated free vibration, then comparing with the actual natural frequency from exact solution and finite element analysis (FEA).
- d. Analyzing the changes of the natural frequency due to a presence of crack
- e. Defining an indicator more sensitive than the fundamental frequency to the presence of crack.
- f. Predicting a crack inception indicator defined in step (e), using neural networks.
- g. Determining the sensitivity of the crack inception indicator, and comparing this with the sensitivity of the natural frequencies to crack inception.

- h. Performing multivariate linear regression analysis to the results to study the relationship between the indicator and the crack depth and location.

1.3 Organisation of the Thesis

The organisation of this thesis is described as follows: Chapter One gives a background of the research, states the scope of work of this research and describes the methodology used.

Chapter Two contains a study of the literature regarding this topic of research. The study will help to give an insight of the problem and the progresses of the researchers that have been done in this area. Also, it gives information about the limitations and advantages of the existing methods in damage identification.

Chapter Three describes theoretical background and mathematical formulations pertaining to the technique used for crack identification in this work. The procedure uses auto-correlation function for determining estimated free vibration response as application of random decrement technique. Then, the function is applied into a neural networks algorithm to determine a parameter from the equation of motion. The parameter is a function of frequency, damping ratio and acceleration of the random response of the beam.

Chapter Four, Experimental Study, contains the detail descriptions of experimental study. It includes the experiment model descriptions, instrumentation, experimental setup, and procedures employed on the experiment. The details of the instrumentation used are also explained in this chapter.

Chapter Five presents the results and discussion of the identification technique used in this experimental work. The changes of natural frequency of each crack condition were observed from the estimated free vibration response. A verification of the predicted natural frequency with the values from exact solution and finite element method is also discussed. Then, results of the neural network identification technique are presented. All the results obtained were tabulated and presented in figures, plots and discussion. A linear multivariable regression is employed to the experiment results to study the experimental results and the model's trend.

Chapter Six gives the conclusions and recommendations of the research for future works.

CHAPTER 2

LITERATURE REVIEW

Research in the area of vibration-based damage identification has been rapidly expanding over the last 30 years. This chapter will explore and review a number of works that have been completed by researchers in the area of damage identification using vibration analysis. An excellent review about vibration-based damage identification has been done by Doebling et al. (1996). Another excellent literature survey in this topic also was done by Wauer (1990). Pappa et al. (2000) provided an on-line bibliographic database of vibration-based damaged detection experiments by researchers around the world. The database can be searched and sorted in many ways and it provides

photographs of test structures where available. This database is available for public use on the Internet.

2.1 Damage Identification

Cole (1971, 1973), Dimarogonas (1970), Adams et al (1975), Cawley (1979), Ibrahim (1977), and Vandiver (1975, 1977, 1982) are a number of the earlier researchers who performed the investigation in identifying damage using vibration analysis. Henry Cole (1971, 1973) first developed the Random Decrement Technique (RDT) for determining modal damping and detecting mechanical failure of aerospace structures. The RDT was developed as a technique in averaging the random response of a structural system under random excitation to obtain an estimation of its free vibration. Cole hypothesised that the random decrement signature is equivalent to the free vibration response of the system. Even if it is based on empirical induction, the basic conclusion has been widely accepted and used in the aerospace industry. The major advantage of the technique is that the free vibration of a structure can be identified by measured random response without disrupting the structure from normal operation condition.

Ibrahim (1977) extended the work and developed another more general vibration analysis technique known as “Ibrahim Time Domain Modal Vibration Testing Technique”. The technique identified the natural frequencies, mode shapes and damping ratios of a structural system by fitting a mathematical model to the free vibration response

of the structure. After Ibrahim's work published, many researchers used and developed either Ibrahim Time Domain Technique or the Random Decrement Technique. Vandiver et al. (1982) established a mathematical interpretation for the Random Decrement Technique of vibration signature analysis, while Yang (1976, 1980, 1984) applied the Random Decrement method in detection of induced cracks and incipient failure on offshore platform models.

In 1970, still in the early development of vibration-based damage identification, Dimarogonas investigated the dynamic response of a cracked rotor. He introduced the bending stiffness description of the rotor crack and determined it from compliance measurements. Cawley and Adams (1979) described a method of crack detection and localisation which uses measurement of the structural natural frequencies. This method gave a rough indication of the magnitude of the damage, although it was not precise.

Imam et al.(1989) developed a new vibration monitoring technique based on the vibration signature analysis called Histogram Technique. Before the histogram analysis was taken, they eliminated the background noise of the vibration data by summing and averaging the identical samples. Then, the histogram analysis is carried out in the following three steps: first, synchronously summing the data in time domain, second, repeating step 1 periodically for crack monitoring purposes and subtracting data in step 1 with data in step 2 in time domain. Lastly, performing a Fourier transform on this difference. They [Imam et al.] used the resulting differential harmonics called histogram

harmonics as a parameter in detecting the cracks. The technique can be performed in on-line mode, but it only works on rotor machines, such as turbines, generators, pumps, and others. They claim that this technique has successfully detected cracks of the order of one to two percents of shaft diameter deep in an on-line mode.

Qian et al. (1990) investigated numerically the dynamic behaviour of a beam. They derived the equation of motion of the beam and its stiffness matrix by applying fracture mechanics and finite element methods. From these equations, the eigenfrequencies were determined for different crack lengths and positions. The results showed that the frequencies were shifted slightly as the crack occurred and grew. The small differences of the frequencies between the beam without a crack and with a crack made the detection scheme difficult to apply.

Rajab et al. (1991) also presented a method for the detection of cracks based on measuring changes in the natural frequencies. The structure observed was Timoshenko shafts. In regards to the fact that the natural frequencies and mode shapes will change due the presence of a crack, they used it inversely to predict the crack characteristics from measurement of those parameters. A functional relationship between the crack parameters and the changes in the structure's dynamic characteristics was determined. The results again show that at the fundamental frequencies, there are only small changes. Therefore, information of the higher frequencies is also needed in order to predict the

crack precisely. The crack location was predicted successfully once the changes in shaft frequencies at several modes were known.

There are a number of other researchers, such as Sekhar and Prabhu.(1992), Shen and Pierre (1990), Hamidi et al. (1992), El-Dannah et al.(1994) and others, who were working on crack detection using the changing of the natural frequencies. Sekhar and Prabhu used a simply supported shaft for the experiment and derived the analytical expression to describe the relationship between crack position, depth and their natural frequencies. Shen and Pierre also used an Euler Beam and derived the mathematical modelling for the beam with symmetric cracks. They showed the results as plots of changing natural frequencies, crack depth, and its position. They also presented the changing of mode shape due to the cracks for several modes. Hamidi et al. developed mathematical models for a rotor system with a crack. They compared the mathematical models with the experimental results to validate them. The results showed an excellent agreement between the analytical models and the experimental results. The results of that study are confined to changes in the system's natural frequencies due to the presence of cracks. El-Dannah et al. modified Rajab's work by adding elastically mounted end masses on the beam. They also derived the equation of motion of the beam and its general solutions. The result was plotted as a variation in natural frequencies in terms of crack depths and locations.

Liao et al.(1992) presented a new technique in crack detection for rotating shafts. The technique used deflection signals, velocity and acceleration signals for FFT signal processing. With proximity probes, the experiment results showed that a crack could be identified even when the change of the shaft frequency due to the crack is about 1%.

Doyle (1995) applied a spectral element method combined with a stochastic generic algorithm to give a scheme in identifying and locating cracks in structural components. The results are demonstrated with experimental data from an aluminium beam with a transverse crack. However, the study still needed more improvement in order to predict the crack accurately and efficiently. The choice of a stochastic search in the scheme is computationally inefficient and less successful in predicting the cracks.

Juneja et al. (1997) developed another approach in damage detection using a combination of changing frequency signature and contrast maximisation approach. Contrast maximisation was applied to find the excitation forces that create maximum differences in the response between the damaged structure and the analytical response of the undamaged structure. The optimal excitations for the damage structure were then matched against a database of optimal excitations to locate the damage. Therefore a prestudy about a number of damage scenarios on the structure was needed for a database. In this work, they verified the success of the method by applying the technique numerically and experimentally on a 36-degree-of-freedom space truss model. The results show an excellent prediction of damage location, but the effectiveness of the

technique depends on the ratio of the magnitude of damage to the cross-sectioned area and errors in the measurements.

Liew and Wang (1998) attempted for the first time, a wavelet theory for the crack identification on structures. The work showed that by using wavelet analysis a crack location could be identified clearly in contrast with the use of eigenfunctions that only gave a minor effect for the cracked beam. They also claimed that the wavelet analysis could be applied easily to investigate the eigenfunctions rather than a tedious application of eigentheory. However, in this technique it is hard to decide which wavelet should be selected in order to get an appropriate result.

Kosmatka and Ricles (1999) developed a new methodology for the nondestructive detection of structure damage based on vibration modal data. This methodology used measured modal data along with a correlated analytical structural modal to locate the damage and conduct a weighted sensitivity analysis. Residual modal force vectors were used to locate the potentially damaged region. By analysing the correlated analytical structural modal data, the change in the stiffness and mass of the existing crack can be determined. From the experimental and numerical work, it is concluded that the method successfully determined the location of potential damage as well as estimated its magnitude. The method works exceptionally well even if the frequency shift due to damage is small. The weakness of this method is the complexity of the approach that

requires a correlated analytical model and the residual force calculation, beside the need of high frequency modes which are hard to obtain in real practice.

Zhao and DeWolf (1999) developed a sensitivity study comparing use of natural frequencies, mode shapes, and modal flexibilities for vibration-based damage monitoring. Their analysis was based on theoretical analysis to determine which dynamic parameters are best for damage monitoring purposes. The result of their study showed that in several different damage scenarios used, modal flexibility indicator is more sensitive to detect damage than either the natural frequencies or the mode shapes. While as, the natural frequencies is a more sensitive indicator than mode shapes to damage identification.

2.2 Auto-correlation Function

In the late 1960's, Cole (1971) developed a new identification technique on structures using random decrement technique. This technique has been used widely in the aerospace industry for the analysis of experimentally generated vibration data in identification of space structures. Vandiver et al. (1982) derived a mathematical relationship between the auto-correlation function and the random decrement signature. In their work, they showed the random decrement signature for a linear system excited using a stationary, Gaussian random excitation represents the free response of the system. Vandiver et al. showed that the auto-correlation function is proportional to the free vibration decay of the linear system for the case of a single degree of freedom oscillator

excited by a white noise, stationary, Gaussian process. Moreover, the auto-correlation function can be used to replace the random decrement signature and usually is more accurate than random decrement signature in estimating the free vibration decays in a single degree of freedom case. Ibrahim (1977), Haddara (1992, 1995, 1998) and Zubaydi et al. (2000) expanded the use of random decrement and auto-correlation function for multi degrees of freedom.

2.3 Summary

There are a great number of researchers who are interested and developed vibration-based damage detection on structures. The vibration-based damage detection can be included in the real time monitoring of damage inspection. The works by researchers in this area can be divided into three categories: analytical, experimental works and combination of both. In its early development, the researchers were trying to investigate the global dynamic behaviour of the structures due to a presence of cracks, and develop a technique to identify the crack without regarding its effectiveness. The most parameter that the researchers were interested in is the fundamental natural frequencies of the system. While after that period, most researchers were interested in developing new techniques in crack detection rather than just observing the changing of the natural frequencies. As well, they were working on sensitivity analysis and developing a technique that has high sensitivities in the prediction of the location and magnitude of the cracks.

From the literature review, one can conclude that identification of the change in modal parameters is of the most interest to the researchers in the area of crack detection. The common parameter used in the studies is the changing of natural frequencies. However, the structure damage or the presence of cracks will not give a major effect on its natural frequencies unless the ratio of the magnitude of the damage is large, or the frequencies observed are of the higher mode. On the other hand, in the real practice it is rather difficult to obtain higher modes of frequencies if the measurement is taken in the real time.

Most of the successful detection methods combined several approaches in predicting the cracks. The hybrid approach will prevent the technique giving mislead information regarding the damage. Moreover, it will increase the sensitivity of the proposed technique.

From the study of literature, we also know that auto-correlation function of a random response system is exactly proportional to the free vibration decay of the linear system for the case of a single degree of freedom oscillator excited by a white noise, stationary, and Gaussian process. Therefore, the auto-correlation function can be used to estimate an approximation of the free vibration responses of a single degree of freedom linear system.

CHAPTER 3

MATHEMATICAL FORMULATION

In this study, we use a Neural Network algorithm to identify structural cracks. The auto-correlation function was used as an input to the algorithm of neural networks in order to estimate a parameter that can be used for crack identification. In this chapter, the mathematical expression, background, and the concept for this technique are presented.

3.1 Equation of Motion

As mentioned earlier, in this study, two beam models were used: one was simply supported, and the other was a fixed-fixed supported beam. The vibrations of the two beams are described using the same basic equation, but they have different boundary

conditions. The equation of motion describing the response of a slender beam acted upon by an external forcing function is given by Thompson (1993):

$$a^2 \frac{\partial^4 w(x,t)}{\partial x^4} + \frac{\partial^2 w(x,t)}{\partial t^2} + c \frac{\partial w(x,t)}{\partial t} = E(t) \quad (3.1)$$

where:

$$a^2 = \frac{EI}{\rho A}$$

E = modulus elastisitas [N/m²]

I = moment inertia [m⁴]

ρ = mass density [kg/m³]

c = the damping coefficient [N.s/m]

$E(t)$ = exciting force (random excitation) [N]

$w(x,t)$ = random response [m]

The beam is assumed to have viscous damping. Consider:

$$w = \theta(x).y(t) \quad (3.2)$$

Equation (3.1) can be written as:

$$a^2 \theta^{IV} y + \theta \ddot{y} + c \theta \dot{y} = E(t) \quad (3.3)$$

$$\ddot{y} + c\dot{y} + \frac{a^2 \theta^{IV} y}{\theta} = \frac{E(t)}{\theta} \quad (3.4)$$

For a fixed value of x , $\frac{a^2 \theta^{IV}}{\theta}$ and c are constants.

The equation (3.1) can be written as:

$$\ddot{y} + \alpha \dot{y} + \gamma y = H(t) \quad (3.5)$$

where $\alpha = c = 2\zeta\omega_n$

$$\gamma = \frac{a^2\theta^{IV}}{\theta} = \omega_n^2 \quad H(t) = \frac{E(t)}{\theta}$$

Equation (3.5) can be written as

$$\ddot{y} + \omega_d^2 y + G(x, y, \dot{y}) = H(t) \quad (3.6)$$

where:

$$\omega_d^2 = \omega_n^2(1 - \zeta^2)$$

$$G(x, y, \dot{y}) = 2\zeta\omega_n\dot{y} + \zeta^2\omega_n^2 y$$

H (t) is assumed to be a Gaussian, zero mean stationary random process. Taking the average of equation (3.6), we get:

$$\ddot{\mu} + \omega_d^2 \mu + G(x, \mu, \dot{\mu}) = 0 \quad (3.7)$$

where $\mu = \langle y \rangle$, and $\langle \rangle$ indicates the time average of the function.

and the function G is expressed in terms of the averages of the deflection y and its derivative. Equation (3.7) is obtained by averaging the stationary random response. It is clear that this equation describes the free vibration of the beam measured at point x . It has been shown by Zubaydi (2001) that this equation also describes the auto-correlation function of the random response of the beam. A detailed explanation regarding the use of auto-correlation function in this study will be presented next in this chapter. The function G above will be used in this study as the indicator to identify a presence of a crack.

3.2 Random Decrement Signature

3.2.1 Random Decrement Technique

The random decrement technique, which was initially developed by Cole in 1973 is an averaging technique applied to the stationary random response of the structure to obtain its free vibration response. This technique has been widely used in aerospace industry to identify the dynamic parameters of structures. Since the technique only needed the measured dynamic response of the structure, the test could be performed on-line without disrupting the normal operation of the structure.

The concept of this technique is that, by averaging the random response, $\{y(t)\}$, of a system in a certain manner, it is possible to obtain the free vibration response of the structure. The estimated free vibration by random decrement technique is usually referred as the random decrement signature $\{x(\tau)\}$. Cole hypothesized that the random decrement signature is equivalent to the free vibration response of the system with initial displacement equal to the threshold level and an initial slope equal to zero. The theory is explained further as follows. The random response of a structural system under random excitation is composed of two components:

- a deterministic (transient) component
- a random (stationary) component

If the excitation is a zero average, white noise random process, then the stationary random response will be also a zero average random process. By averaging samples of the stationary random response, the random component of the response will average out to zero, and only the deterministic component is left, which is the random decrement signature.

A trigger value is chosen. The trigger value corresponds to the initial displacement for the free response. The stationary random response is divided into segments of equal length. Each segment starts when the trigger value intersects the response. Some of these segments will start with a positive slope and an equal number will start with a negative slope. Thus, when all these segments are averaged, the result will be a curve similar to the free response of the system with initial displacement equal to the trigger value and zero slope. If $y(t)$ is a segment of the random response, N is the number of segments, and τ is time length, the random decrement signature is given by:

$$\{x(\tau)\} = \frac{1}{N} \sum_{n=1}^N \{y(t_n + \tau)\} \quad (3.8)$$

N = number segments,

$y(t_n) = y_s$ = threshold or trigger level when $n = 1, 2, 3, \dots$

$\dot{y}(t) \geq 0$, when $n = 1, 3, 5, \dots$, and $\dot{y}(t) \leq 0$ when $n = 2, 4, 6, \dots$. The function of $\{x(\tau)\}$ is only defined in the time interval of $0 \leq \tau \leq \tau_1$, where τ_1 is the time length of response.

3.2.2 Auto-correlation Function

Vandiver et al (1982) established a mathematical basis for the random decrement technique and derived the relationship between the auto-correlation function of a random process and the random decrement signature. They have shown that the random decrement signature is related to the auto-correlation function by:

$$x(\tau) = \frac{R_{yy}(\tau)}{R_{yy}(0)} y_s \quad (3.9)$$

where y_s is the trigger value and R_{yy} is the auto-correlation function of the random process $y(t)$. For the case of a single degree of freedom, excited by a white noise, stationary, gaussian process, the auto-correlation function is shown to be proportional to the free vibration decay from a specified initial displacement.

In this study, the auto-correlation function is used to estimate the free vibration response of the beam because it is much easier and more reliable (Zubaydi, 2001) to calculate the auto-correlation of the response rather than attempt to calculate the average value of the response. Therefore, the average of deflection y and its derivative that are employed in the equation (3.7) are replaced with the auto-correlation function of the random response at point x and its derivative. In equation (3.7), the variable μ and $\dot{\mu}$ denote the auto-correlation function and its derivative. This equation will be used in determining the function G .

The mathematical expression of the auto-correlation function is given as (McConnel, 1995):

$$R_{yy}(t) = \frac{1}{N-t} \sum_{j=1}^{N-t} y(j)y(j+t) \quad (3.10)$$

Another mathematical term that is important in determining dynamic characteristic of vibration data is Power Spectral Density (PSD). PSD provides information on the random response in the frequency domain. In fact, PSD is the Fast Fourier Transform (FFT) of $R_{yy}(t)$ as shown in Equation (3.11):

$$S_{yy}(\omega) = \int_{-\infty}^{\infty} R_{yy}(t)e^{-i\omega t} dt \quad (3.11)$$

Therefore, the auto-correlation function can also be determined in the form of an Inverse Fast Fourier Transform (IFFT) of the PSD. From the PSD plot, the dominant frequency of the random response can also be obtained. In this study, PSD plot was used to check the predicted natural frequency from the estimated free vibration.

3.3 Neural Networks Technique

3.3.1 Artificial Neural Networks Computing

Artificial Neural Networks computing is biologically inspired. It is inspired by human brain characteristics and biological neuron architecture. Artificial neural networks are composed of elements that perform in a manner that is analogous to the most elementary functions of the biological neuron. Like the characteristics of the brain, artificial neural networks can learn from experience or training, generalize from previous examples to new ones, and abstract essential characteristics from inputs containing relevant data.

In biological terms, neurons are complex cells that respond to electrochemical signals. They are composed of a processing body or a cell body, a nucleus, numerous dendrites, transmitting axon, and receiving synapses. The concept of biological neurons is explained as follows. Dendrites extend from the cell body to other neurons where they receive signals at a synapse. On the receiving side of the synapse, these inputs are conducted to the cell body. There they are summed with some inputs tending to excite the cell, others tending to inhibit its firing. When the cumulative excitation in the cell body exceeds a threshold, the cell fires, sending a signal down the axon to other neurons.

While it sounds simple, this basic functional outline has many complexities and exceptions. However, artificial neural networks model these simple characteristics. As an example, a computational unit or an artificial neuron could be modelled as a single nerve cell. The receiving sites/input represent the synapses, while the receiving connections represent the dendrites of the cell. A processing element is representing the cell body and the transmitting connections to output is representing axons which connect to other neuron. In mathematical expression, it could be described as an input layer, one or more hidden/middle layer and an output layer of neurons. The connections are associated with different weights that are representative of the strength of the connection. The rest of this section will present the basics of the artificial neural network algorithm applied in this study.

3.3.2 The Neural Network Algorithm

A neural network technique was used to predict the function G , using μ and $\dot{\mu}$ as inputs. As mentioned earlier in the previous section, μ and $\dot{\mu}$ are the auto-correlation function of the measured random response of the beam at point x , and its derivative, respectively. A block diagram showing the network used in this work is shown in figure 3.1. A three layers network is used; an input layer, an output layer and a hidden or middle layer. In the input and middle layers, each layer contains a bias neuron with input unity. The input to neuron k in the middle layer is obtained as:

$$Z_k = \sum_{j=0}^2 W_l^{(jk)} u_j \quad (3.12)$$

where: $u_0 = 1$, $u_1 = \mu$, and $u_2 = \dot{\mu}$

The output of the k neuron in the middle layer is:

$$M_k = f(Z_k) \quad (3.13)$$

where f is called the squashing function and is given by:

$$f(i) = \frac{1 - e^{-i}}{1 + e^{-i}} \quad (3.14)$$

The network output, G function, is then obtained as

$$G(x, \mu, \dot{\mu}) = \sum_{k=0}^6 W_0^{(k)} M_k \quad (3.15)$$

$W_l^{(jk)}$ are the weights employed to the input through Z_k to obtain the input to the hidden/middle layer neurons, while $W_0^{(k)}$ are the weights applied to the hidden layers output to produce the $G(x, \mu, \dot{\mu})$ function.

Since we cannot measure values for G corresponding to μ and $\dot{\mu}$, we have to use a hybrid approach. In this approach, the function G predicted by the network (Eq. 3.15) is substituted in equation (3.7) and the equation is integrated numerically to obtain the corresponding values of μ or the auto-correlation function. The estimate or predicted auto-correlation function is then compared with the input auto-correlation function obtained using equation (3.10) from the measured random response. The error obtained in terms of the difference between the actual values of μ and that obtained from the

integration of equation (3.7) was used as a criterion to optimize the network. A least square technique was used and the process was continued until the values of G obtained minimized the mean square error between measured and predicted μ .

The values of the G function is used as the indicator to identify the crack presence. The next chapter will present the details of the experiment performed in this study and discuss how the data was analyzed.

3.4 Summary

This chapter provided the mathematical approach used in the present study and the basic concept of the method of analysis. Section 3.1 described the mathematical formulation of the equation of motion of the beams and the derivation of the parameter that would be used as a crack indicator. Basically, it derived the equation of motion of beams under forced vibration. The other section discussed the use of the auto-correlation in this study, based on the random decrement technique. The section also provided the basic theory of the random decrement technique. The last section described the neural network concept and how it would be employed in the study.

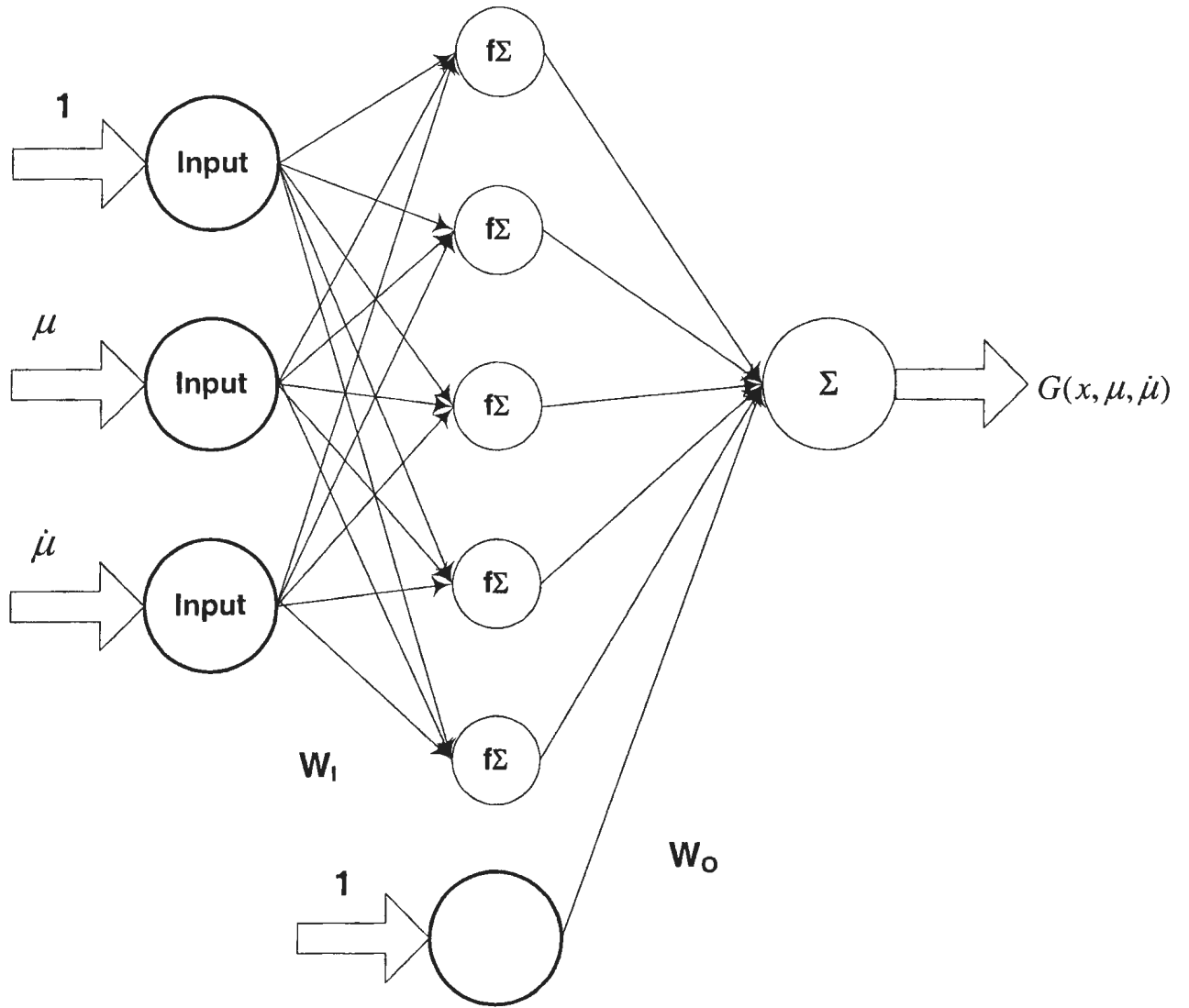


Figure 3.1 Block diagram for the Neural Network used in crack identification.

CHAPTER 4

EXPERIMENTAL STUDY

An extensive experimental program was designed and carried out to validate the identification technique developed to predict crack inception and progression. The experimental study was carried out in the Structural Laboratory of the Faculty of Engineering and Applied Science. In this chapter, the details of the experimental program are described. These include descriptions of the model, instrumentation, experimental setup, scope, and procedure.

4.1 Model Description

Two sets of beam models were tested. One set was with a fixed-fixed support, while the other was simply supported. Each set consisted of seven aluminium beams. Model dimensions are shown in Figure 4.1. Table 4.1 shows the material properties of the models. Cracks were made using saw-cuts on the model. The models were tested intact and with cracks at different locations and with different depths. The depth of each crack ranged from 1/10 in (2.54 mm) to 7/10 in (17.78 mm). The cracks were located at a distance from the support, which ranged from 1/16 L to 11/16 L, where L is the length between the supports. Two notches were introduced at the ends of the simply supported beams to simulate the simply supports, as shown in Figure 4.2. Figures 4.3 and 4.4 show pictures of the models.

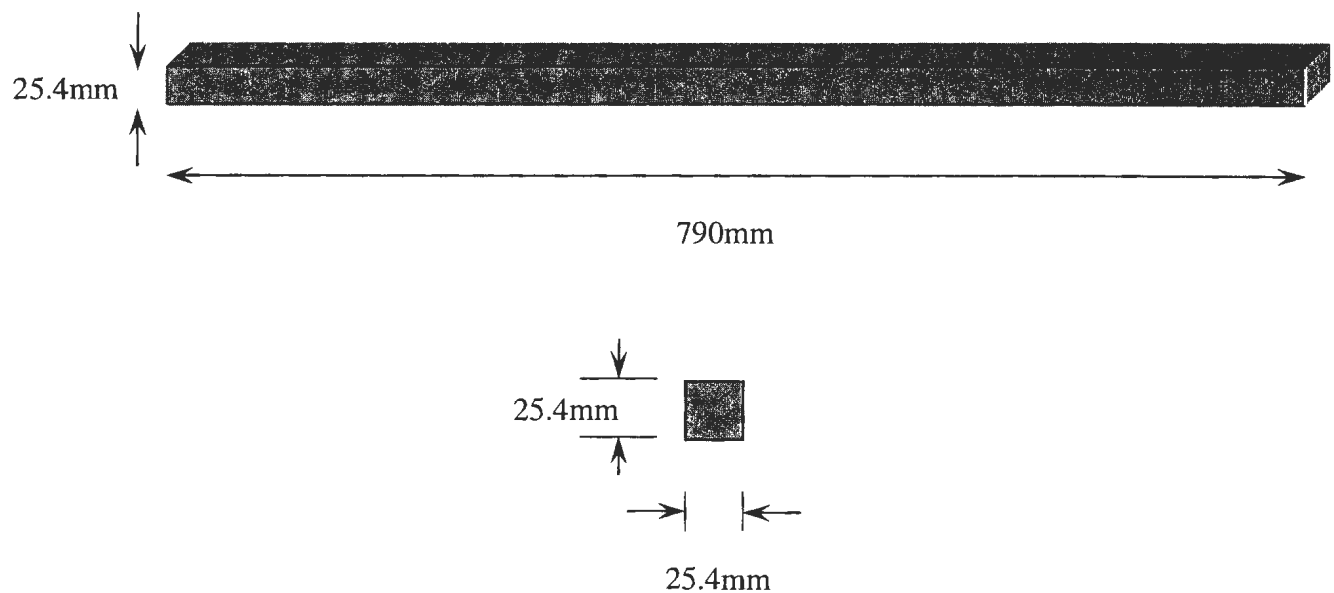


Figure 4.1. Aluminium beam model and its dimensions.

Table 4.1: Material properties of the beam model.

| Material Properties | |
|---------------------|-------------------------------|
| Material Type | Aluminium |
| Mass | 12.3 gr. |
| Young's Modulus E | 70 Gpa |
| Density (ρ) | 2.696 gr/cm^3 |
| Poisson ratio | 0.35 |

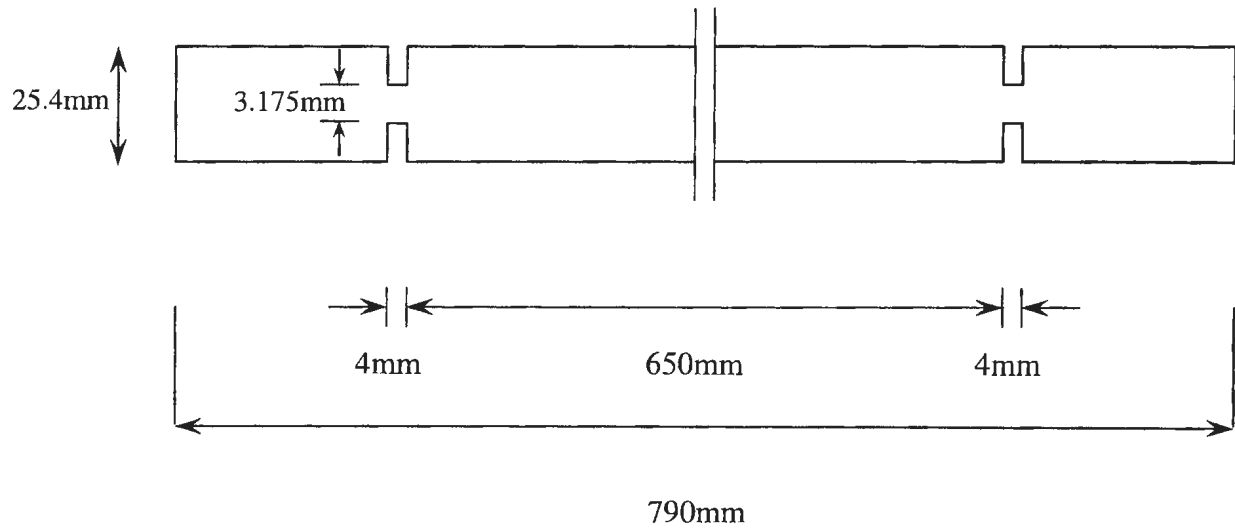


Figure 4.2. The idealisation and dimensions for the simply-supported beam model.

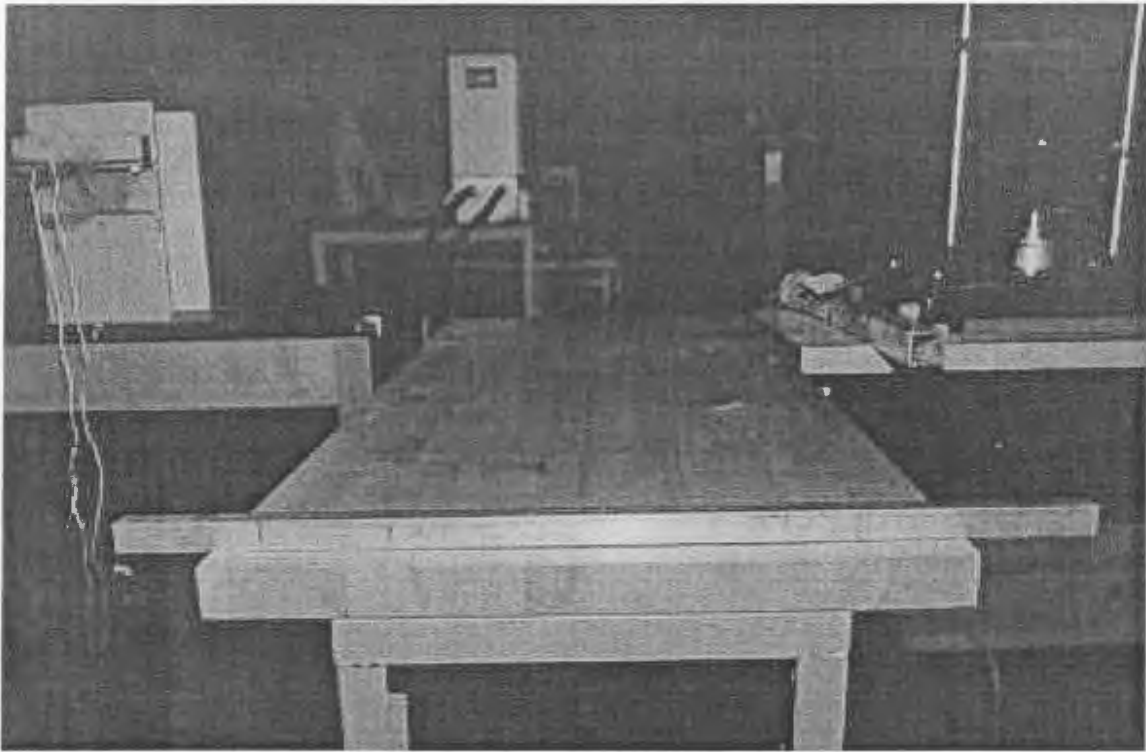


Figure 4.3. The fixed-fixed beam.



Figure 4.4. The simply-supported beam.

4.2 Instrumentation

This section briefly describes the instruments used in the experiments. The instruments are a signal generator, a vibration exciter, transducers, power amplifiers, a load cell, an oscilloscope, and a personal computer. It is very important to have a proper selection and functioning of the instruments to obtain reliable results.

4.2.1 Signal Generator

There are many types of signal generators that are commonly used in vibration testing. Generally, they can be divided into two types: impact and continuous signal generators. In this experiment we used a continuous signal generator with a random exciting force so that we could measure the random response of the beam. The identification technique developed in this work is based on the analysis of the random response of the structure. A pseudo-random signal is used to excite the beam model so that the dynamic response of the model can be obtained. The signal generator used in this experiment is a WAVETEK model 132 noise generator. This generator can generate signals varying over a frequency range of 0.2 Hz to 2.0 MHz in 6 decade-ranges.

4.2.2 Vibration Exciter

Signals generated from the generator were sent to a power amplifier and then transmitted to a vibration exciter. The purpose of the exciter is to generate a dynamic force that will excite the structures. There are many different types of exciters that are employed in vibration testing. The selection of the proper exciter will significantly influence the test results. In this experiment, an electromagnetic exciter was used. It was a B&K 4809 vibration exciter with a force rating of 44.5 N (10 lbf), which can be used for vibrating small specimens at a range of frequency 10 Hz to 20 kHz. The vibration exciter is shown in Figure 4.5.

4.2.3 Load Cell

The function of the load cell is to measure force signal delivered to the model. By measuring the force, we can also monitor the amplitude of the force signal using an oscilloscope. The load cell used was a Kistler model 912-2010 quartz type. Before performing the vibration testing, the load cell should be calibrated. The scheme of the load cell position can be seen in Figure 4.5.

4.2.4 Power Amplifiers

As mentioned above, before the force signal can be applied on the structure it must be amplified using a Power amplifier. The reason is that the force will have enough

magnitude to vibrate the structure. Thus, the dynamic characteristics of the structures can be observed. Other power amplifiers are also needed to amplify the signal from the accelerometers, so that the structure response signal can be observed properly. Three amplifiers were used during the experiment. One was a small size B&K power amplifier type 27067 that amplified the signal from generator to exciter. The other two were a charge and a differential amplifier to amplify the signal from the accelerometers and load cell, respectively. The charge amplifier used was a Dual-Mode Amplifier Model 504E while the differential amplifier was a PCB 433A .

4.2.5 Transducers

The function of transducers is to measure the structure's response. Piezoelectric accelerometers were selected for measuring the response in this experiment. Accelerometers are compact, light weighted, and suitable for measuring high frequency vibrations. The model of the Piezoelectric transducers used was STRUCTCEL No.330A. In this experimental setup, there were seven accelerometers attached to the model. The reason for using a number of accelerometers was to investigate which one would yield the best measured signal. The detailed locations of the accelerometers will be described in the experimental setup part of this chapter. Before the accelerometers can be used, they must be calibrated first. The characteristics of the accelerometers and their sensitivities after calibration are shown in Table 4.2 and 4.3, respectively.

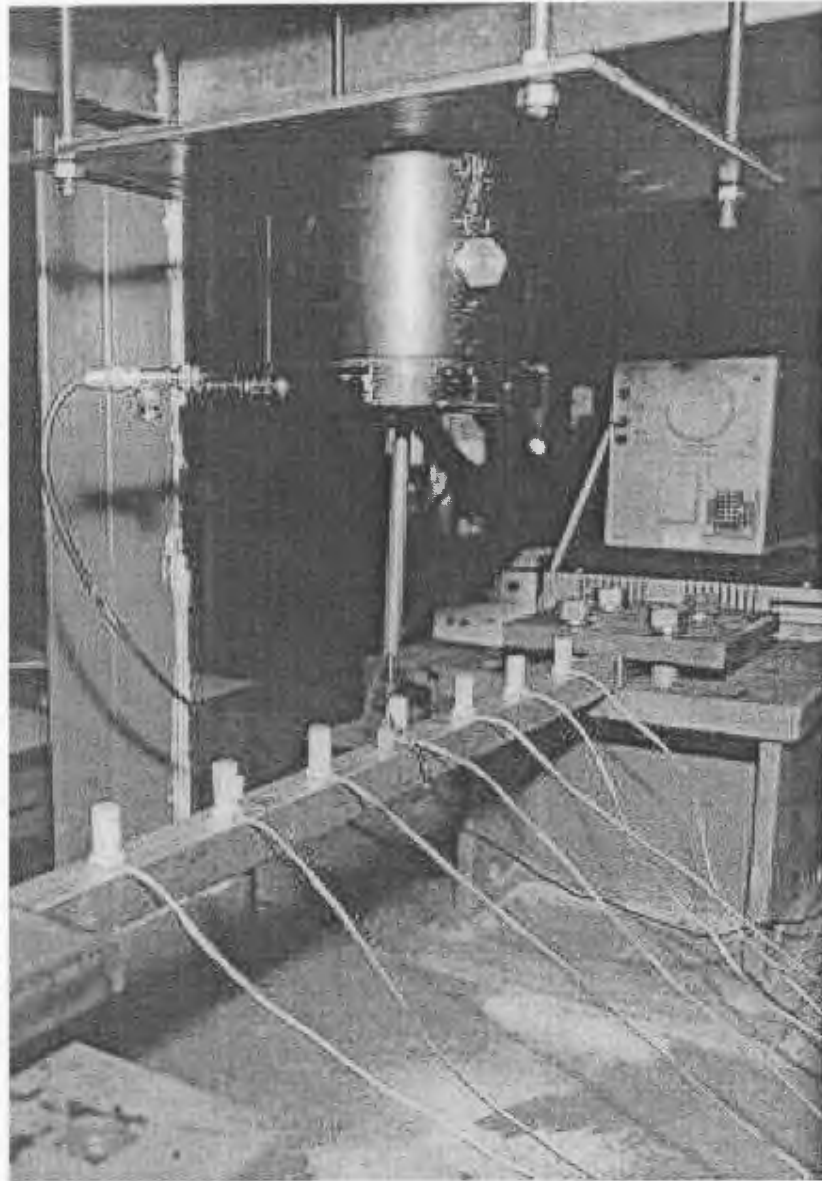


Figure 4.5. Vibration Exciter B&K 4809, Load Cell and Accelerometers.

Table 4.2: Characteristics of accelerometers.

| | |
|-----------------------------------|-----------|
| Resolution (G) | 0.001 |
| Range ($\pm 10V$) (G) | 10 |
| Shock (max) (G) | 5000 |
| Range of frequency | 1-1000 Hz |
| Excitation ($\pm DVC$) | 15 |
| Temperature Range ($^{\circ}F$) | 0-130 |
| Mass | 2 gm |
| Connectors (Pins) | 3 |

Table 4.3: Sensitivities of calibrated accelerometers.

| Accelerometer No. | Series Number (S/NO) | Sensitivity (mV/g) |
|-------------------|----------------------|--------------------|
| 1 | 20093 | 160 |
| 2 | 20502 | 180 |
| 3 | 20503 | 180 |
| 4 | 20504 | 200 |
| 5 | 20403 | 200 |
| 6 | 19906 | 160 |
| 7 | 19907 | 200 |
| 8 | 20505 | 170 |

4.2.6 Oscilloscope

The purpose of the oscilloscope in the vibration testing is to monitor one or two signals from either the force or the accelerometer. By monitoring the signals, an improper signal or noise can be discovered. The oscilloscope was also used to recheck the amplitude, frequency, or the phase of the force and structure response signals.

The detailed block diagram for the instrumentation scheme can be seen in Figure 4.6, while a picture of the setup is given in Figure 4.7.

4.3 Experimental Setup

The support for the beam models consisted of two stiff steel H-section columns. The beam model was clamped at each end using two thick square steel plates on the top of the H-sections columns. The exciter was suspended using a square flat plate which was fixed on top of a steel frame. The complete experimental setup is shown in Figure 4.8.

As mentioned previously, in order to determine the best location for the accelerometer, seven accelerometers were attached to each beam model at seven different locations for acquiring the responses of the model. The detailed locations of the accelerometers can be seen in Figure 4.9.

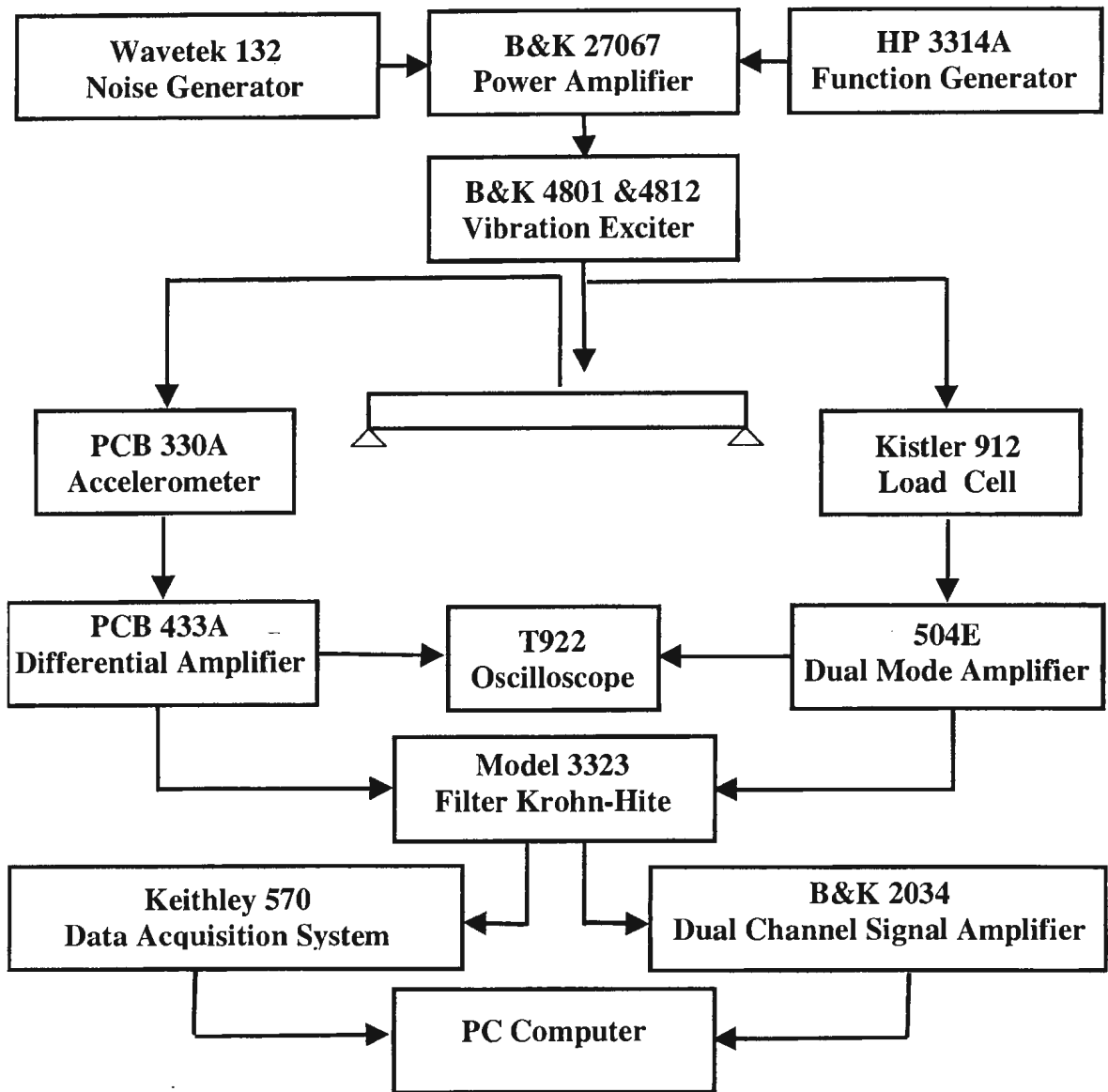


Figure 4.6. Detailed vibration testing instrumentation scheme.



Figure 4.7. Instrumentation setup

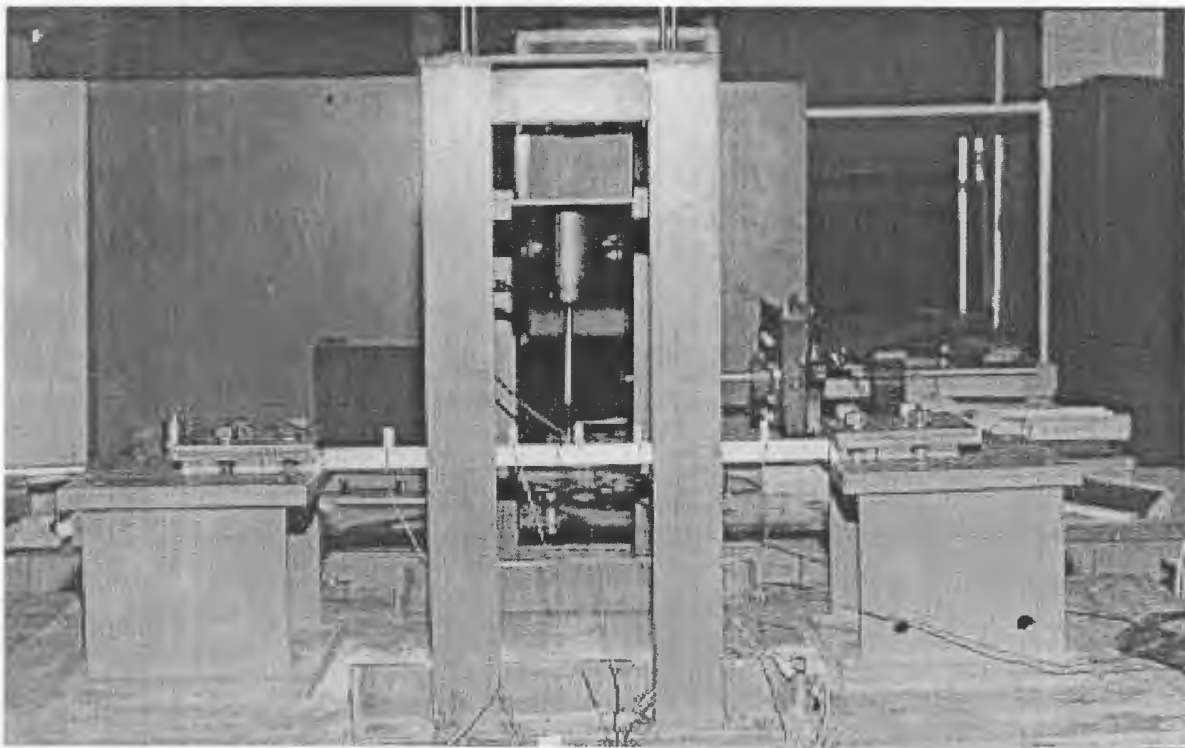


Figure 4.8. Experimental setup

4.4 Experimental Procedure

First, the intact model was tested and its response to the random excitation was measured. The measurements were recorded at a rate of 1/9000 sec and the length of each data sample was 1 sec. The signal was digitised, manipulated and stored on the hard disk drive of a personal computer. Then, a crack of depth 1/10 in (2.54 mm) was created at a particular location on the model. The crack was made by a thin saw-cut (around 0.4mm thick). The test was repeated for that crack depth. The crack depth was then increased to the next depth and the test was repeated again. The process was continued with crack depths increasing at an increment of 1/10 in (2.54 mm) until the crack depth reached a magnitude of 7/10 in (17.78 mm).

In every set, seven beams were tested with cracks of different depths and at different locations. The testing was carried out very carefully to obtain a reliable set of data with a high degree of accuracy. Table 4.4 gives the locations of the cracks on each beam. Table 4.5 shows the dimensions of the cracks. Examples of the beams tested are shown in Figures 4.10 and 4.11.

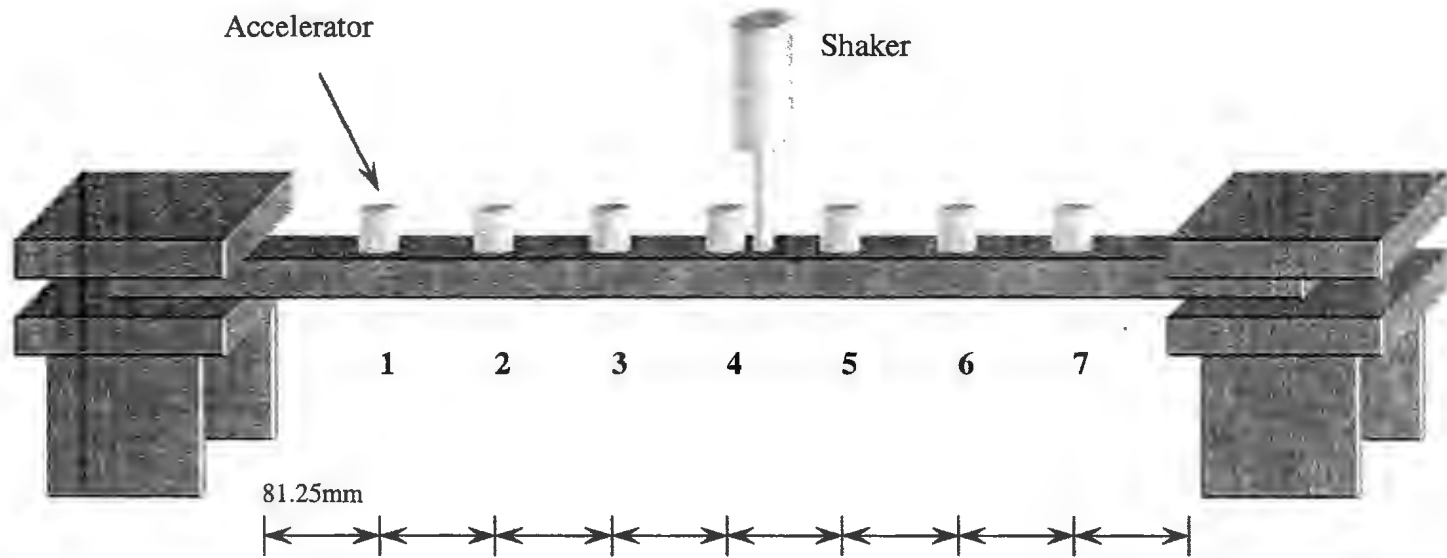


Figure 4.9. Locations of accelerometers

Table 4.4: Crack Location

| Beam Specimen No. | Crack position from one end (mm) | | |
|-------------------|----------------------------------|------------------|------------------|
| | L = 650 mm | Fixed-Fixed Beam | Simply-Supported |
| 1 | Uncracked | uncracked | uncracked |
| 2 | 1/16 L | 41 | 41 |
| 3 | 3/16 L | 122 | 122 |
| 4 | 5/16 L | 203 | 203 |
| 5 | 7/16 L | 284 | 284 |
| 6 | 8/16 L | 325 | 325 |
| 7 | 11/16 L | 447 | 447 |

Table 4.5: Crack Depth

| Depth No. | Depth of cuts (mm) | |
|-----------|--------------------|-------|
| | d = 25.4 mm | |
| 1 | 1/10 d | 2.54 |
| 2 | 2/10 d | 5.08 |
| 3 | 3/10 d | 7.62 |
| 4 | 4/10 d | 10.16 |
| 5 | 5/10 d | 12.70 |
| 6 | 6/10 d | 15.24 |
| 7 | 7/10 d | 17.78 |

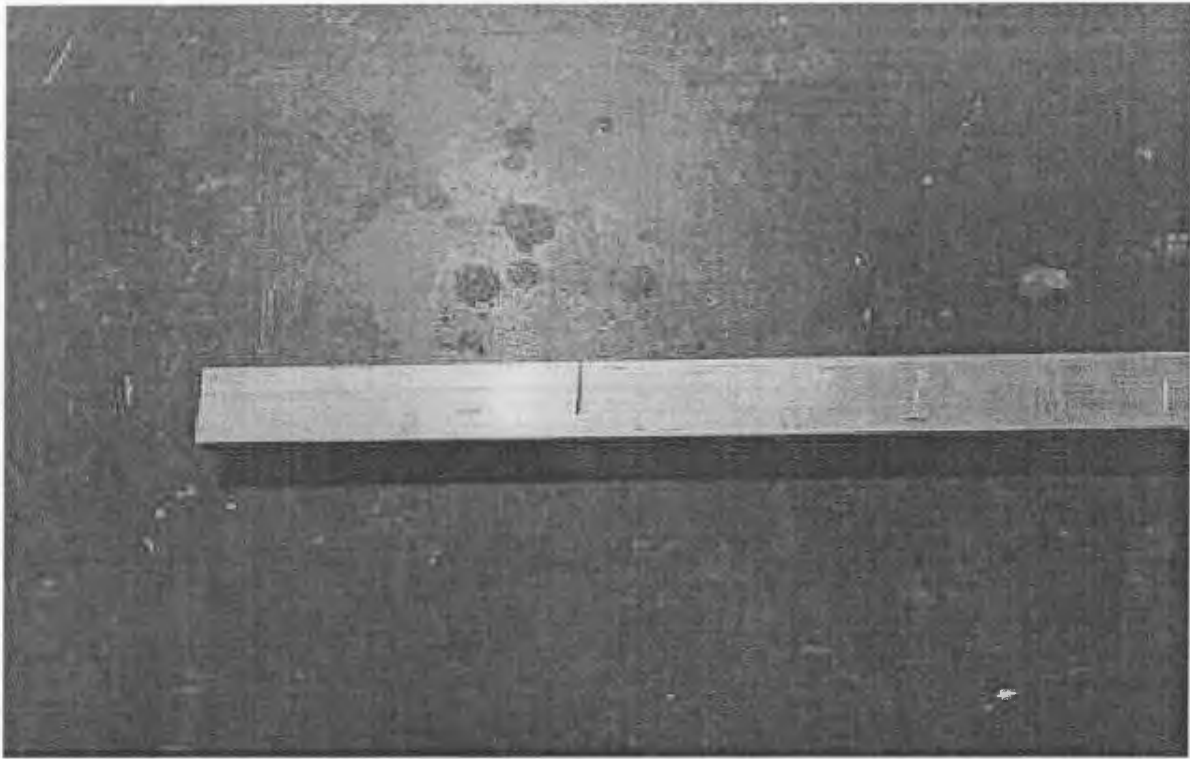


Figure 4.10. A Fixed-fixed beam with a crack at $1/16 L$.

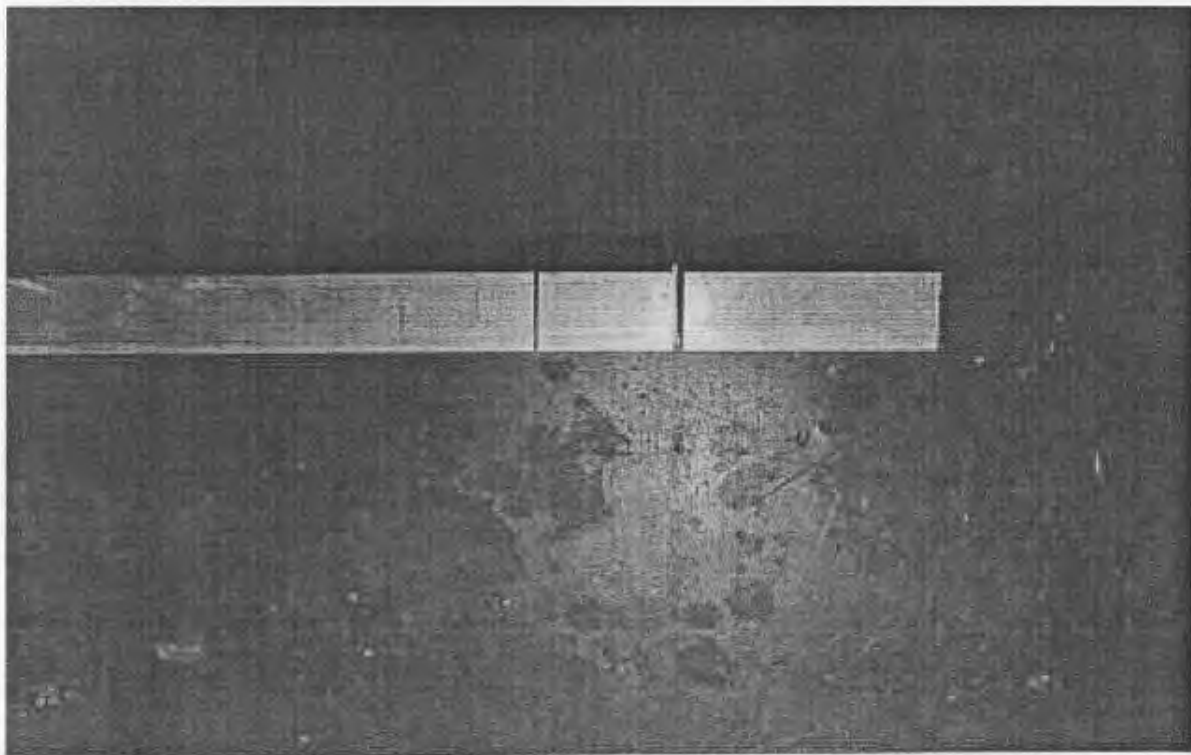
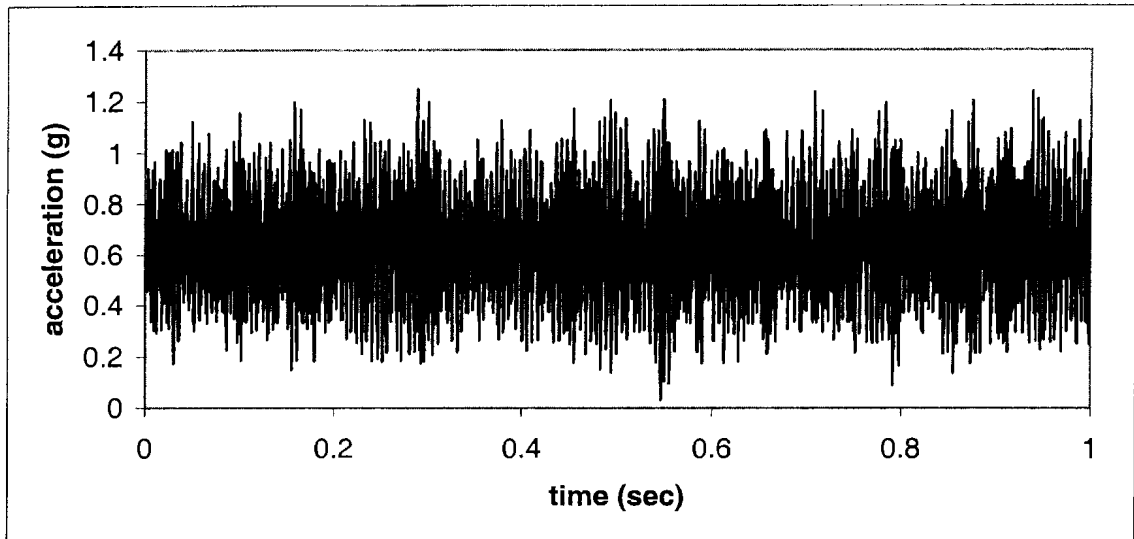


Figure 4.11. A Simply-supported beam with a crack at $1/16 L$.

4.4.1 Auto-correlation Calculation

In this work, random responses of the beam model at different locations were measured using accelerometers. Initially, the experiment was started with seven accelerometers to determine the best location for measurements. Comparing the signals measured by the different accelerometers, we found that accelerometers 3 and 4 gave clear and reliable signals. Since accelerometer 4 is located at mid length, it was decided to choose measurements obtained for accelerometer number 3 for analysis. Because of symmetry, accelerometer 4 lies at the node of asymmetric modes. Figure 4.12 shows an example of signals taken by accelerometer number 3.

As mentioned previously in this chapter, before the analysis can be done, the data should be calibrated using calibration sheets for the accelerometers and the load cell. Next, the acceleration random response was filtered using a wide-band frequency filter to reduce the noise. The filtered signature then was analysed by using Equations 3.16 to obtain the Auto-correlation function. Not only the low frequencies from the noise, ground and building vibration were taken out in the filtering process, but also the frequencies higher than the first mode were eliminated. The filtering process was performed using MATLAB 5.3 software package (The Math Works, Inc, 1999). Figure 4.13 shows the procedure used in this experiment for obtaining the auto-correlation function of a random response.



**Figure 4.12 A random response data taken from accelerometer No. 3
(after calibration).**

As discussed in previous chapter, the auto-correlation function is used to estimate the free vibration response of the structure. Then, by calculating the period of the response the fundamental natural frequency can be determined. The signal processing scheme from filtering until obtaining the natural frequency of the model was shown in Figure 4.14.a – 4.14.d. The predicted natural frequency of the structure and its auto-correlation function then were used as input to the neural networks algorithm for crack identification.

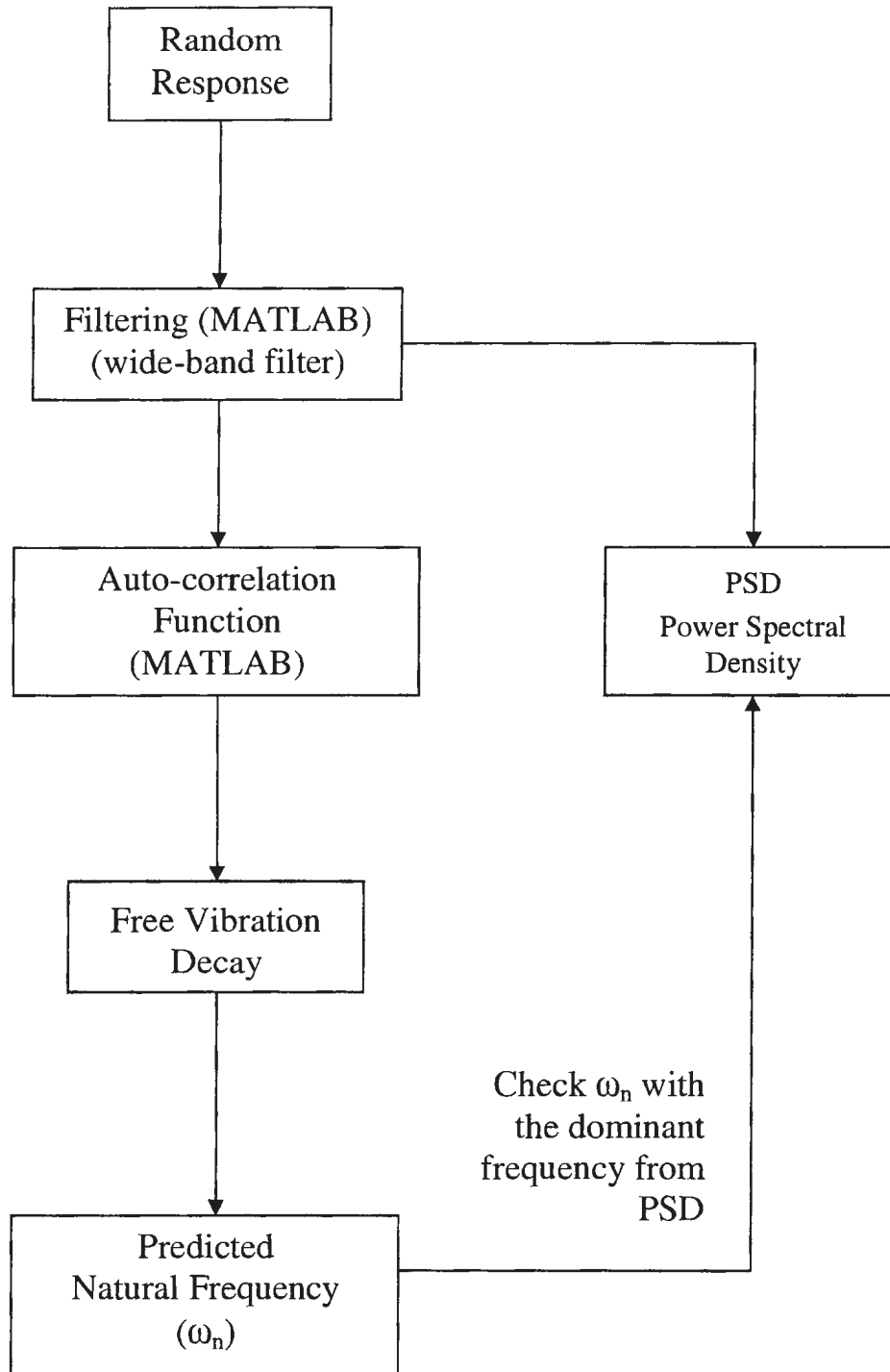


Figure 4.13. Procedure for obtaining the Auto-correlation function.

Signal Processing Scheme



Figure 4.14.a. Random response from an accelerometer, before Filtering.



Figure 4.14.b. Random response from an accelerometer, after Filtering.



Figure 4.14.c. The auto-correlation function (half side, only circled part is used in the analysis).

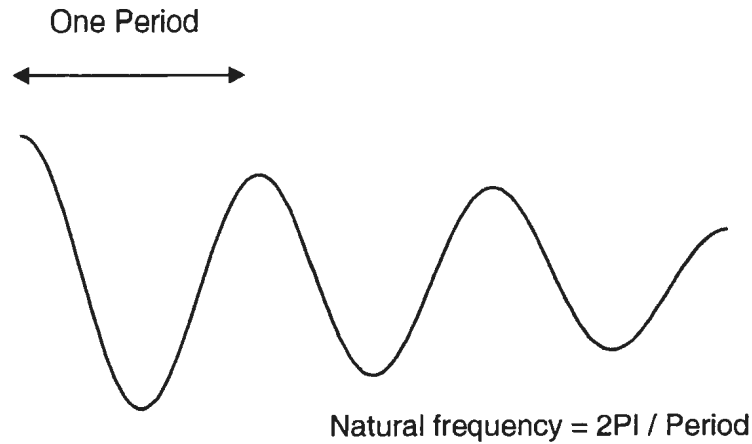


Figure 4.14.d. The Free vibration decay (the first 3 cycles).

4.5 Summary

The complete experimental setup, model and equipment descriptions used in this work, were briefly described in this chapter. To obtain accurate and reliable results, the experiment should have proper experimental setup, calibration and careful test treatment. The chapter also provides the experiment procedure, pictures and sample of calculations performed during the data analysis. These procedures have been carefully followed in the present study in order to minimize the errors occurred. The results obtained were analyzed, tabulated, and discussed in Chapter Five follows.

CHAPTER 5

RESULTS AND DISCUSSION

In this work, a technique for crack identification in beams using neural networks was developed. First, the recorded random responses of the beam were filtered and analyzed. Then, the auto-correlation function was obtained from the filtered random response. The auto-correlation function represents the free vibration response of the beam as discussed in Chapter 3, and it can be used in the identification of the vibration characteristics of the beam. The fundamental natural frequency of the beam was estimated from the period of the auto-correlation function. The estimated natural frequency was compared to the values of the natural frequencies obtained from a finite element model and the exact solution. Following this, the changes of the natural frequencies for each crack condition were observed and analyzed. Next, the auto-

correlation function and its derivative were used as inputs to the neural network algorithm. The neural network algorithm was employed to identify the function $G(x, \mu, \dot{\mu})$, which is used as an indicator for crack inception and progression. Appendix A provides the FORTRAN program 'neural.for' that was used in this study. In this chapter, all the results and discussions of the technique are presented.

5.1 Natural Frequency Prediction

In this study, the auto-correlation function was obtained from the random response to predict the natural frequency of the first mode (fundamental frequency) of the beam based on the random decrement technique described in Chapter 3. As mentioned in the previous chapter, only a small number of cycles of the auto-correlation are used in representing the free vibration of the beam. The natural frequency is obtained from the measured period of the auto-correlation as: $\varpi_d = \frac{2\pi}{T_d}$.

5.1.1 Filtering

In predicting the natural frequency using the auto-correlation, the filtering process plays an important role. The noise from low frequencies (ground/building, machinery vibration, etc) and high mode frequencies affect the accuracy of the calculations. The filter window should eliminate frequencies of the higher modes of the beam's dynamics as well as the low frequency noise. A wide band filter from MATLAB was used in this

work. Figure 5.1 shows an example of the auto-correlation of the simply supported beam before and after filtering the process.

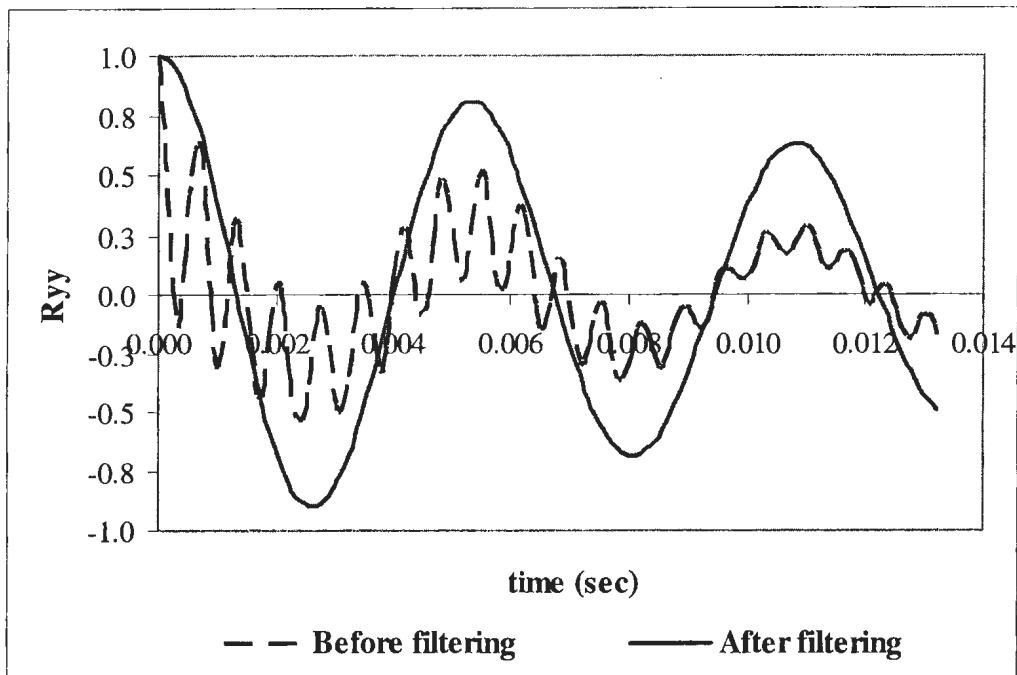


**Figure 5.1 Comparison of the auto-correlation function before and after filtering.
(simply-supported, no crack)**

In figure 5.1, the auto-correlation function before filtering contains high frequencies caused by the superposition of two (or more) sinusoids at different frequencies. The filter succeeded in eliminating the high frequency noise. After filtering, the function becomes more representative of the free vibration of the beam. All random response measurements from the experiment were filtered and analyzed carefully and consistently for each crack condition and location.

5.1.2 Experimental Results

The auto-correlation function for each crack condition was normalized. Figure 5.2 to 5.8 present the auto-correlations for the case of fixed-fixed beam with a center crack, having a depth that varies from 2.54mm to 17.78mm (1/10, 2/10, 3/10, 4/10, 5/10, 6/10 and 7/10 of the beam's depth). Appendix B contains the auto-correlation functions for the case of simply-supported beam. To show the effect of crack depth on the auto-correlation function, the auto-correlation functions obtained at the same location for cases of different crack depths are plotted together in Figure 5.9. The plots of the auto-correlation function for different end conditions, crack positions and crack depths are presented in Appendix B.

The estimated natural frequencies obtained from the auto-correlation functions are shown in Tables 5.1 and 5.2 for the fixed-fixed and simply supported beams, respectively. The natural frequencies were normalized and plotted as a function of crack depth, for each crack location. Figure 5.10 and 5.11 show the changes in the natural frequency as functions of crack depths and crack locations for the simply supported and fixed-fixed beams, respectively. The same information have been plotted in three dimensional plots in Figure 5.12.

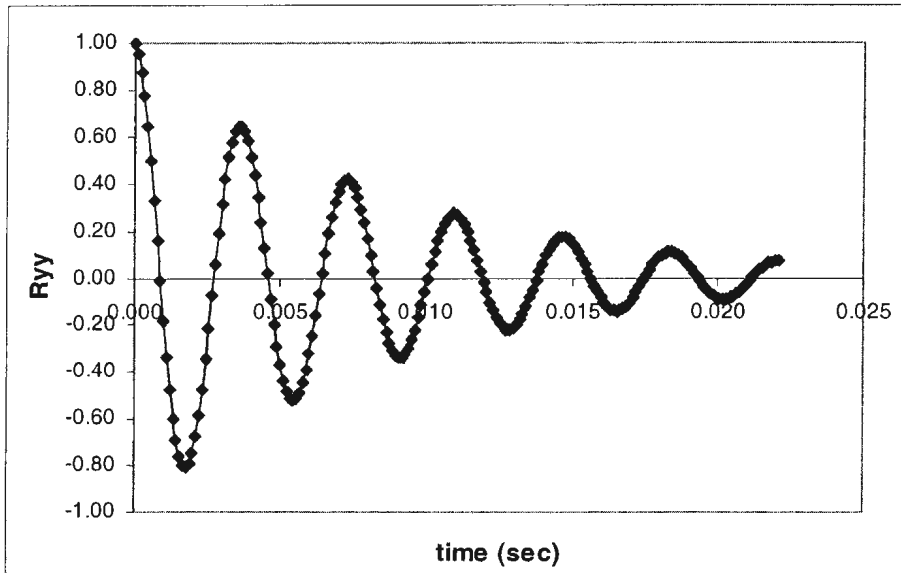


Fig 5.2 Estimated free vibration (auto-correlation function) of fixed-fixed beam with a 2.54mm crack depth at the center of the beam

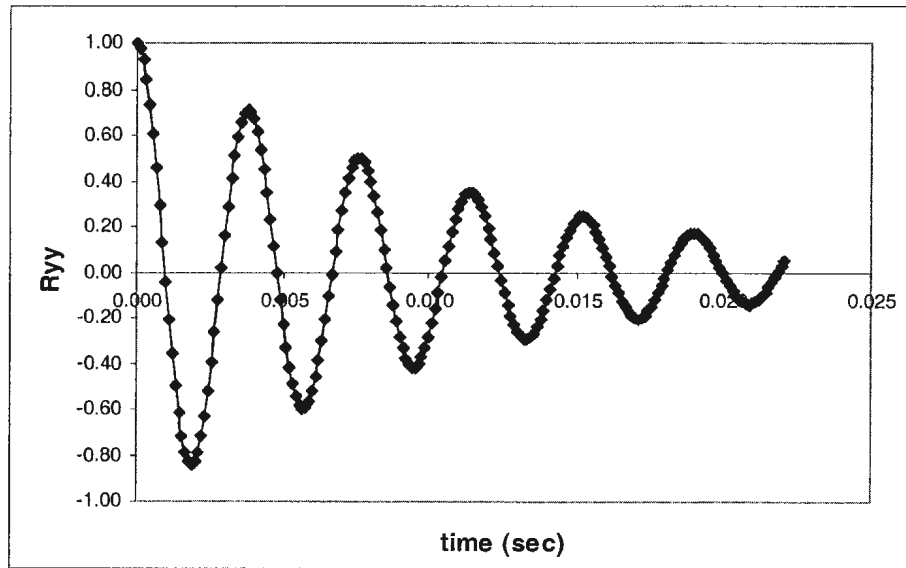


Fig 5.3 Estimated free vibration (auto-correlation function) of fixed-fixed beam with a 5.08mm crack depth at the center of the beam

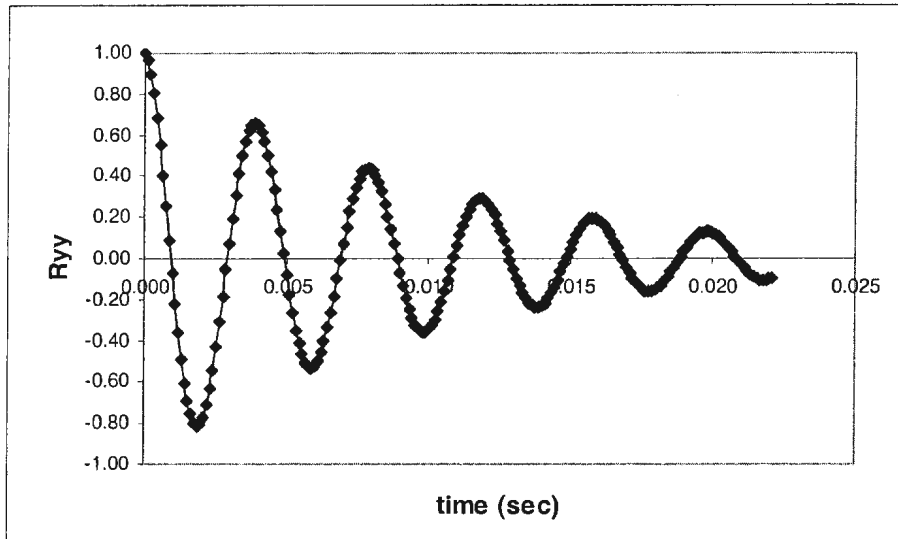


Fig 5.4 Estimated free vibration (auto-correlation function) of fixed-fixed beam with a 7.62mm crack depth at the center of the beam

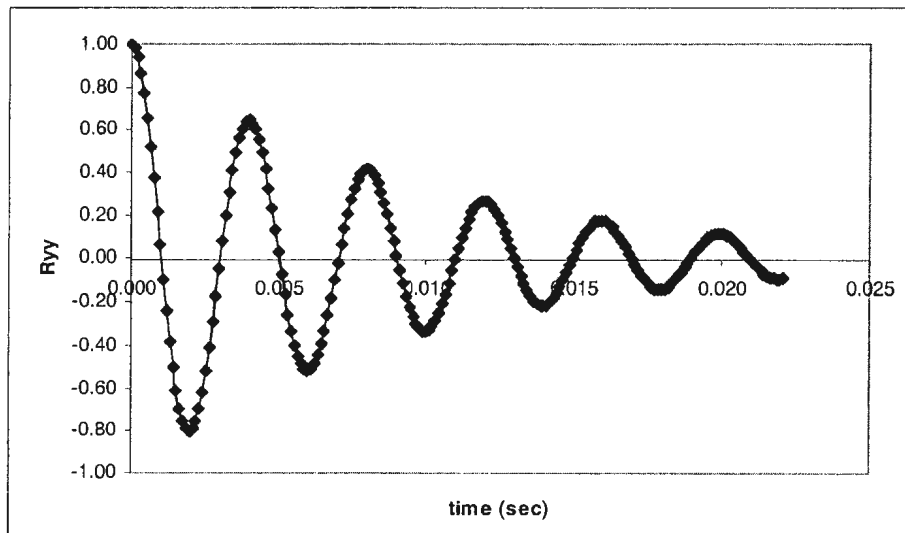


Fig 5.5 Estimated free vibration (auto-correlation function) of fixed-fixed beam with a 10.16mm crack depth at the center of the beam

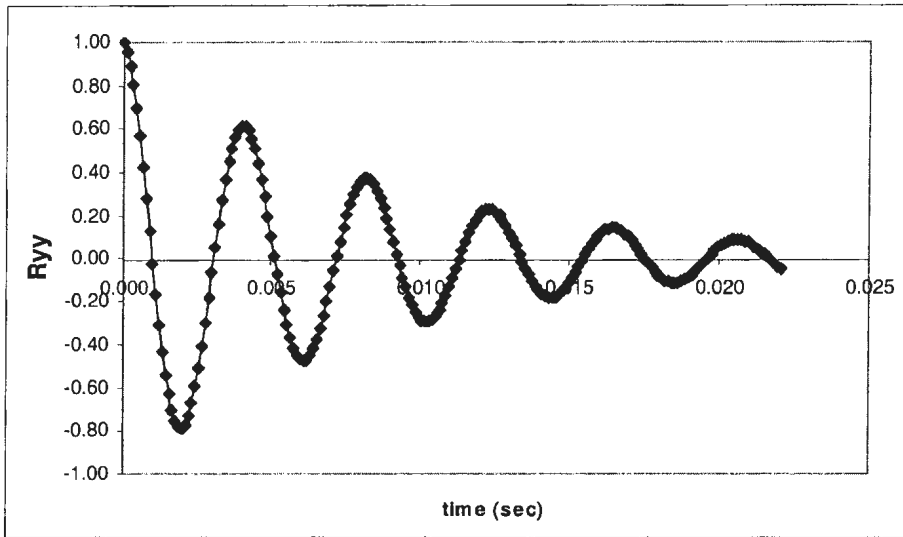


Fig 5.6 Estimated free vibration (auto-correlation function) of fixed-fixed beam with a 12.70mm crack depth at the center of the beam

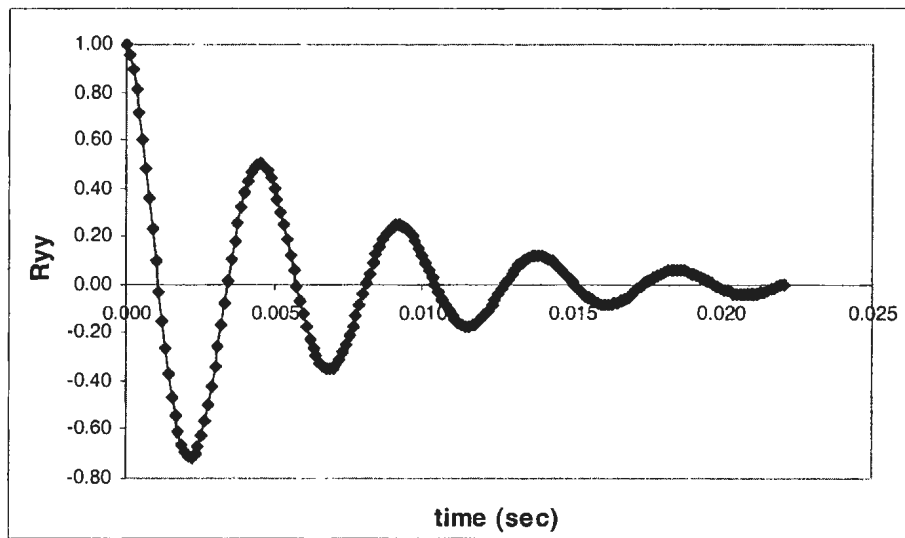


Fig 5.7 Estimated free vibration (auto-correlation function) of fixed-fixed beam with a 15.24mm crack depth at the center of the beam

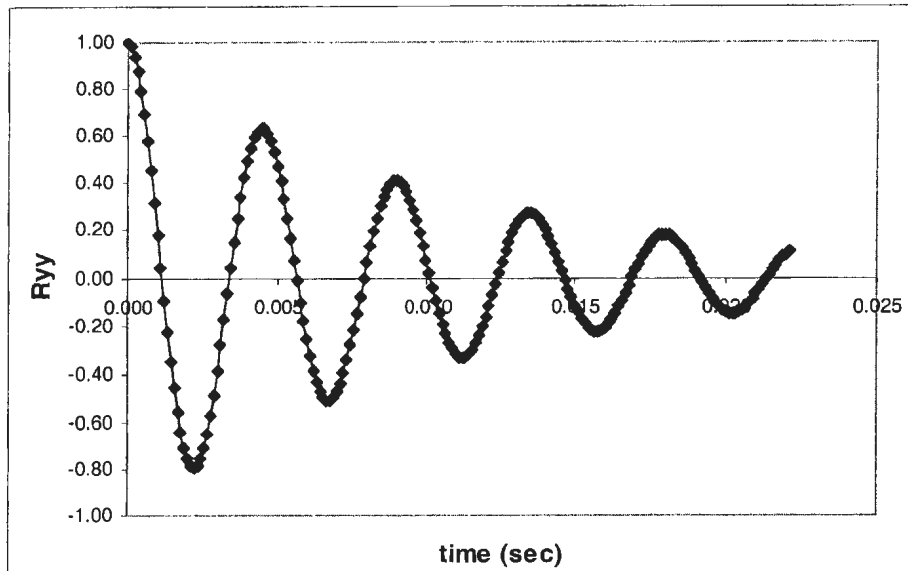


Fig 5.8 Estimated free vibration (auto-correlation function) of fixed-fixed beam with a 17.78mm crack depth at the center of the beam

Table 5.1: Predicted fundamental frequency for different crack depths and locations on simply supported beam.

| Crack depth [mm] | Crack location from one end (L = beam's length) | | | | | |
|---------------------|---|---------|---------|---------|---------|---------|
| | 1/16 L | 3/16 L | 5/16 L | 7/16 L | 8/16 L | 11/16 L |
| No crack | 135.9195 | | | | | |
| 2.54 | 134.831 | 133.601 | 134.459 | 133.856 | 132.817 | 133.587 |
| 5.08 | 132.322 | 132.284 | 133.149 | 133.725 | 131.123 | 133.070 |
| 7.62 | 131.395 | 131.608 | 131.758 | 127.867 | 130.710 | 128.895 |
| 10.16 | 126.521 | 130.389 | 125.286 | 125.802 | 128.995 | 125.104 |
| 12.70 | 126.435 | 128.536 | 124.465 | 118.342 | 122.249 | 124.429 |
| 15.24 | 113.100 | 125.092 | 117.323 | 116.320 | 110.478 | 113.011 |
| 17.78 | 115.642 | 112.763 | 107.880 | 102.388 | 94.528 | 113.982 |

Table 5.2: Predicted fundamental frequency for different crack depths and locations on fixed-fixed beam.

| Crack depth [mm] | Crack location from one end (L = beam's length) | | | | | |
|---------------------|---|---------|---------|---------|---------|---------|
| | 1/16 L | 3/16 L | 5/16 L | 7/16 L | 8/16 L | 11/16 L |
| No crack | 282.363 | | | | | |
| 2.54 | 274.336 | 276.306 | 274.733 | 275.512 | 274.224 | 277.360 |
| 5.08 | 271.571 | 273.415 | 273.508 | 270.055 | 269.509 | 274.592 |
| 7.62 | 259.824 | 258.773 | 256.212 | 266.803 | 251.350 | 266.635 |
| 10.16 | 251.433 | 247.819 | 243.658 | 247.188 | 252.444 | 259.219 |
| 12.70 | 248.202 | 245.871 | 239.211 | 242.827 | 236.859 | 240.875 |
| 15.24 | 239.523 | 245.008 | 228.114 | 210.963 | 211.160 | 215.652 |
| 17.78 | 236.767 | 217.952 | 217.935 | 216.757 | 224.288 | na |

Table 5.3: The reduction of natural frequencies due to a presence of a 1/10 d crack (2.54 mm) for simply supported and fixed-fixed beam model.

| Crack Location (L = beam's length) | Simply Supported Beam (%) | Fixed-Fixed Beam (%) |
|---------------------------------------|------------------------------|-------------------------|
| 1/16 L | 0.801 | 2.843 |
| 3/16 L | 1.706 | 1.772 |
| 5/16 L | 1.074 | 2.702 |
| 7/16 L | 1.518 | 2.426 |
| 8/16 L | 2.283 | 2.882 |
| 11/16 L | 1.716 | 2.145 |

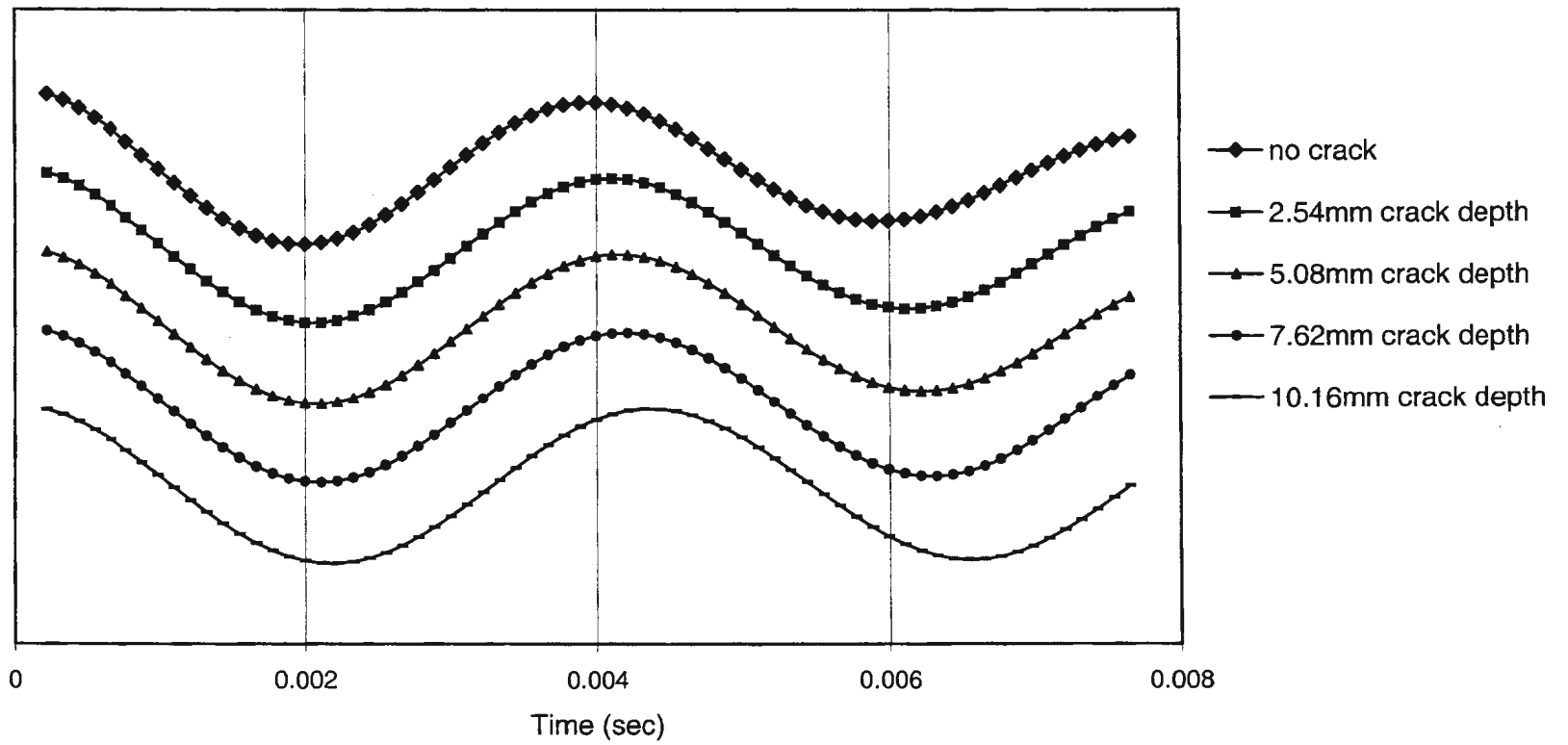


Figure 5.9 Auto-correlation functions for simply supported, crack at 8/16 L.

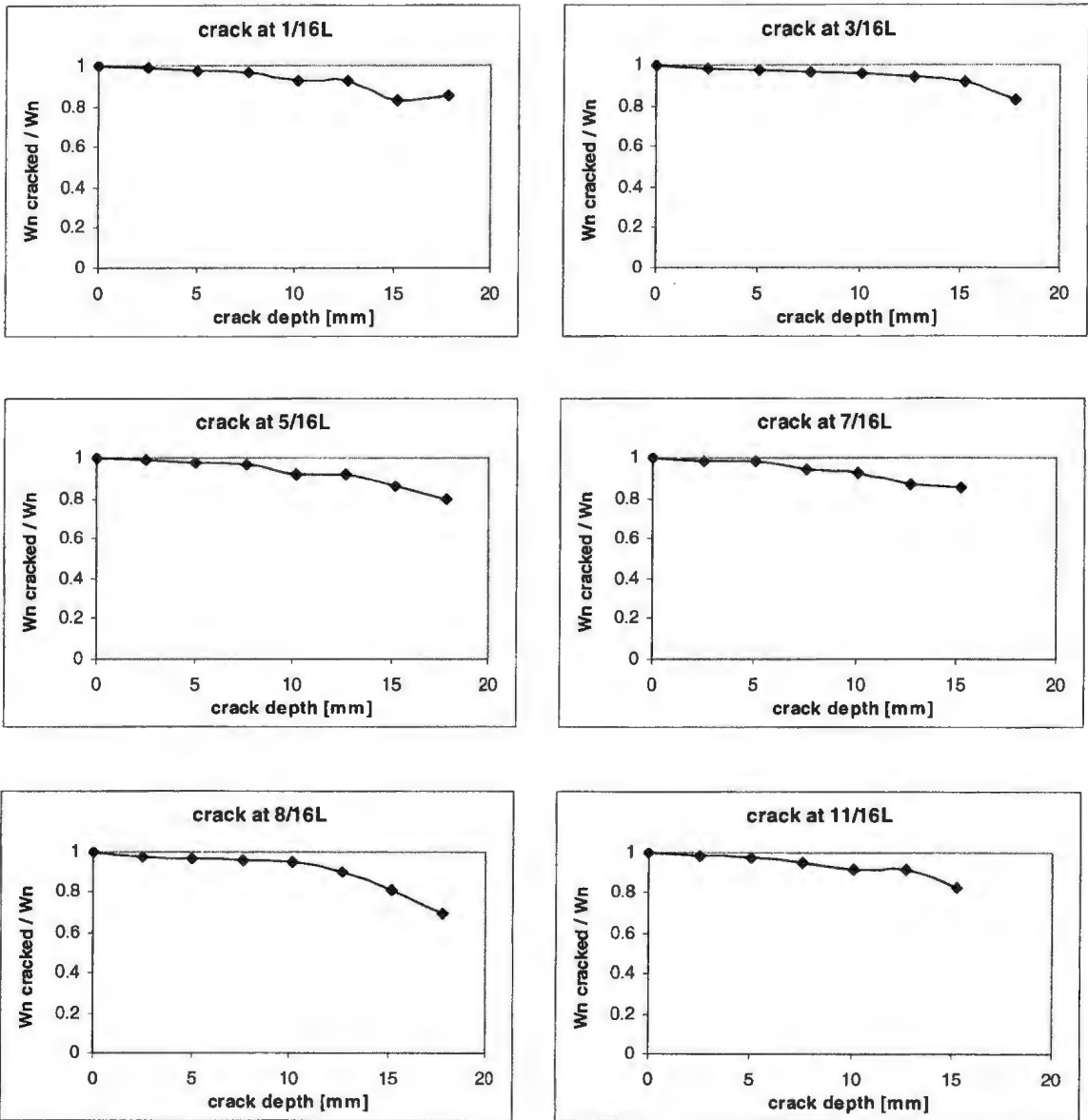


Fig 5.10 Fundamental frequency ratio ($\omega_{n \text{ crack}}/\omega_{n \text{ nocrack}}$) as a function of crack depth and location on the simply supported beam.

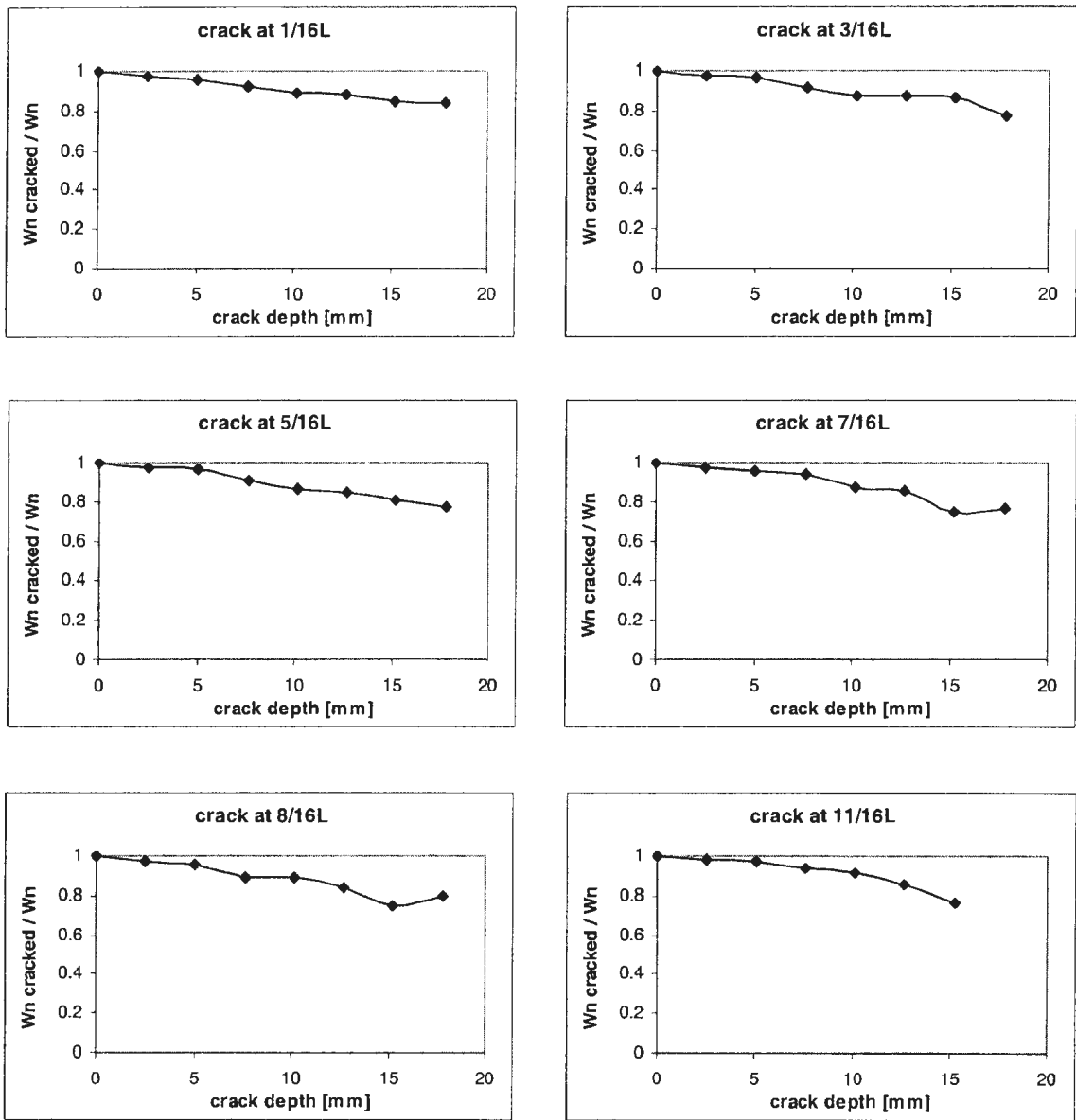
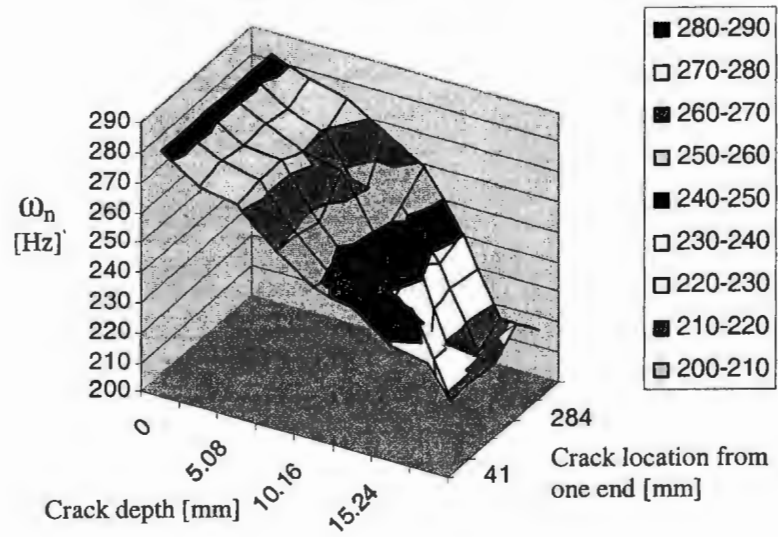
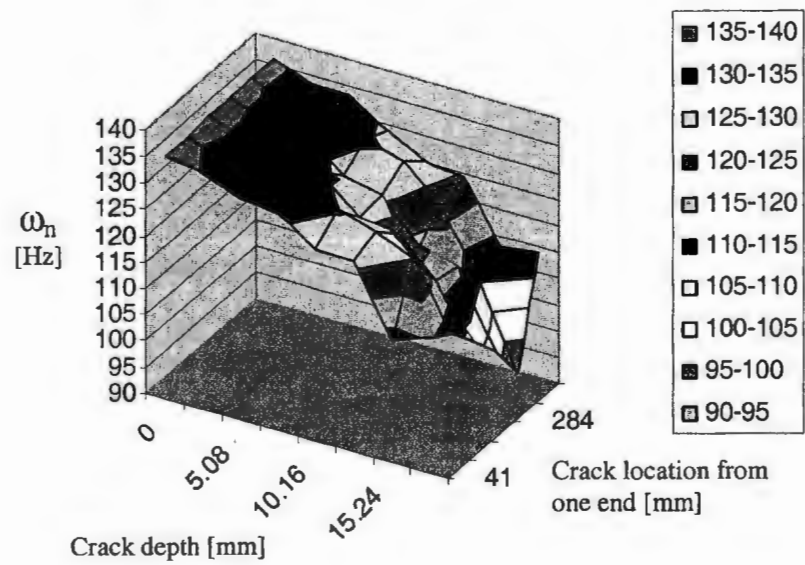


Fig 5.11 Fundamental frequency ratio ($\omega_{n \text{ crack}} / \omega_{n \text{ no crack}}$) as a function of crack depth and location on the fixed-fixed beam.



Fixed-fixed beam



Simply supported beam

Fig 5.12 3D plots of the natural frequencies for different crack locations and depths.

5.1.3 Exact and Finite Element Solution

The natural frequency for the beam without crack were obtained using the exact solution, see DeSilva (1999). The exact solution was obtained as follows:

$$\omega_n = \left(\frac{\lambda_i}{L}\right)^2 \sqrt{\frac{EI}{m}}$$

where $\lambda_i = 4.730041$ for the simply supported beam and $\lambda_i = \pi$ for the fixed-fixed beam.

A finite element model for the beam was formulated using ABAQUS. The beams were modeled using 2D beam elements. The model used a notch section to represent a crack. The notched section was replaced by a section having a smaller cross-section of the beam. The results show good agreement between the experiment, the exact solution and the finite element solution. Table 5.4 shows the comparisons.

Table 5.4: The comparison of the natural frequencies obtained from the experiment, the exact solution and the finite element solution.

| Beam with no crack | | | |
|---------------------------|-----------------------------|-----------------------|------------------------------|
| Model | Experimental Results | Exact Solution | Finite Element Method |
| Simply Supported | 135.919 | 138.553 | 138.550 |
| Fixed-fixed | 282.363 | 314.448 | 314.070 |

| Simply supported beam, crack at the center | | | |
|---|----------------------|-----------------------|--------------|
| Crack depth [mm] | Experimental results | Finite Element Method | % Difference |
| 2.54 | 134.831 | 138.320 | 2.522 |
| 5.08 | 132.322 | 137.910 | 4.052 |
| 7.62 | 130.710 | 137.200 | 4.730 |
| 10.16 | 128.995 | 135.890 | 5.074 |
| 12.70 | 126.435 | 133.360 | 5.193 |

| Fixed-fixed beam, crack at the center | | | |
|--|----------------------|-----------------------|--------------|
| Crack depth [mm] | Experimental results | Finite Element Method | % Difference |
| 2.54 | 274.22 | 313.79 | 12.609 |
| 5.08 | 269.51 | 313.22 | 13.955 |
| 7.62 | 251.35 | 312.14 | 19.475 |
| 10.16 | 252.44 | 310.11 | 18.595 |
| 12.70 | 236.86 | 306.13 | 22.628 |

For the fixed-fixed beam, the difference between the experimental results and the exact solution or finite element method is significant. This may be caused by the fact that the experimental setup could not simulate the fixed-fixed boundary conditions accurately.

5.1.4 Discussion

It is clear from the results presented that the auto-correlation function gives a good approximation of the free response. The auto-correlation function can be easily obtained from the random response of the system. The natural frequency obtained from the auto-correlation function is in good agreement with the ones that were obtained from the exact solution and the finite element method. For the simply supported beam, the difference between the natural frequency obtained from the auto-correlation function and that obtained from the analytical solutions is less or equal than 5%. This is within the range of experimental error. For the fixed-fixed beam, the difference reaches 23 %. This may be caused by the way the beam is supported in the experiment. The beam ends were clamped between two thick plates. This is the nearest we can come experimentally to a fixed supported. However, this support does not completely prevent the beam ends from rotating during the test.

Figures 5.10 and 5.11 show that the fundamental frequency decreases as the crack grows. This is true for both boundary conditions and for all crack locations. The difference between the natural frequency for the beam with crack and the natural frequency of the beam with no crack reaches an average of 2.28% for a crack depth of 2.54mm and 30% for a crack depth of 17.78mm, for the simply supported beam. For the fixed-fixed beam the values are 2.88% for a crack depth of 2.54mm and 20.6% for a crack length of 17.78mm.

For the simply supported beam, the reduction in frequency is minimum when the crack is at a distance of $1/16L$ from the support and the maximum reduction when the crack is at midlength. For the fixed-fixed beam the minimum change in the frequency occurs when the crack is located at a distance of $3/16L$ from the support, while the maximum change occurs for a crack at midlength. It seems then that the crack affects the natural frequency most when it occurs at the maximum deflection point, for both beams. However, it should be noted that even the maximum change in the frequency is not appreciable. The maximum change is shown to be in the range of 2-3%. This is not going to be an effective tool for crack detection. In the next section, we discuss a more effective tool for crack detection.

5.2 Identification of $G(x, \mu, \dot{\mu})$

In this work, we will use $G(x, \mu, \dot{\mu})$ function as a second criterion for identifying the occurrence and progression of a crack. A neural network algorithm is used to obtain the magnitude of the $G(x, \mu, \dot{\mu})$ function using $\mu(t)$ and $\dot{\mu}(t)$ as inputs.

5.2.1 Results

Figures 5.13 to 5.19 show samples of the comparison between the original auto-correlation functions and their predictions from the neural network training for the case of crack at the center and crack depth from 2.54mm to 17.78mm. The results for all cases

can be seen in Appendix C. Figures 5.20 to 5.26 show the plots of $G(x, \mu, \dot{\mu})$ as a function of time. As can be seen from those figures, the amplitude of $G(x, \mu, \dot{\mu})$ decreases as the crack depth increases. The decrease in the $G(x, \mu, \dot{\mu})$ amplitude is used in identifying the presence of a crack. Table 5.5 and 5.6 summarize the amplitude of $G(x, \mu, \dot{\mu})$ for both the simply supported and fixed-fixed beam.

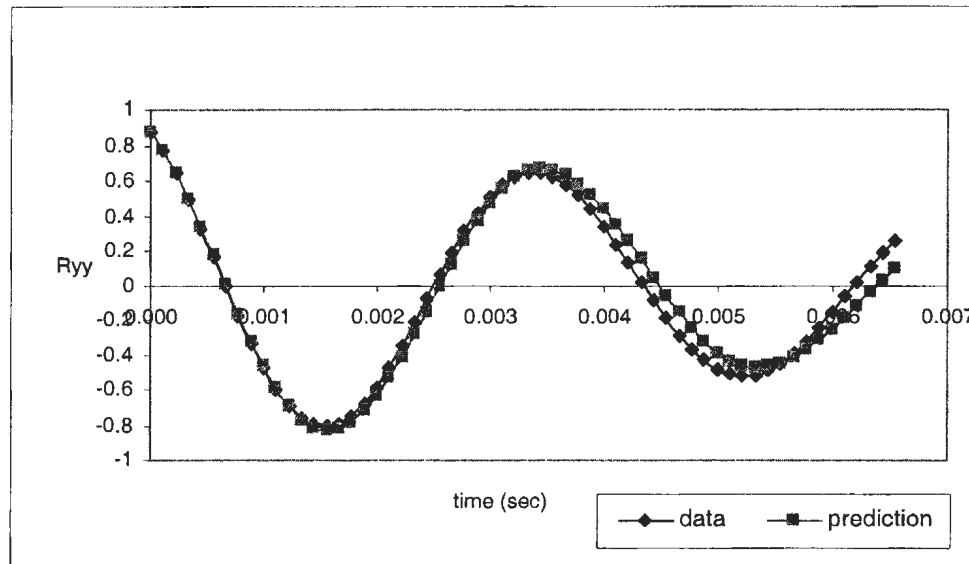


Fig 5.13 Comparison between original Auto-correlation function and the neural network prediction for fixed-fixed beam (2.54mm crack depth, center crack).

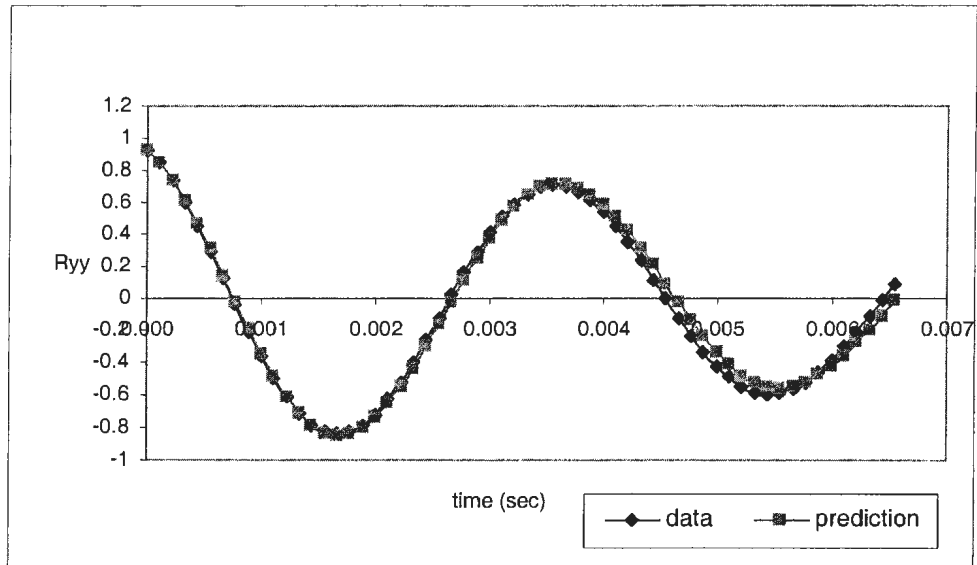


Fig 5.14 Comparison between original Auto-correlation function and the neural network prediction for fixed-fixed beam (5.08mm crack depth, center crack).

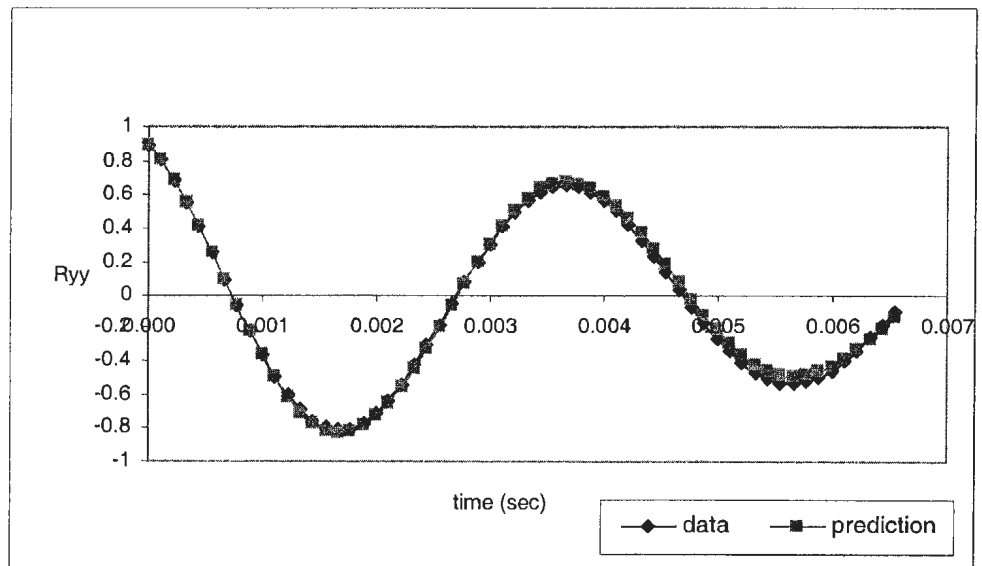


Fig 5.15 Comparison between original Auto-correlation function and the neural network prediction for fixed-fixed beam (7.62mm crack depth, center crack).

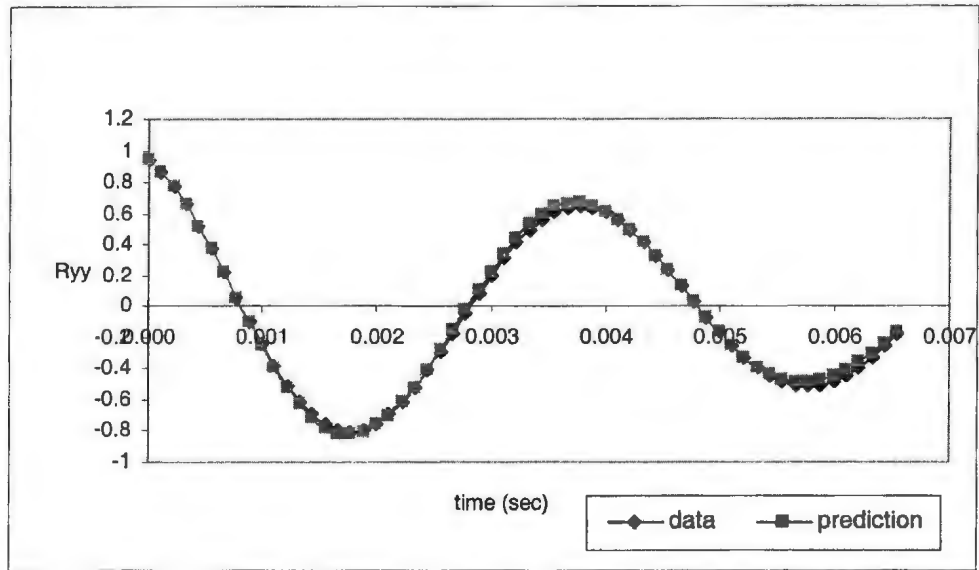


Fig 5.16 Comparison between original Auto-correlation function and the neural network prediction for fixed-fixed beam (10.16mm crack depth, center crack).

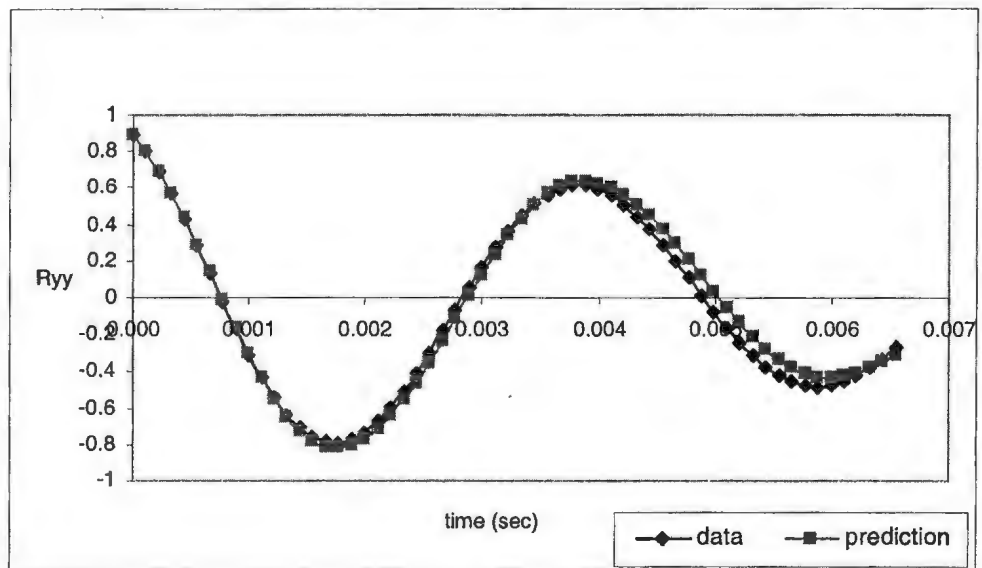


Fig 5.17 Comparison between original Auto-correlation function and the neural network prediction for fixed-fixed beam (12.70mm crack depth, center crack).

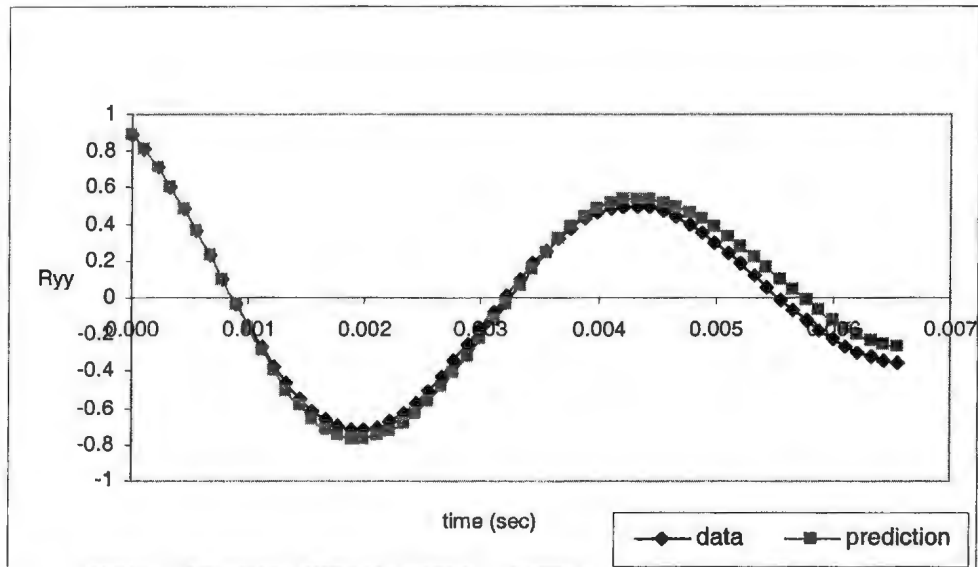


Fig 5.18 Comparison between original Auto-correlation function and the neural network prediction for fixed-fixed beam (15.24mm crack depth, center crack).

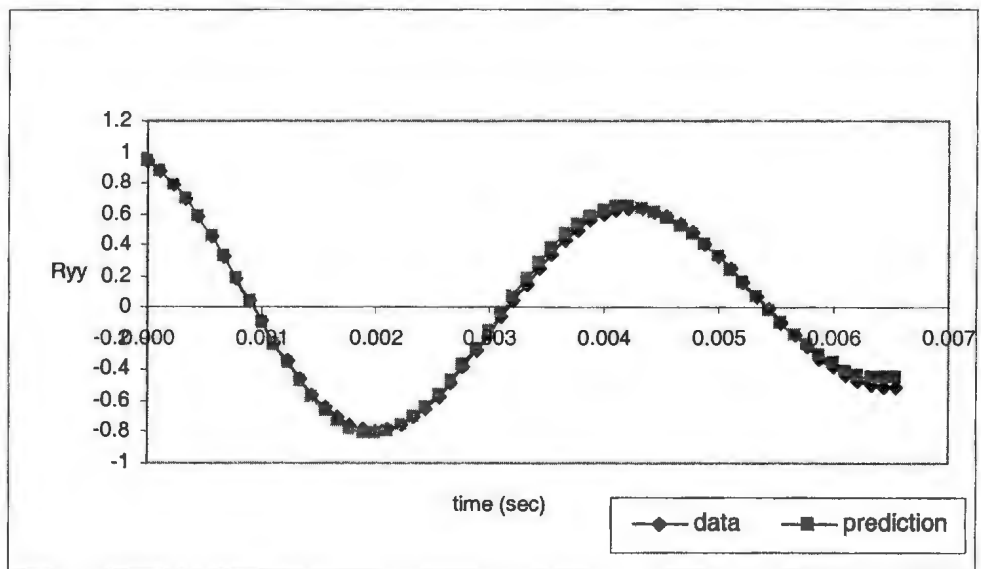


Fig 5.19 Comparison between original Auto-correlation function and the neural network prediction for fixed-fixed beam (17.78mm crack depth, center crack).

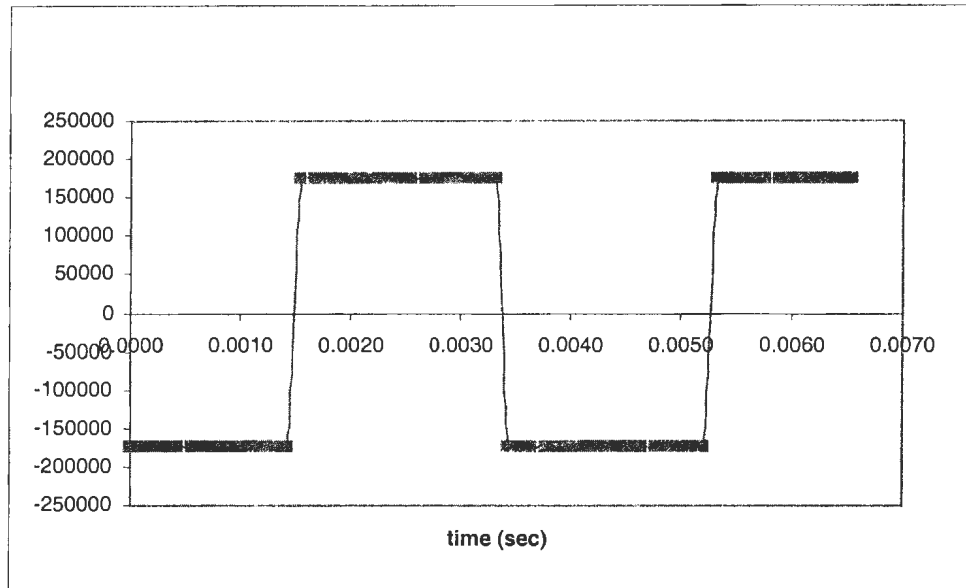


Fig 5.20 Plot of $G(x, \mu, \dot{\mu})$ function as a function of time, for fixed-fixed beam (2.54mm crack depth, center crack).

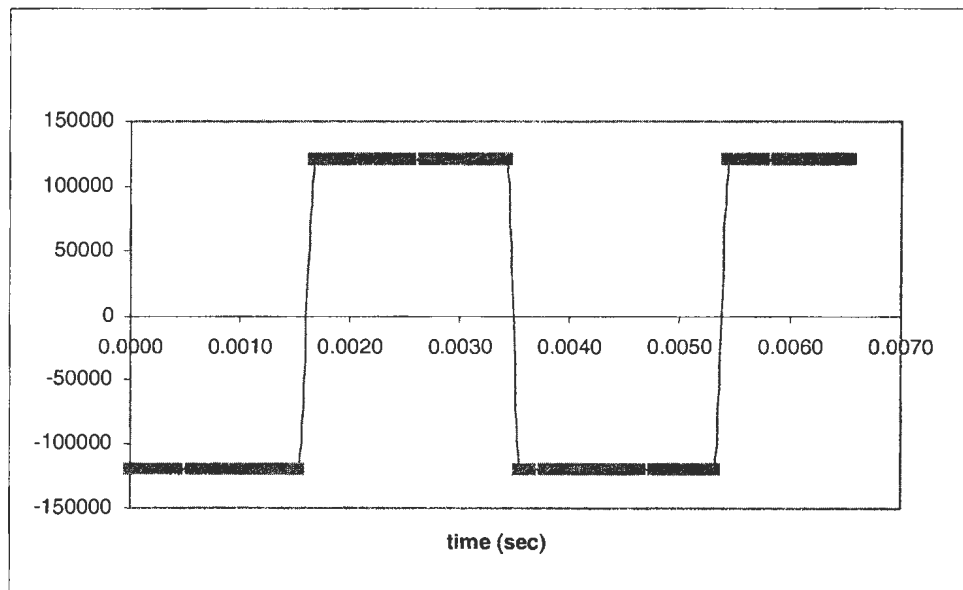


Fig 5.21 Plot of $G(x, \mu, \dot{\mu})$ function as a function of time, for fixed-fixed beam (5.08mm crack depth, center crack).

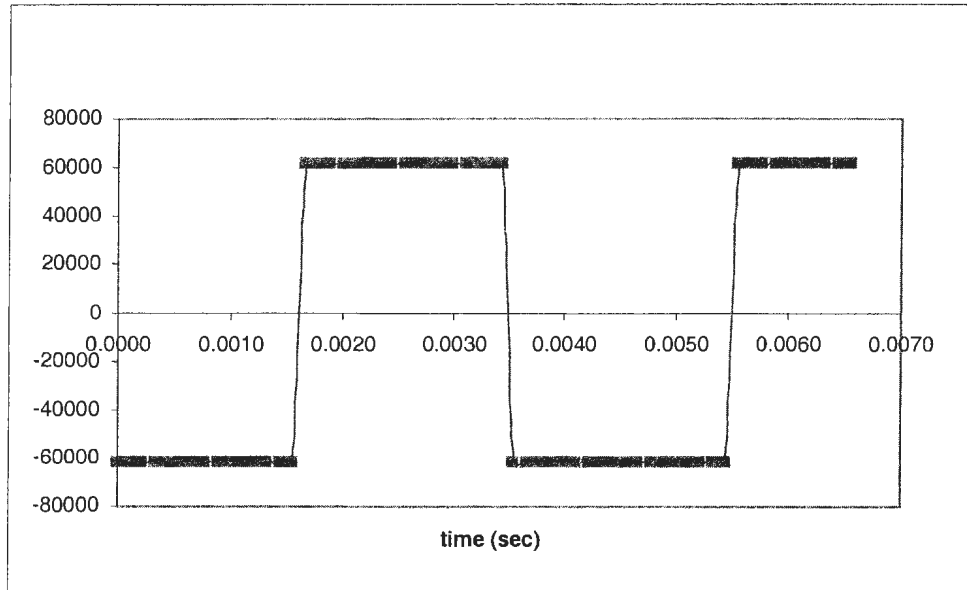


Fig 5.22 Plot of $G(x, \mu, \dot{\mu})$ function as a function of time, for fixed-fixed beam (7.62mm crack depth, center crack).

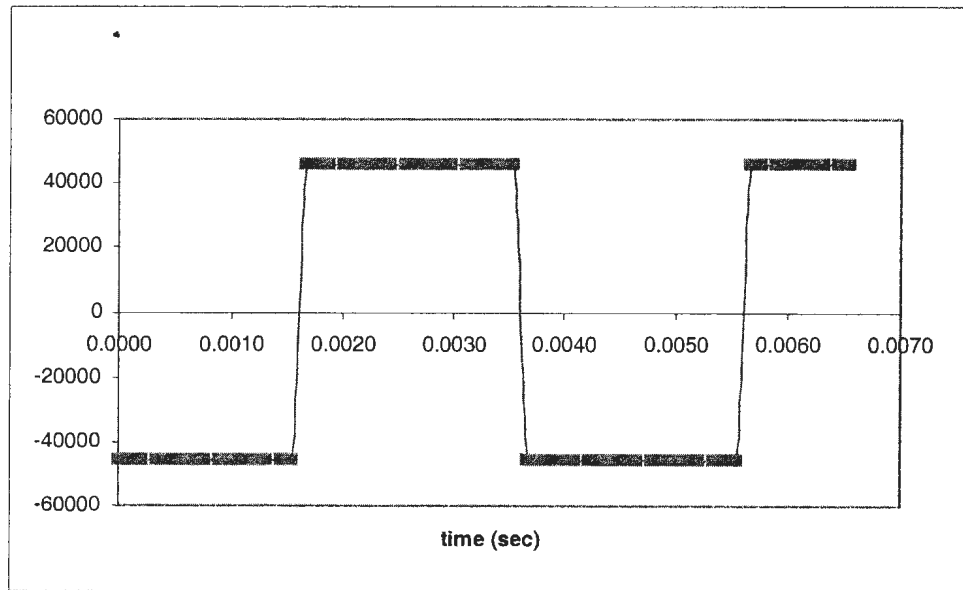


Fig 5.23 Plot of $G(x, \mu, \dot{\mu})$ function as a function of time, for fixed-fixed beam (10.16mm crack depth, center crack).

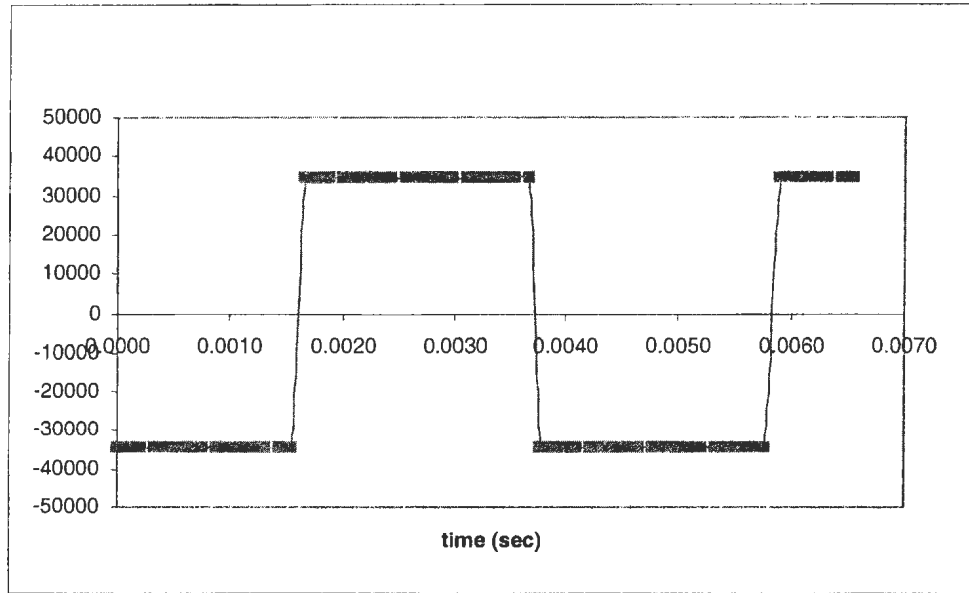


Fig 5.24 Plot of $G(x, \mu, \dot{\mu})$ function as a function of time, for fixed-fixed beam (12.70mm crack depth, center crack).

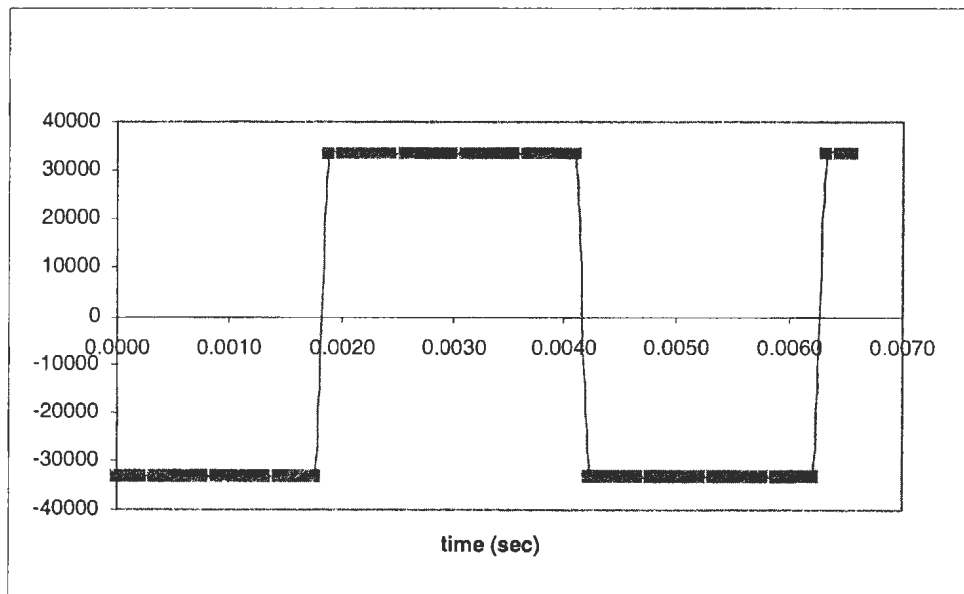


Fig 5.25 Plot of $G(x, \mu, \dot{\mu})$ function as a function of time, for fixed-fixed beam (15.24mm crack depth, center crack).

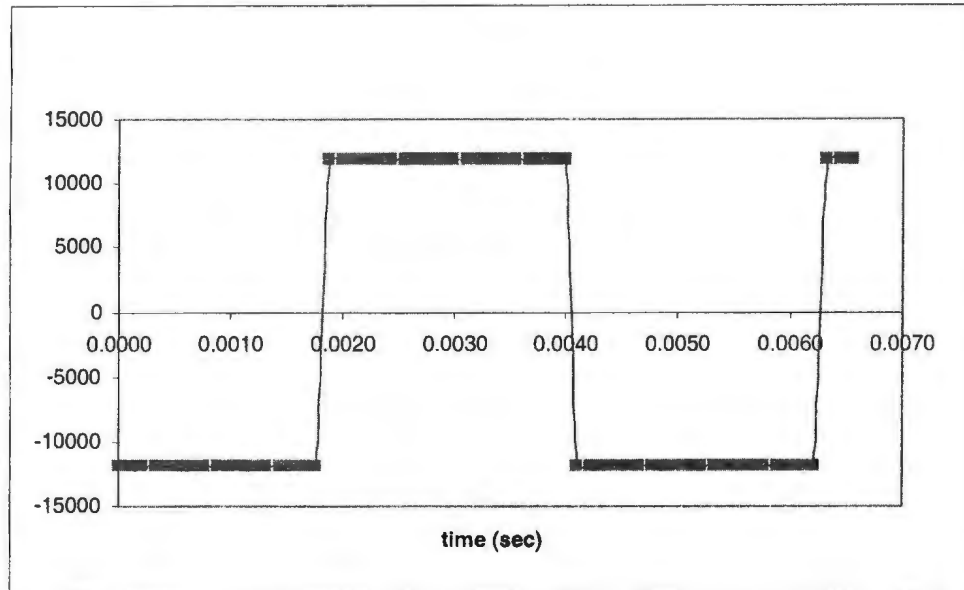


Fig 5.26 Plot of $G(x, \mu, \dot{\mu})$ function as a function of time, for fixed-fixed beam (17.78mm crack depth, center crack).

The amplitude is normalized by dividing by the highest value (the amplitude of $G(x, \mu, \dot{\mu})$ for the beam without crack), then plotted in Figure 5.27 for fixed-fixed supported beam with crack located at 1/16, 3/16, 5/16, 7/16 and 8/16 of the beam's length. Figure 5.28 shows plots of the normalized $G(x, \mu, \dot{\mu})$ amplitude for simply supported beam. Figure 5.29 presents the 3D plot of the amplitude in terms of crack location and crack length for fixed-fixed beam, while Figure 5.30 shows for the case of simply supported beam. Table 5.7 summarizes the percentage change in the amplitude of G for fixed-fixed and simply- supported beam due to the presence of a 2.54mm crack.

Table 5.5: Amplitude of $G(x, \mu, \dot{\mu})$ for different crack depths and locations on simply supported beam.

| Crack depth [mm] | Crack location from one end (L = beam's length) | | | | | |
|---------------------|---|--------|--------|--------|--------|---------|
| | 1/16 L | 3/16 L | 5/16 L | 7/16 L | 8/16 L | 11/16 L |
| No crack | 162320 | 162320 | 162320 | 162320 | 162320 | 162320 |
| 2.54 | 154400 | 134185 | 116602 | 89100 | 73369 | 98000 |
| 5.08 | 147550 | 95674 | 67092 | 47837 | 38269 | 60469 |
| 7.62 | 126779 | 72230 | 55915 | 66607 | 33541 | 66607 |
| 10.16 | 124641 | 73003 | 45441 | 55915 | 25915 | 36607 |

Table 5.6: Amplitude of $G(x, \mu, \dot{\mu})$ for different crack depths and locations on fixed-fixed beam.

| Crack depth [mm] | Crack location from one end (L = beam's length) | | | | |
|---------------------|---|--------|--------|--------|--------|
| | 1/16 L | 3/16 L | 5/16 L | 7/16 L | 8/16 L |
| No crack | 222678 | 222678 | 222678 | 222678 | 222678 |
| 2.54 | 196495 | 179982 | 179982 | 179982 | 173898 |
| 5.08 | 170221 | 141156 | 139482 | 129618 | 120879 |
| 7.62 | 168696 | 124830 | 121986 | 101538 | 61578 |
| 10.16 | 154499 | 96703 | 96442 | 55980 | 45441 |
| 12.70 | 80368 | 64295 | 41328 | 38818 | 34320 |
| 15.24 | 102960 | 72013 | 35086 | 34320 | 33541 |
| 17.78 | 72013 | 42642 | 30510 | 24024 | 23859 |

Table 5.7 Reduction in the amplitude of $G(x, \mu, \dot{\mu})$ in presence of a 1/10d crack (2.54 mm) for simply supported and fixed-fixed beam.

| Crack Location (L = beam's length) | Simply-Supported Beam (%) | Fixed-Fixed Beam (%) |
|---|--------------------------------------|---------------------------------|
| 1/16 L | 4.88 | 11.75814 |
| 3/16 L | 17.33 | 19.17387 |
| 5/16 L | 28.17 | 19.17387 |
| 7/16 L | 45.11 | 19.17387 |
| 8/16 L | 54.80 | 21.90607 |
| 11/16 L | 39.63 | Na |

5.2.2 Discussions

A number of observations can be made from these results:

- The neural network has predicted the auto-correlation function accurately. Figures 5.13 to 5.19 show good agreement between the original auto-correlation and the neural network's predictions. This shows that the network can identify the $G(x, \mu, \dot{\mu})$ function, accurately.
- The predicted $G(x, \mu, \dot{\mu})$ for all cases have the same pattern corresponding to their auto-correlation functions in terms of their dependence on time. When the period of the auto-correlation function increases, the period of the $G(x, \mu, \dot{\mu})$ also increases. It can also be seen that the magnitude of the $G(x, \mu, \dot{\mu})$ decreases consistently as the crack grows larger.

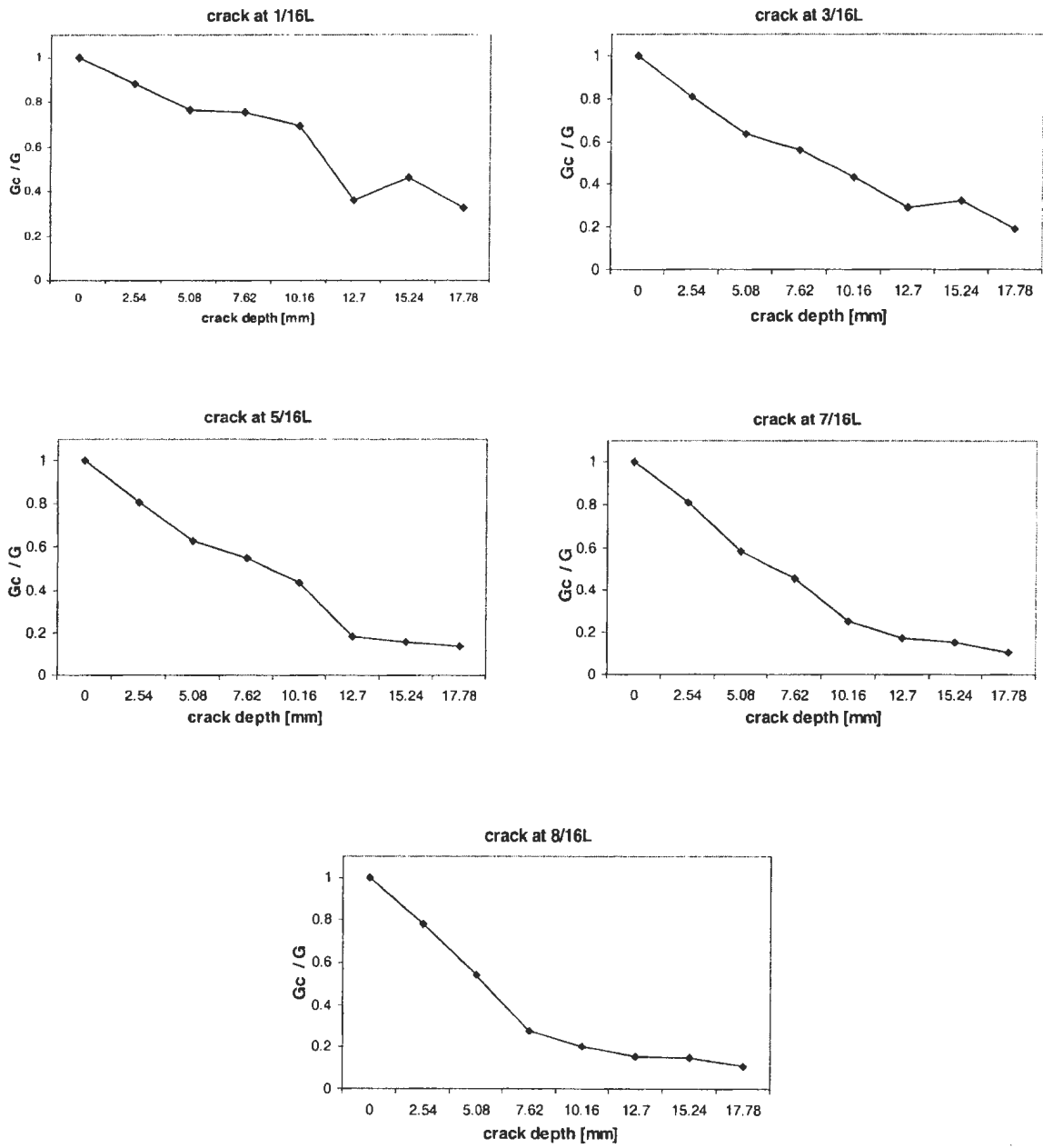


Fig 5.27 Plot of normalized $G(x, \mu, \dot{\mu})$ amplitude for fixed-fixed beam.

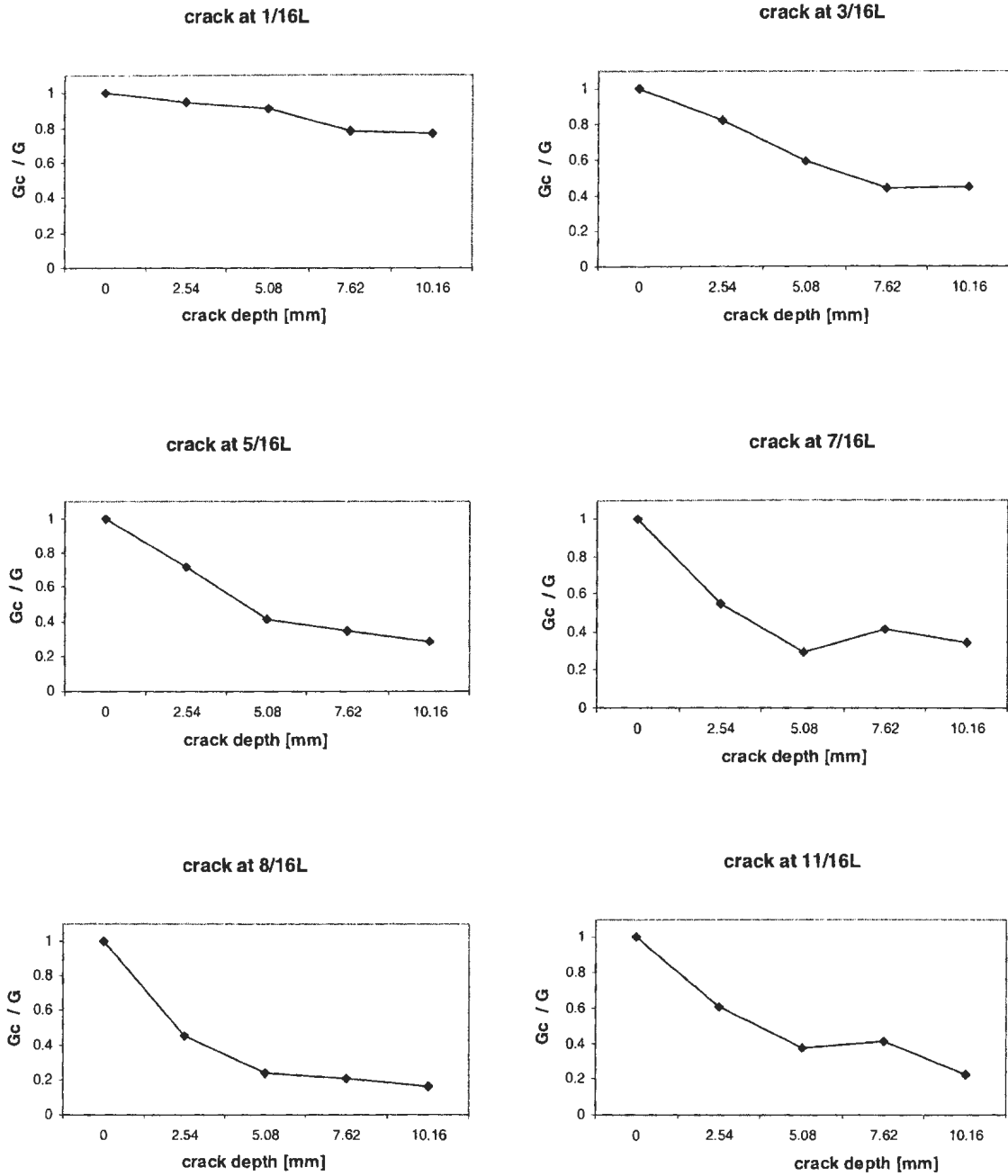


Fig 5.28 Plot of normalized $G(x, \mu, \dot{\mu})$ amplitude for simply supported beam.

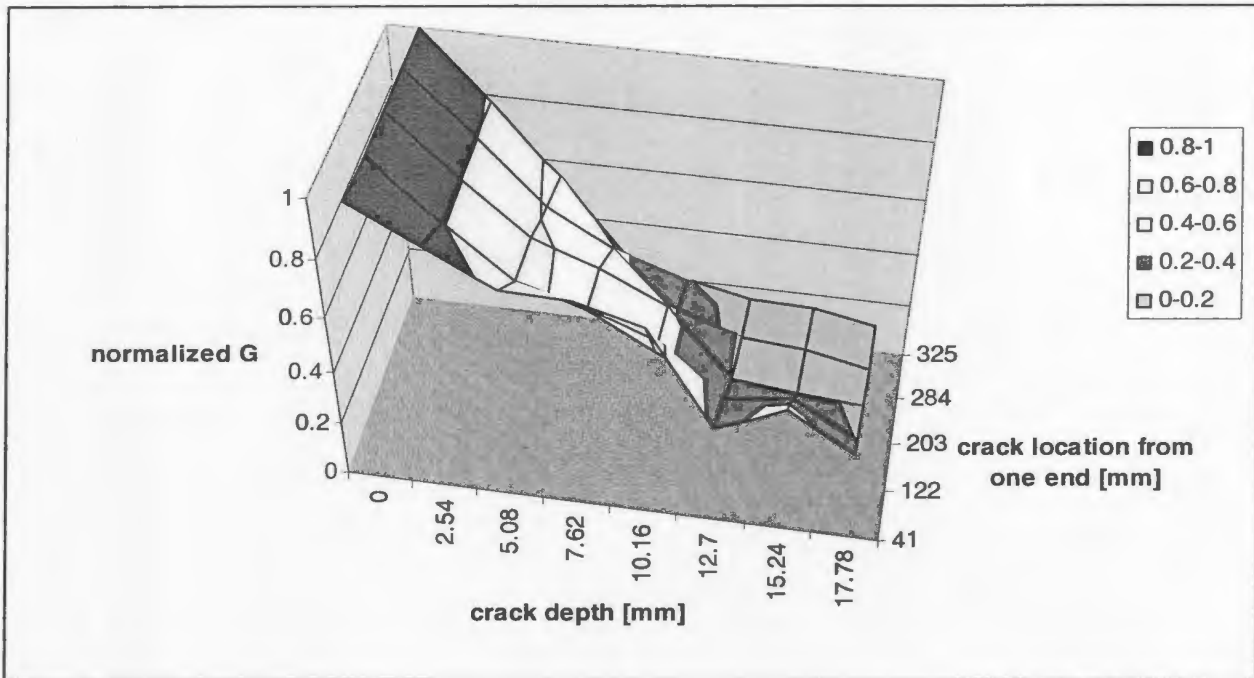


Fig 5.29 3D Plot of normalized $G(x, \mu, \dot{\mu})$ amplitude for fixed-fixed beam.

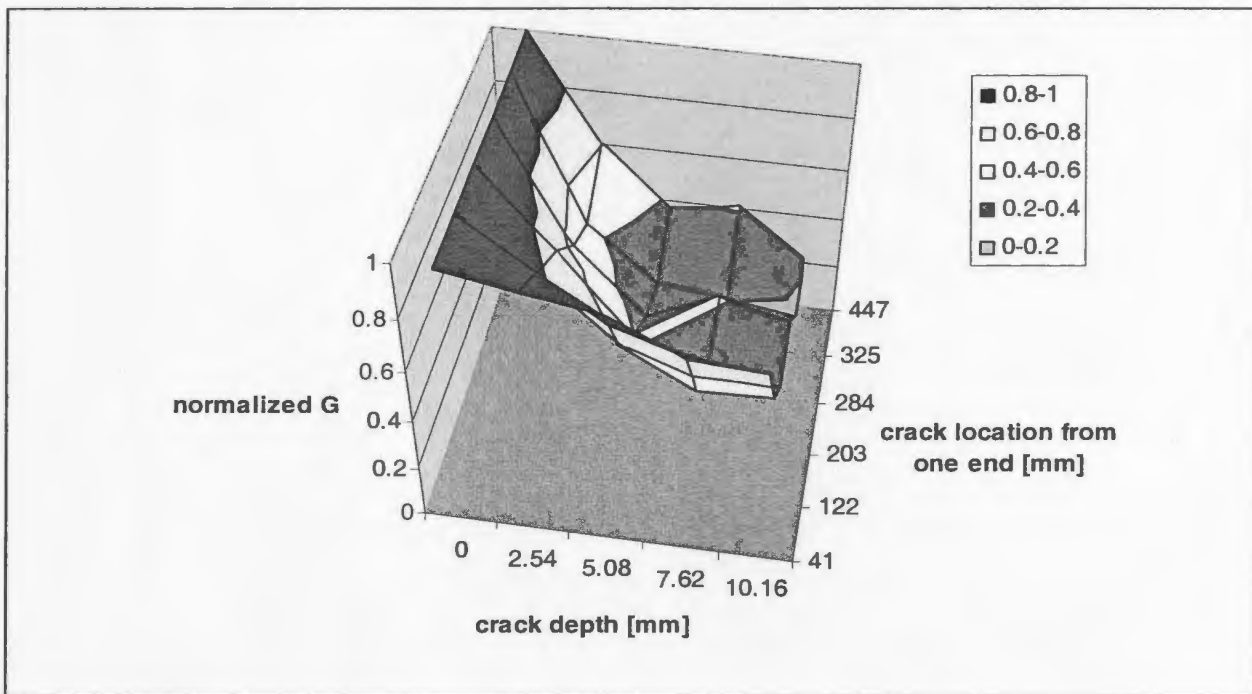


Fig 5.30 3D Plot of normalized $G(x, \mu, \dot{\mu})$ amplitude for simply supported beam.

- The change of the amplitude of $G(x, \mu, \dot{\mu})$ can be used as an indicator to identify the occurrence of a crack. This amplitude decreases significantly and consistently as the crack grows larger. This applies for both simply supported and fixed-fixed beam for a crack at any location.
- The amplitude of G is a function of the crack depth. The amplitude decreases as the crack depth increases. For the fixed-fixed support, the percentage decrease in the amplitude takes the values of 11.7% to 89.3% for crack depths 2.54mm to 17.78mm, respectively. For the simply supported, the percentage decrease in the amplitude of G is 4.8% to 84% for crack depths of 2.54mm to 10.16mm, respectively.
- These results lead us to conclude that the value of the amplitude of the function can be used as an indicator for the occurrence of a crack. The changes in the amplitude of G are much more significant than the corresponding changes in the natural frequency. G is a nonlinear function of both the natural frequency and the damping coefficient. This makes the amplitude of G sensitive to the occurrence of cracks.

5.2.3 Multivariate Linear Regression

A multivariate regression is performed to study the experimental results as a model for crack identification using $G(x, \mu, \dot{\mu})$. The regression analysis is performed using Minitab software. A multivariate regression analysis will explore the relationship

between a response variable and several independent variables from the available data. The amplitude of $G(x, \mu, \dot{\mu})$ is used as the response variable, while crack locations and depths are the independent variables. Table 5.8 and 5.9 summarize the results of the analysis for both models.

Table 5.8: Summary output for fixed-fixed beam.

| <i>Regression Equation</i> | |
|---|--|
| $G(x, \mu, \dot{\mu}) = -10368.1 * crackdepth - 182.4 * cracklocation + 239819.9$ | |

| <i>Residuals Statistics</i> | |
|-----------------------------|---------|
| Multiple R | 95.50 % |
| R Square | 91.19 % |
| Adjusted R Square | 90.72 % |

Table 5.9: Summary output for simply supported beam.

| <i>Regression Equation</i> | |
|--|--|
| $G(x, \mu, \dot{\mu}) = -9637.64 * crackdepth - 148.03 * cracklocation + 180030.6$ | |

| <i>Residuals Statistics</i> | |
|-----------------------------|---------|
| Multiple R | 85.40 % |
| R Square | 72.93 % |
| Adjusted R Square | 70.92 % |

The residual square values from the output regression analysis, 91% for fixed-fixed beam and 73% for simply supported beam, show the goodness of fit obtained from the regression models. The numbers mean that the model would represent at least 91%

and 73% of the experimental data points, for the fixed-fixed beam and simply supported beam, respectively. This shows that the multivariate regressions have successfully modeled the experimental results on the particular beam models. Using the equation from the multivariate regression output, the amplitudes of $G(x, \mu, \dot{\mu})$ are predicted and plotted as functions of crack depth and location. Figure 5.31 to 5.34 show the amplitude of $G(x, \mu, \dot{\mu})$ and the predicted value corresponding to the crack depths and locations for both fixed-fixed and simply supported beam. The figures show excellent agreement between the amplitudes of $G(x, \mu, \dot{\mu})$ and the predicted values correspond to the crack depths and locations. This brings the conclusion that the equations can be used to identify and predict an occurrence of a crack in beam for particular beam models used in this experiment.

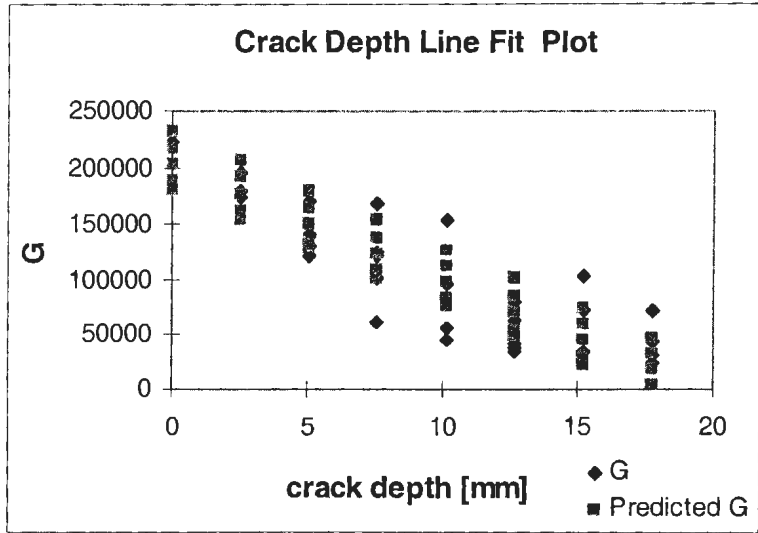


Figure 5.31 Plot of amplitude G and the predicted value versus crack depth for fixed-fixed beam.

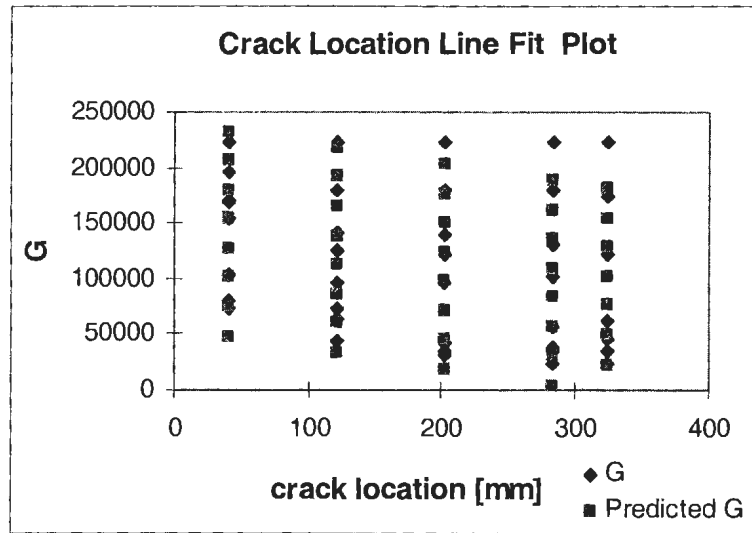


Figure 5.32 Plot of amplitude G and the predicted value versus crack location for fixed-fixed beam

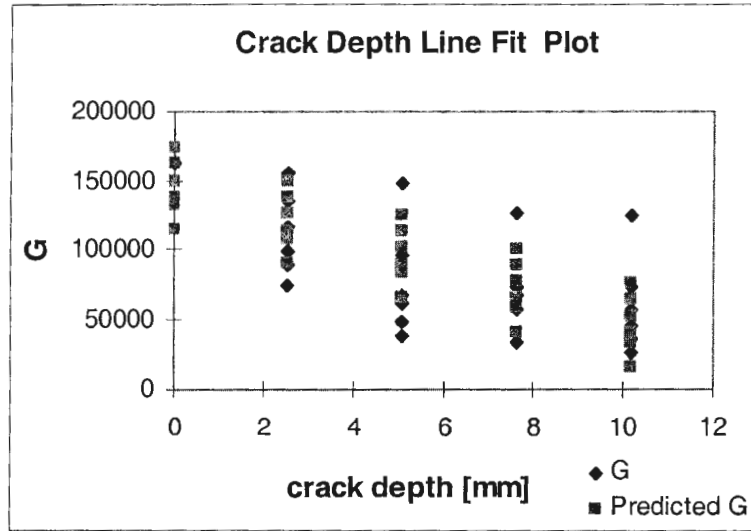


Figure 5.33 Plot of amplitude G and the predicted value versus crack depth for simply supported beam.

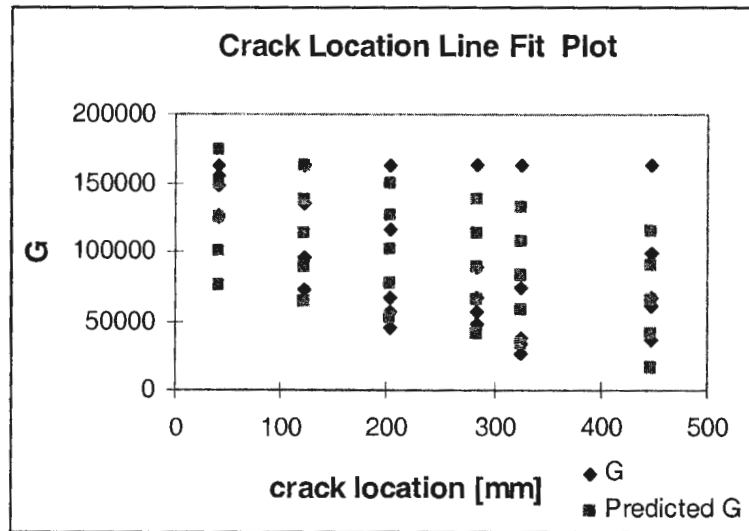


Figure 5.34 Plot of amplitude G and the predicted value versus crack location for simply supported beam

CHAPTER 6

CONCLUSIONS AND RECOMMENDATIONS

6.1 Conclusions

The main objective of this study is to develop a methodology for the identification of crack inception in structures. The study is comprised of two components: experimental and analytical. In the experimental study, two beam models were used: a simply supported model and a fixed-fixed model. The models were made out of aluminum and cracks of different depths and at different locations on the models were

made using a saw blade. The stationary response of a beam model subjected to a random excitation was measured in each case. The auto-correlation function was obtained from the stationary random response. The analytical study was performed to check the experimental results. The natural frequencies of the models were obtained using exact solution formulation and finite element technique. Two indicators were considered for the detection of crack inception: the change in the natural frequency and the change in the amplitude of a function, G . G is a nonlinear function of the natural frequency and the damping of the system. The function G was obtained using a neural network technique.

The results of this study show that:

1. The auto-correlation function of the random response of structures proved to be a powerful tool to estimate the free vibration of structures when the excitation is a white noise, stationary, Gaussian process. The auto-correlation function can be used to predict the natural frequency accurately. The process is simple and can be performed on the structure during normal operation (on-line mode). The prediction of the natural frequency has been verified using results from the exact solution and finite element analysis. The verification shows an excellent agreement between the experimental and the analytical results.
2. The natural frequency decreased consistently as a crack occurred and grew larger. The reduction depends on the crack depth ratio and the location of the crack. The maximum decrease occurs when the crack is located at the center

of the beam. This applies both for the simply supported and the fixed-fixed beam. This can be explained by the fact the stiffness of the beam would decrease most when the crack located at the point of highest deflection.

3. The change in values of the natural frequency of the model as the result of crack occurrence is not appreciable. The changes are within the experimental error limits. Thus, a change in the natural frequency cannot be used as a reliable indicator in detecting crack inception and growth.
4. The amplitude of the function G changes appreciably as a crack occurs and grows. The amplitude of the function G can be used as a reliable indicator for crack occurrence and growth.
5. A multi-variable regression analysis was used to obtain the relationship between crack depth and the function G , and the crack location. The results show that this relationship is reliable.

6.2 Recommendations

The present study has demonstrated the use of auto-correlation function in predicting natural frequency and the use of neural networks in predicting $G(x, \mu, \dot{\mu})$ for identifying crack inception. The results of the study were verified using the exact solution and the finite element method. The regression analysis models the experimental

results and studies the correlation for each independent variable to the experiment results.

The following recommendations are drawn for future studies:

- (a) Another experiment can be conducted using more complicated type of structure to ensure that the technique developed in this study could be applied in the field.
- (b) To verify the effectiveness of the technique in the field, it is also suggested to use random excitation that close to the field conditions, such as excitations from wave generator in a wave basin. An experiment using a model scale conducted in wave basin is recommended.
- (c) A more detailed study about the characteristics and behaviour of the $G(x, \mu, \dot{\mu})$ function as a parameter of damage identification would be a benefit before applying the technique in industry.
- (d) Developing more advanced neural network algorithm based on the equation of motion that can identify not only the crack inception, but also its extent and location accurately. It is recommended to train the network using data obtained from finite element analysis on the structure for a number of locations and depths of crack.

References

1. Adams, R. D., Walton, D., Flitcroft, J. E., and Short, D., 1975. "Vibration Testing as a Non-destructive Test Tool for Composite Materials". Composite Reliability, ASTM STP 580 1975 (Amer. Soc. For Testing and Mtls.), pp. 159-175.
2. Alexander, I., and Morton, H., 1990. "An Introduction to Neural Computing". Chapman and Hall, ISBN 0 412 37780 2.
3. Allemang, R.J., and Brown, D.L, 1996. "Modal Analysis and Testing ", Shock and Vibration Handbook, Fourth Edition, McGraw-Hill inc.
4. Barai, S.V., and Pandey, P.C., 1995. "Vibration Signature Analysis using Artificial Neural Networks". Journal of Computing in Civil engineering, Vol. 9, No. 4, pp. 259-265.
5. Bruel & Kjaer Inc., 1987. "Instruction Manual of B & K 2034 Dual Channel Signal Analyzer". Vol. 1, 2, 3.
6. Cawley, P., and Adams, R.D., 1979. "The Location of Defects in Structures from Measurements of Natural Frequencies". Journal of Strain Analysis, Vol 14, No. 2, pp. 49-57.
7. Cole, H. A., 1971. "Failure Detection of a Space Shuttle wing Flutter Model by Random Decrement". NASA TMX-62, 041.
8. Cole, H.A., 1973. "On-line Failure Detection and Damping Measurement of Aerospace Structures by Random Decrement Signatures". NASA CR-2205.

9. Chen, F.L., and Xu, T.X., 1999. "Dynamic Behaviour of a Clamped Plastic Beam with Cracks at Supporting Ends Under Impact". *Journal of Pressure Vessel Technology*, Vol. 121, pp. 406-412.
10. Chong-Won Lee, Jong-Seop Yun and Oh Sung Jun, 1992. "Modeling of a Simple Rotor with a Switching Crack and Its Experimental Verification". *Journal of Vibration and Acoustics*, Vol. 114, pp. 217-225.
11. Cramer, E.H., Loseth, R., and Bitner-Gregersen, E., 1993. "Fatigue in Side Shell Longitudinal Due to External Wave Pressure". *Safety and Reliability Proceedings of the International Conference on Offshore Mechanics and Arctic Engineering (OMAЕ)*, Vol. 2, pp. 267-272.
12. Chiang, D.Y., and Lai, W.Y., 1999. "Structural Damage Detection using the Simulated Evolution Method". *American Institute of Aeronautics and Astronautics Journal*, Vol. 37, No. 10, pp. 13331-3.
13. DeSilva, C. W., 1999. "Vibration: Fundamentals and Practice", CRC Press.
14. Dimarogonas, A. D., 1970. "Dynamic Response of Cracked Rotors". General Electric Co., Schenectady NY.
15. Doyle, J.F., 1995. "Determining the Size and Location of Transverse Cracks in Beams". *Journal of Experimental Mechanics*, Vol. 35, pp. 272-80.
16. Doebling, S. W., Farrar, C. R., Prime, M. B. and Shevitz, D. W., 1996. "Damage Identification and Health Monitoring of Structural and Mechanical Systems from Changes in Their Vibration Characteristics: A Literature Review". Los Alamos National Laboratory Report LA-13070-MS.

17. Ewins, D.J., 1996. "Modal Testing: Theory and Practice". Research Studies Press Ltd, England.
18. Elkordy, M.F., 1992. " Application of Neural Networks in Structural damage Diagnosis and Condition Monitoring". Dissertation, Faculty of Graduate School of State University of New York, Buffalo.
19. El Dannah, E.H., and Farghaly, S.H., 1994. "Natural Vibrations of Cracked Shafts Carrying Elastically Mounted End Masses". Journal of Sound and Vibration, Vol. 170 (5), pp. 607-620.
20. Friswell, M. I., Penny, J. E. T. and Wilson, D. A. L., 1994. "Using Vibration Data and Statistical Measures to Locate Damage in Structures". Modal Analysis: The International Journal of Analytical and Experimental Modal Analysis, 9(4), 239-254.
21. Haddara, M.R., 1992. " On the Random Decrement for Nonlinear Rolling Motion". Proceedings of the Eleventh International Conference on Offshore Mechanics and Arctic Engineering, Vol. 11, Safety and reliability, pp. 321-324.
22. Haddara, M.R., 1995. " On the Use of Neural Network Techniques for the Identification of Ship Stability Parameters at Sea". Proceedings of the Fourteenth International Conference on Offshore Mechanics and Arctic Engineering, Vol. II, Safety and Reliability, pp. 127-135.
23. Haddara, M.R., and Xu, J., 1998. " On the Use of Random Decrements in the Identification of Two Degrees of Freedom Systems". Proceedings of CSME Forum, Vol. 4, pp. 499-507.

24. Hamidi, L., Piaud, J.B., and Massoud M., 1992. "A Study of Cracks Influence on the Modal Characteristics of Rotors". Paper C432/066, I. Mech. E. Conference, Vibrations in Rotating Machinery.
25. Hearn, G., and Testa, R.B., 1992. "Modal Analysis for Damage Detection in Structures". Journal of Structural Engineering, Vol 117, No. 10, pp. 3042-3063.
26. Ibrahim, S. R., 1977. "Random Decrement Technique for Modal Identification of Structures". The AIAA Journal of Space Craft and Rockets, Vol. 14, No. 11, pp. 696-700.
27. Imam, I., Azzaro, S.H., Bankert, R.J., and Scheibel, J., 1989. "Development of an On-Line Rotor Crack Detection and Monitoring System". Journal of Vibration, Acoustics, Stress, and Reliability in Design, July, V.111, pp. 241-250.
28. Idichandy, V.G, Ganapathy, C., and Srinivasa Rao, P., 1990. "Structural Integrity Monitoring of Fixed Offshore Platform". Experimental Mechanics, December.
29. Iwatsubo, T., and Oks, A., 1992. "Detecting of a Transverse Crack in a Rotor Shaft by Adding External Force". Paper C432/093, I. Mech. E. Conference, Vibrations in Rotating Machinery.
30. Juneja, V., Haftka, R.T., and Cudney, H.H., 1997. "Damage Detection and Damage Detectability-Analysis and Experiments". Journal of Aerospace Engineering, Vol. 10, No. 4, pp. 135-142.
31. Kosmatka, J.B., and Ricles, J.M., 1999. "Damage Detection in Structures by Modal Vibration Characterization." Journal of Structural Engineering, vol. 125, No. 12, pp. 1384-1392.

32. Liao, M. and Gasch, R., 1992. "Crack Detection in Rotating Shafts - an Experimental Study". Paper C432/106, I. Mech. E. Conference, 1992, Vibrations in Rotating Machinery.
33. Liew, K.M., and Wang, Q., 1998. " Application of Wavelet Theory for Crack Identification in Structures". Journal of Engineering Mechanics, Vol. 124, No. 2, pp. 152-157.
34. McConnell, K. G., 1995. " Vibration Testing: Theory and Practice". J. Wiley.
35. Owolabi, G. M., 2001. "Crack Identification Procedures In Beams Using Experimental Modal Analysis". Theses (M. Eng), Faculty of Engineering and Applied Science, Memorial University of Newfoundland.
36. Pappa, R.S., Doebling, S. W., and Kholwad, T.D, 2000. " On-Line Database of Vibration-Based Damage Detection Experiments". Sound and Vibration, January, pp. 28-33.
37. Qian, G. L., Gu, S.N., and Jiang, J.S., 1990. " The Dynamic Behavior and Crack detection of a Beam with a Crack". Journal of Sound and Vibration, Vol. 138, No. 2, pp. 233-243.
38. Rytter, A., Krawczuk, M., and Kirkegaard, P.H., 2000. "Experimental and Numerical Study of Damaged Cantilever". Journal of Engineering Mechanics, Vol 126, No. 1, pp. 60-65.
39. Rajab, M.D. and Al-Sabeeh, A., 1991. "Vibrational Characteristics of Cracked Shafts". Journal of Sound and Vibration, Vol. 147 (3), pp. 465-473.
40. Sekhar, A. S. and Prabhu, B. S., 1992. "Crack Detection and Vibration Characteristics of Cracked Shafts". Journal of Sound and Vibration, Vol. 157 (2), pp. 375-381.

41. Shen, M.H.H., and Pierre, C., 1990. "Natural Modes of Bernoulli-Euler Beams with Symmetric Cracks". *Journal of Sound and Vibration*, Vol. 138 (1), pp. 115-134.
42. Sharivar, F. Bouwkamp, 1986. "Damage detection in offshore platforms using vibration information". *ASME symposium on Offshore Mechanics and Arctic Engineering*, pp 174-185.
43. Sundstrand Data Control Inc., 1972. "Instruction Manual for Load Cells, Series Model 912 (X) and Model 922 (X).
44. Thompson, W.T., 1993. "Theory of Vibration with Applications" Fourth Editions, Prentice Hall.
45. Vandiver, J. K., 1975, "Detection of Structural Failure on Fixed Platforms by Measurement of Dynamic Response". *Proceedings, Offshore Technology Conference, OTC 2267, Houston, Texas.*
46. Vandiver, J. K., 1977, "Detection of Structural Failure on Fixed Platforms by Measurement of Dynamic Response". *Journal of Petroleum Technology*, March, pp. 305-310.
47. Vandiver, J. K., Dunwoody, A. B., and Campbell, R. B., 1982. " A Mathematical Basic for the Random Decrement Vibration Signature Analysis Technique ". *Journal of Mechanical Design*, Vol. 104, pp. 307-313.
48. Yang, J. C. S., and Caldwell, D. W., 1976. " The Measurement of Damping and The Detection of Damages in Structures by the Random Decrement Technique", *46th Shock and Vibration Bulletin*, pp. 29-36.

49. Yang, J. C. S., Dagalakis, N. G., and Hirt, M., 1980. "Application of the Random Decrement Technique in the Detection of Induced Cracks on an Offshore Platform Model in Computational Methods for Offshore Structures". ASME, AMD, Vol. 37.
50. Yang, J. C. S., Chen, J., and Dagalakis, N. G., 1984. "Damage Detection in Offshore Structures by the Random Decrement Technique ". Journal of Mechanical Design, March, Vol. 106, pp. 38-42.
51. Qian, G.L., Gu S.N., and Jiang, J.S., 1990. "The Dynamic Behaviour and Crack Detection of a Beam with a Crack". Journal of Sound and Vibration, Vol. 138 (2), pp. 233-243.
52. Wauer, J., 1990. "On the Dynamics of Cracked Rotors: A Literature survey". Application Mechanics Review, Jan, V.43 (No. 1), pp. 13-17.
53. Zubaydi, A., Haddara, and M.R., Swamidas, A.S.J., 1999. "Damage Identification in Stiffened Plates Using the Random Decrement Technique". Proceedings of the 5th Canadian Marine Hydromechanics, and Structures Conference, St. John's, Canada.
54. Zubaydi, A., Haddara, M.R., and Swamidas, A.S.J., 2000. "Random Decrement Technique for Damage Identification of Stiffened Plates". Proceedings of the 18th International Modal Analysis Conference, San Antonio, Texas, USA.
55. Zubaydi, A., 2001. "Use of Neural Networks for the Identification of Damage in Ship Structures". Dissertation, School of Graduate Studies, Faculty of Engineering and Applied Science, Memorial University of Newfoundland.
56. Zhao, J., and DeWolf, J.T., 1999. "Sensitivity Study for Vibrational Parameters Used in Damage Detection". Journal of Structural Engineering. Vol. 125, No. 4, pp. 410-416.

APPENDIX A

NEURAL.FOR

```
* Input layer weight--->wi
* Output layer weight-->wo
* Suspension inputs---->ri
* Suspension outputs--->ro
* Middle layer outputs->rm
* Natural frequency---->rr
* Time end & time step-->tend & deltt
* Middle layer neurons-->Net
* Number of inputs----->kin
* Number of outputs----->kon
* variation of data points--> rate
* # of iterations:kit, and Counter for iterations: it
* Logical IF operator mig
* Natural roll Frequency rr
* If statment condition for RM(i) - power
* Weight manipulator del
* Number of input velocities,and angles data npoint
* Use old or new weights CHOICE (choice < 0 old, choice > 0 new)
* Declare variables
  implicit real*8 (a-z)
  integer i,j,count1,kin,kon,net,met,jf
  integer npoint,mf,mig,kit,it,nfiles
  character*20 ff,ff1
  dimension timer2(2500),result3(2500),sense(25000)
  dimension res1(2500),res2(2500)
  common/block1/ met,net,kin,kon,big,choice,power,del,rr,tend,
*   deltt,time,count1,mig,wig,wrong,yi(2),wo(15,15),wi(15,15),rm(15)
*   ,ri(15),ro(15),kl(2),k2(2),k3(2),k4(2),rsim(2500,4),
*   result1(2500),result2(2500),oo(15,15,15),oi(15,15,15)

* input constants and initial variable values
  open(1,file='initial.d',status = 'old')
  read(1,*) rate,big,wig,mig,power,del
  read(1,*) net,kin,kon
  read(1,*) deltt,tend,kit
  read(1,*) choice,ddel
  close(1)
  print *, ' rate:?????:',rate
  print *, '# of Middle layer neurons: net = ',net
  print *, 'Number of inputs:kin = ',kin
  print *, 'Number of outputs:kon = ',kon
  print *, 'Total time ',tend,'and time step',deltt
  print *, 'big',big,'wig',wig
  print *, '# of iterations:',kit,'Counter for iterations: it'
  print *, 'Logical IF operator mig: ',mig

  print *, 'If statment condition for RM(i): power = ',power
  print *, 'Weight manipulator: del = ',del

  print *, 'Use old or new wieghts(choice > 0 old, choice < 0 new)'
```

```

print *, 'choice = ',choice
open(1,file='data.d',status = 'old')
write(1,*)' rate:?????:',rate
write(1,*)'# of Middle layer neurons: net = ',net
write(1,*)'Number of inputs:kin = ',kin
write(1,*)'Number of outputs:kon = ',kon
write(1,*)'Total time ',tend,'and time step',delt
write(1,*)'big',big,'wig',wig
write(1,*)'# of iterations:',kit,'Counter for iterations: it'
write(1,*)'Logical IF operator mig: ',mig

write(1,*)'If statment condition for RM(i): power = ',power
write(1,*)'Weight manipulator: del = ',del

write(1,*) 'choice = ',choice
close(1)
* input weight inputs and outputs
met = net + 1
open(1,file='filenames.txt', status = 'old')
read(1,*) nfiles
do jf = 1, nfiles
    read(1,*) ff
    ff1 = trim(ff) // ".d"

* input structure natural frequency and freq rate
open(2, file= ff1 ,status = 'old')
read(2,*) rr, npoint
npoint = 60
do count1 = 1,npoint
    read(2,*) dummy,rsim(count1,1),rsim(count1,2)

end do
close(2)
do count1 = 1, npoint
    rsim(count1,2) = rsim(count1,2)
end do
print *, 'Natural Frequency rr',rr
print *, 'Number of input velocities, and angles data = ',npoint
it = 1
crit = 1
sense(it) = 1
do while (it.lt.kit)
* loops to end of program
* do while (crit.gt.ddel )
time = 0.d0
count1 = 1
deep = 0.d0
result1(1) = rsim(1,1)
result2(1) = rsim(1,2)

mf = 2
do while(time .lt. tend)

```

```

* call Middle layer and net output subroutine
    ri(1) = result1(mf-1)
    ri(2) = result2(mf-1)

    ri(kin) = 1.d0
    call mid_net_out
    call runge
    result3(mf - 1) = ro(1)
    mf = mf + 1
    result1(mf-1)= ri(1)
    result2(mf-1)= ri(2)
    count1 = count1 + 1
    wrong = ri(1) - rsim(count1,1)

    if (mig.eq.0) then
        deep = deep + wrong**2
    else if (mig.eq.1) then
        deep = deep + DABS(wrong)
    end if
* do while time < tend loop ends
    end do

    it = it + 1
    Sense(it) = sqrt(deep)/npoint
    crit = sense(it)/rsim(1,1)
    write(*,*) it,sense(it), crit
    call wi_oi(result3)
    call wo_oo(timer2,result3)
    call corcalc(cor,rate)
    if (it > kit) then
        go to 3
    else if (it < kit) then
        go to 5
    end if

* do while it < kit loop ends
5    end do
3    call results(npoint,timer2,result3,sense,kit,ff,ff1)
    end do
    close (1)
    end

subroutine intweight
implicit real*8 (a-z)
integer met,net,kin,kon,i,j,count1
integer mig
integer*4 iseed
character*30 string,string1
common/block1/ met,net,kin,kon,big,choice,power,del,rr,tend,
*   delt,time,count1,mig,wig,wrong,yi(2),wo(15,15),wi(15,15),rm(15)
*   ,ri(15),ro(15),k1(2),k2(2),k3(2),k4(2),rsim(2500,4),
*   result1(2500),result2(2500),oo(15,15,15),oi(15,15,15)
If (choice.GE.0) Then

```

```

open(1,file='weights.d',status='old')
  read(1,5) string
5     format(a)
      do 20 j = 1,met
      do 20 i = 1,kon
          read (1,*) wo(j,i)
20     continue
      read(1,15) string1
15     format(a)
      do 30 j = 1,net
      do 30 i = 1,kin
          read (1,*) wi(j,i)
30     continue
      close(1)
  else
* initialize random layer weight input and output
      iseed = 123457
      do 40 j = 1,met
      do 40 i = 1,kon
          gwo = RAN(iseed)*big
          wo(j,i)=gwo
40     continue
*
      do 50 j = 1,net
      do 50 i = 1,kin
          gwo = ran(iseed)*big
          wi(j,i) = gwo
50     continue
  end if
  return
end

subroutine mid_net_out
implicit real*8 (a-z)
integer i,j,net,met,kin,kon,count1
integer mig
common/block1/ met,net,kin,kon,big,choice,power,del,rr,tend,
* deltt,time,count1,mig,wig,wrong,yi(2),wo(15,15),wi(15,15),rm(15)
* ,ri(15),ro(15),k1(2),k2(2),k3(2),k4(2),rsim(2500,4),
* result1(2500),result2(2500),oo(15,15,15),oi(15,15,15)
* middle layer output

      do 60 i = 1,net
      rm(i) = 0.d0
      do 70 j = 1,kin
          rm(i)= rm(i) + wi(i,j)*ri(j)
70     continue
      if(rm(i).ge.power) then
          rm(i)=1.0d0/(1.0d0+dexp(-rm(i)))
      else if(rm(i).lt.power) then
          rm(i)=0.d0
      end if

```

```

        rm(i) = 2.d0*(rm(i)- 0.5d0)
60      continue
        rm(met)=1.0d0
* net ouput calculation
        do 80 i=1,kon
            ro(i)= 0.d0
        do 80 j=1,met
            ro(i)= ro(i) + wo(j,i)*rm(j)
80      continue
        return
        end

```

```

Subroutine runge
implicit real*8 (a-z)
integer n,i,net,met,kin,kon,count1
integer mig
common/block1/ met,net,kin,kon,big,choice,power,del,rr,tend,
* del,t, time,count1,mig,wig,wrong,yi(2),wo(15,15),wi(15,15),rm(15)
* ,ri(15),ro(15),k1(2),k2(2),k3(2),k4(2),rsim(2500,4),
* result1(2500),result2(2500),oo(15,15,15),oi(15,15,15)

n = 2
ti = time
do 90 i = 1,n
    yi(i) = ri(i)
90  continue

    rslt = - rr**2* ri(1) - ro(1)
    k1(1) = del*t*ri(2)
    k1(2) = del*t*rslt
do 100 i = 1,n
    ri(i) = yi(i) + k1(i)/2.d0
100 continue
    call mid_net_out
    time = ti + del*t/2
    rslt = - rr**2*ri(1) - ro(1)
    k2(1) = del*t*ri(2)
    k2(2) = del*t*rslt
do 150 i = 1,n
    ri(i) = yi(i) + k2(i)/2.d0
150 continue
    call mid_net_out
    rslt = -rr**2* ri(1) - ro(1)
    k3(1) = del*t*ri(2)
    k3(2) = del*t*rslt
do 120 i = 1,n
    ri(i) = yi(i) + k3(i)
120 continue
    call mid_net_out
    time = ti + del*t
    rslt = -rr**2* ri(1) - ro(1)
    k4(1) = del*t*ri(2)

```

```

        k4(2) = delt * rslt
        do 130 i = 1, n
        ri(i)= yi(i) + (k1(i) +2.d0*(k2(i) + k3(i))
*           + k4(i))/6.d0
130      continue
        call mid_net_out
        return
        end

subroutine corcalc(cor,rate)

implicit real*8 (a-z)
integer n,i,net,met,kin,kon,count1
integer mig
common/block1/ met,net,kin,kon,big,choice,power,del,rr,tend,
*  delt,time,count1,mig,wig,wrong,yi(2),wo(15,15),wi(15,15),rm(15)
*  ,ri(15),ro(15),k1(2),k2(2),k3(2),k4(2),rsim(2500,4),
*  result1(2500),result2(2500),oo(15,15,15),oi(15,15,15)

do i = 1,kon
do j = 1,met
cor = (oo(j,i,1)-oo(j,i,2))/2.d0/del
wo(j,i) = wo(j,i) - cor*rate
end do
end do
do i = 1,kin
do j = 1,net
cor = (oi(j,i,1)-oi(j,i,2))/2.d0/del
wi(j,i) = wi(j,i) - cor*rate
end do
end do
return
end

subroutine wi_oi(result3)
implicit real*8 (a-z)
integer n,i,net,met,kin,kon,count1,ii,jj,kk
integer mig
dimension result3(2500),result4(2500),result5(2500)
*  ,result6(2500),res1(2500),res2(2500)
common/block1/ met,net,kin,kon,big,choice,power,del,rr,tend,
*  delt,time,count1,mig,wig,wrong,yi(2),wo(15,15),wi(15,15),rm(15)
*  ,ri(15),ro(15),k1(2),k2(2),k3(2),k4(2),rsim(2500,4),
*  result1(2500),result2(2500),oo(15,15,15),oi(15,15,15)

do 999 jj = 1,net
do 999 ii = 1,kin
wi(jj,ii) = wi(jj,ii)+del
do 888 kk=1,2
oi(jj,ii,kk)=0.d0
time = 0.d0
count1 = 1
result5(1) = rsim(1,2)

```

```

result4(1) = rsim(1,1)

mf = 2
do while(time .lt. tend)
ri(1) = result4(mf-1)
ri(2) = result5(mf-1)

ri(kin) = 1.d0
call mid_net_out
call runge
result6(mf - 1) = ro(1)
mf = mf + 1
result4(mf-1)= ri(1)
result5(mf-1)= ri(2)
count1 = count1 + 1
wrong = ri(1) - rsim(count1,1)
wrong = wrong/wig
if (mig.eq.0) then
oi(jj,ii,kk)=oi(jj,ii,kk)+wrong**2
else if (mig.eq.1)then
oi(jj,ii,kk)=oi(jj,ii,kk)+DABS(wrong)
end if
* end of do while TIME loop
end do
wi(jj,ii)=wi(jj,ii)-2.d0*del
888 continue
wi(jj,ii)=wi(jj,ii)+del
999 continue
return
end

subroutine wo_oo(timer2,result3)
implicit real*8 (a-z)
integer n,i,net,met,kin,kon,count1,ii,jj,kk
integer mig
dimension timer2(2500), result3(2500),result7(2500)
* ,result8(2500),res1(2500),res2(2500)
common/block1/ met,net,kin,kon,big,choice,power,del,rr,tend,
* delt,time,count1,mig,wig,wrong,yi(2),wo(15,15),wi(15,15),rm(15)
* ,ri(15),ro(15),k1(2),k2(2),k3(2),k4(2),rsim(2500,4),
* result1(2500),result2(2500),oo(15,15,15),oi(15,15,15)
do 777 jj = 1,met
do 777 ii = 1,kon
wo(jj,ii) = wo(jj,ii)+del
do 666 kk=1,2
oo(jj,ii,kk)=0.d0
time = 0.d0
count1 = 1

result8(1) = rsim(1,2)
result7(1) = rsim(1,1)

timer2(1) = time

```

```

mf = 2
do while(time .lt. tend)
ri(1) = result7(mf-1)
ri(2) = result8(mf-1)

ri(kin) = 1.d0
call mid_net_out
call runge
mf = mf + 1
timer2(mf -1) = time
result7(mf-1)= ri(1)
result8(mf-1)= ri(2)
count1 = count1 + 1
wrong = ri(1) - rsim(count1,1)
wrong = wrong/wig
if(mig.eq.0)then
oo(jj,ii,kk)=oo(jj,ii,kk)+wrong**2
else if (mig.eq.1)then
oo(jj,ii,kk)=oo(jj,ii,kk)+DABS(wrong)
end if

* end of do while TIME loop
end do
wo(jj,ii)=wo(jj,ii)-2.d0*del
666 continue
777 wo(jj,ii)=wo(jj,ii)+del
continue
return
end

subroutine results(npoin,timer2,result3,sense,kit,ff,ff1)
implicit real*8(a-z)
integer i,j,net,met,kin,kon,count1,npoin,count3
integer mig,kit
character*20 ff,ff1,ff2,ff3,ff4,ff5,ff6
dimension timer2(2500),result3(2500),sense(25000)
common/block1/ met,net,kin,kon,big,choice,power,del,rr,tend,
* delt,time,count1,mig,wig,wrong,yi(2),wo(15,15),wi(15,15),rm(15)
* ,ri(15),ro(15),k1(2),k2(2),k3(2),k4(2),rsim(2500,4),
* result1(2500),result2(2500),oo(15,15,15),oi(15,15,15)

* print net outputs
ff2 = trim(ff) //" .a"
ff3 = trim(ff) //" .w"
ff4 = trim(ff) //" .v"
ff5 = trim(ff) //" .r"
ff6 = trim(ff) //" .e"
open(2,file=ff2,status = 'replace')
open(3,file=ff3,status = 'replace')
open(4,file=ff4,status = 'replace')
open(5,file=ff5,status = 'replace')
open(6,file=ff6,status = 'replace')
do 140 count3 = 1, npoin

```

```

write(2,*) timer2(count3),rsim(count3,1),result1(count3)
140   continue
do 170 count3 = 1,npoint
write(4,*) timer2(count3),rsim(count3,2),result2(count3)
170   continue
do 180 i = 1, npoint
write(5,*) result1(i),result3(i)
180   continue
do 190 i =1, kit
write(6,*) sense(i)
190   continue
write(3,*) 'WO - Output layer weights'
do 150 j = 1,met
do 150 i = 1,kon
write(3,*) wo(j,i)
150   continue
write(3,*) 'WI - Input layer weights'
do 160 j = 1, net
do 160 i = 1,kin
write(3,*) wi(j,i)
160   continue
close(3)
close(4)
close(2)
close(5)
close(6)
return
end

```

APPENDIX B

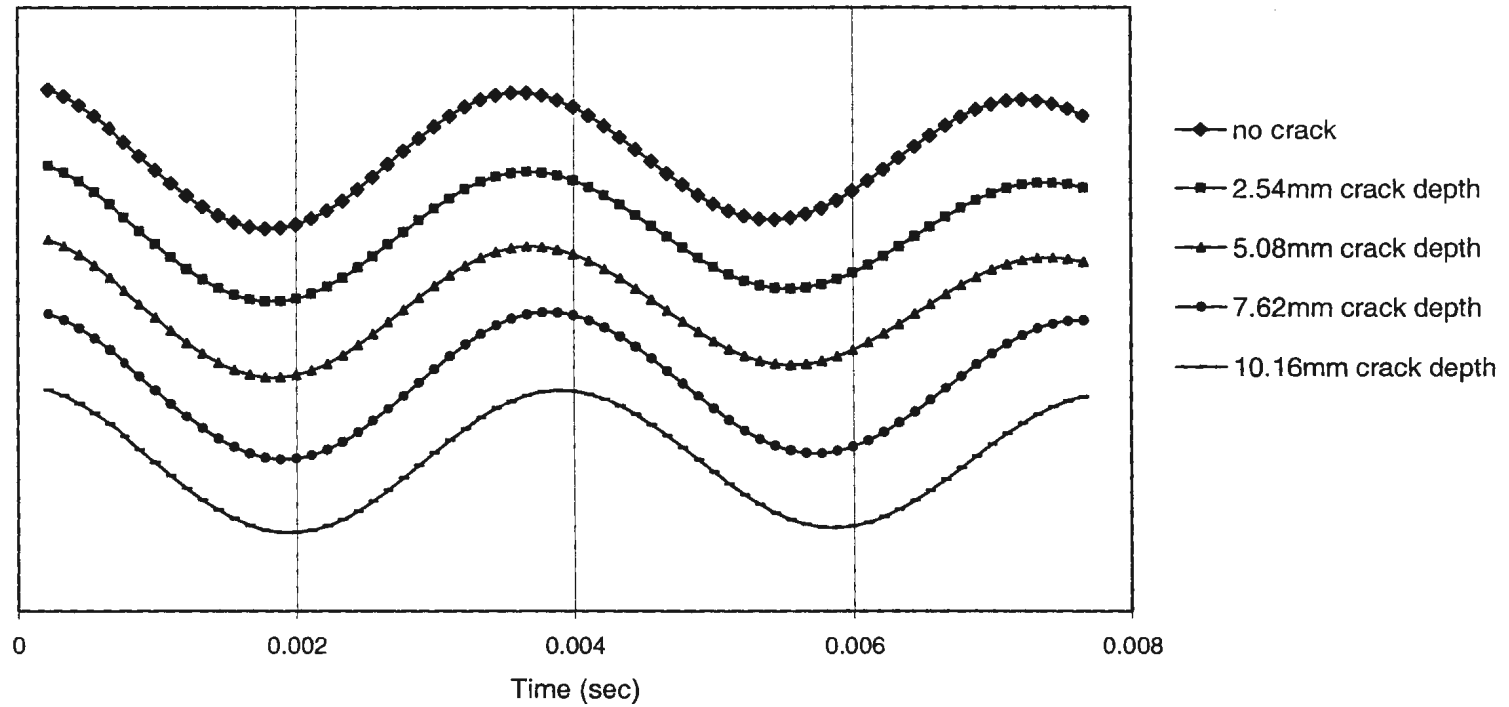


Figure B.1 Auto-correlation functions for fixed-fixed beam, crack at $1/16 L$.

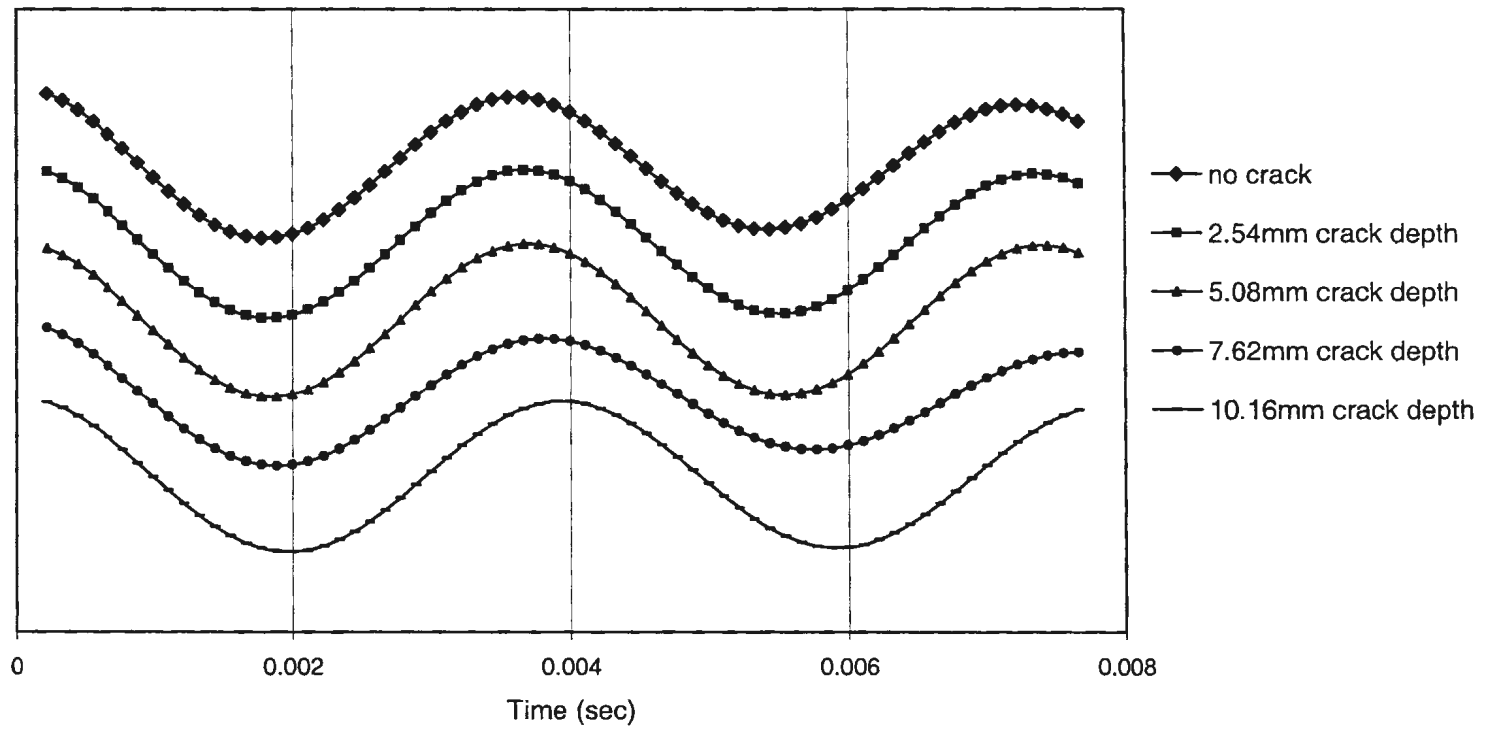


Figure B.2 Auto-correlation functions for fixed-fixed beam, crack at 3/16 L.

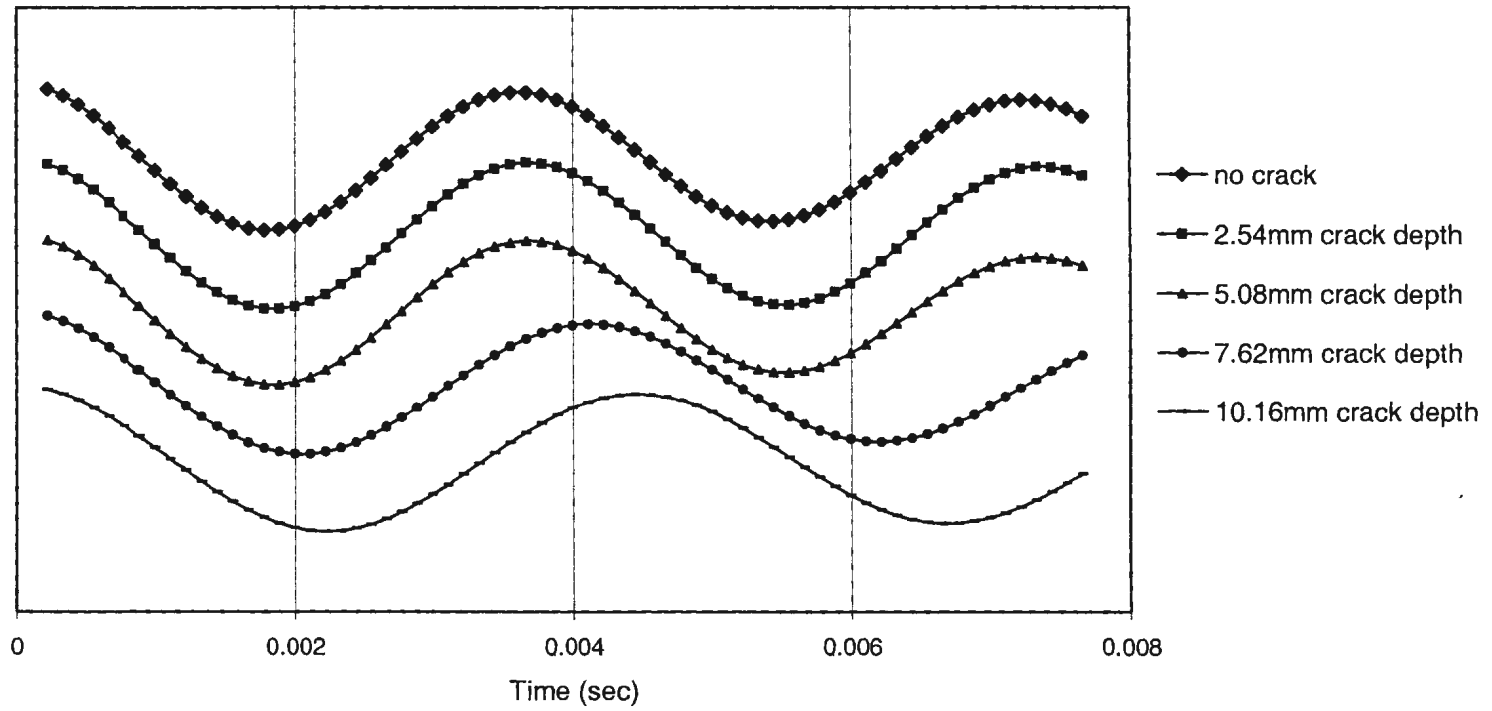


Figure B.3 Auto-correlation functions for fixed-fixed beam, crack at $5/16 L$.

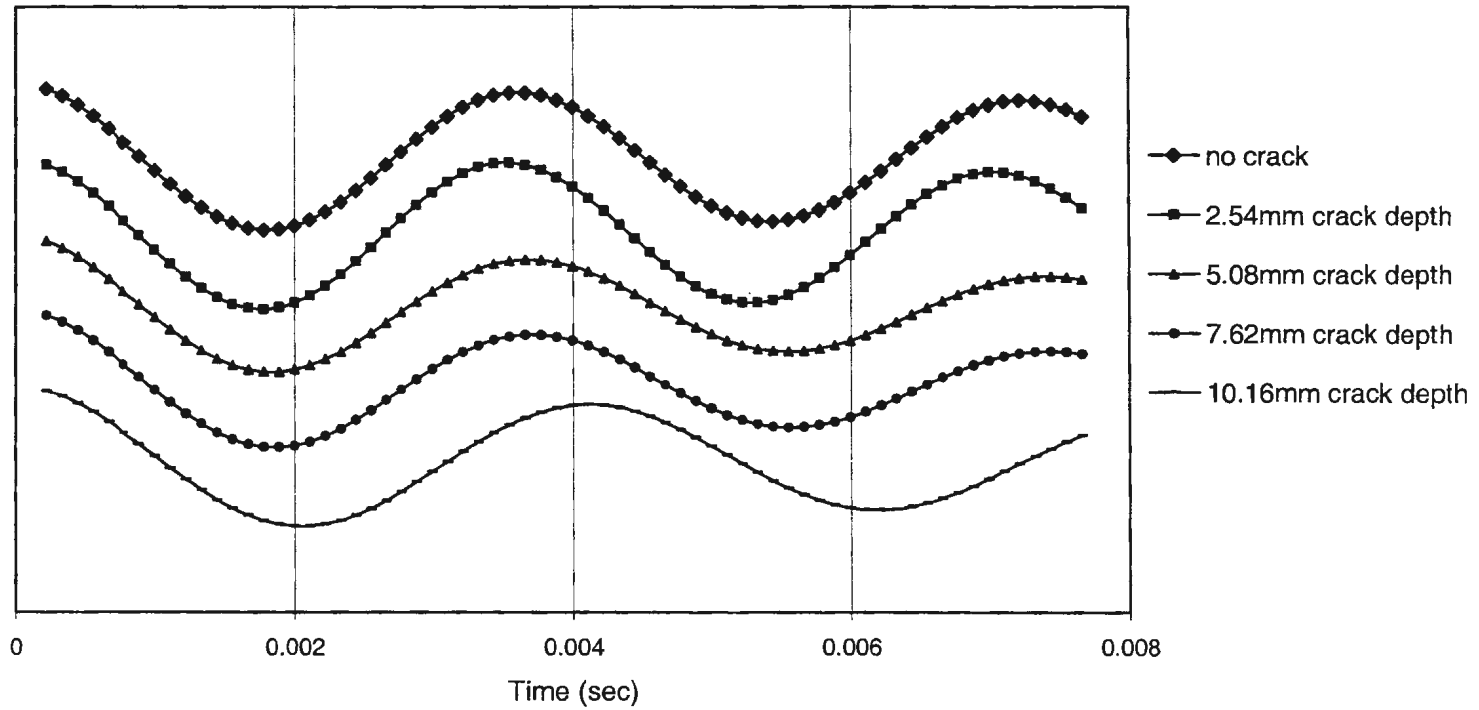


Figure B.4 Auto-correlation functions for fixed-fixed beam, crack at 7/16 L.

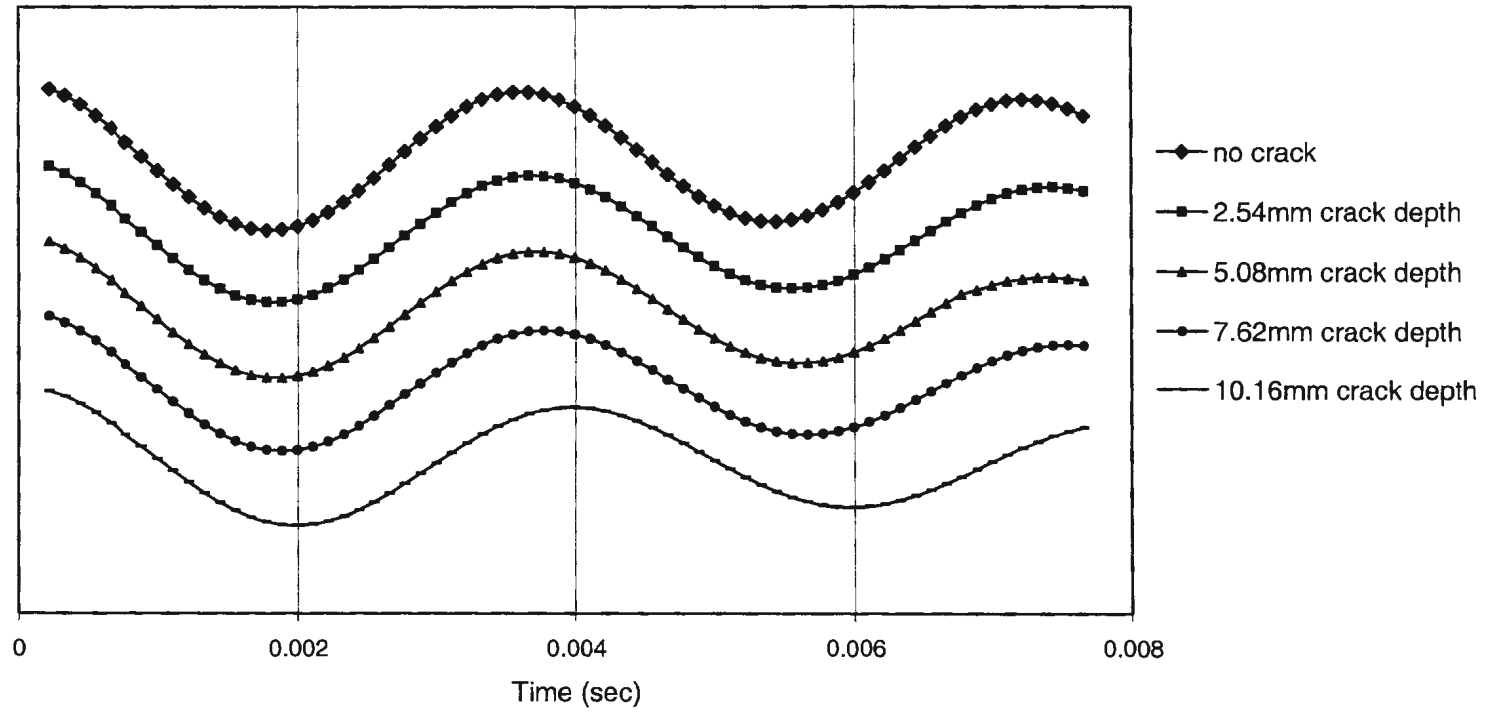


Figure B.5 Auto-correlation functions for fixed-fixed beam, crack at 8/16 L.

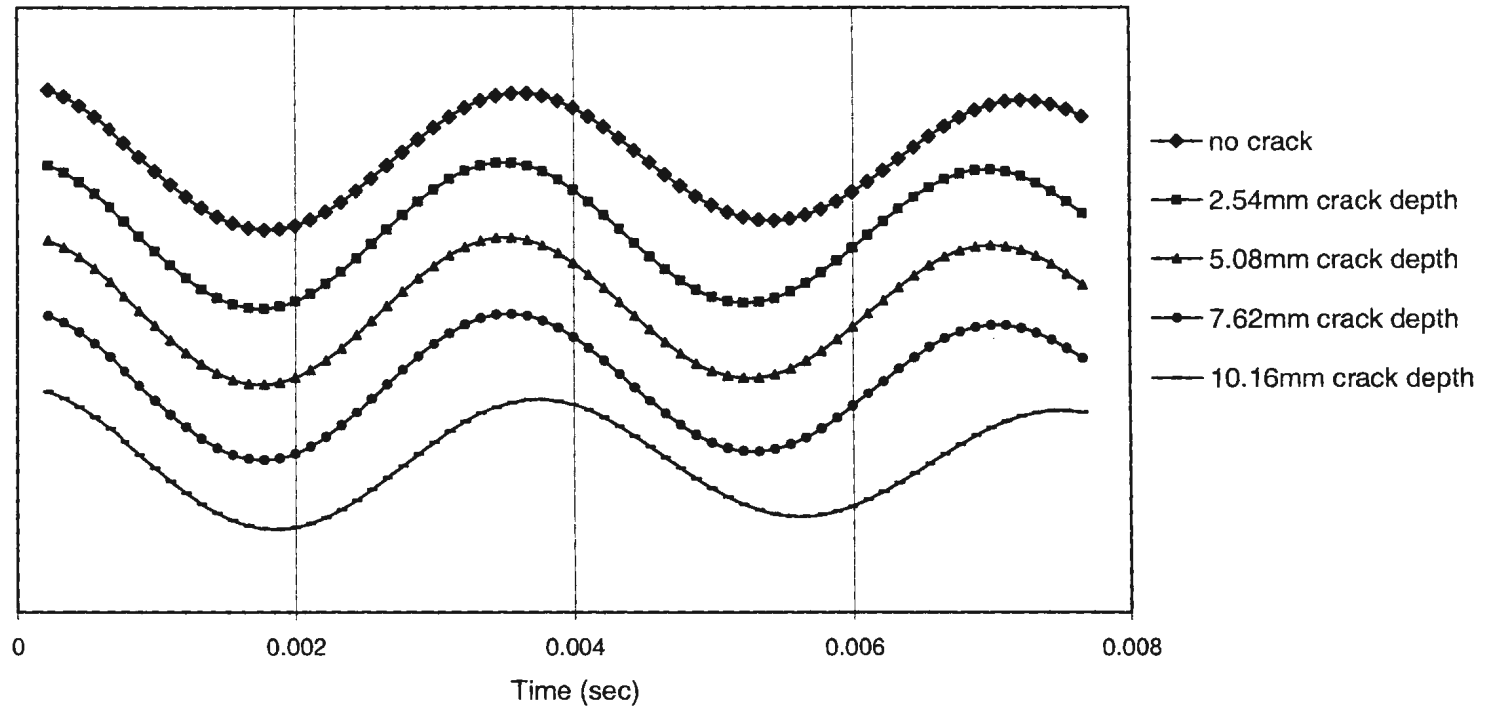


Figure B.6 Auto-correlation functions for fixed-fixed beam, crack at $11/16 L$.

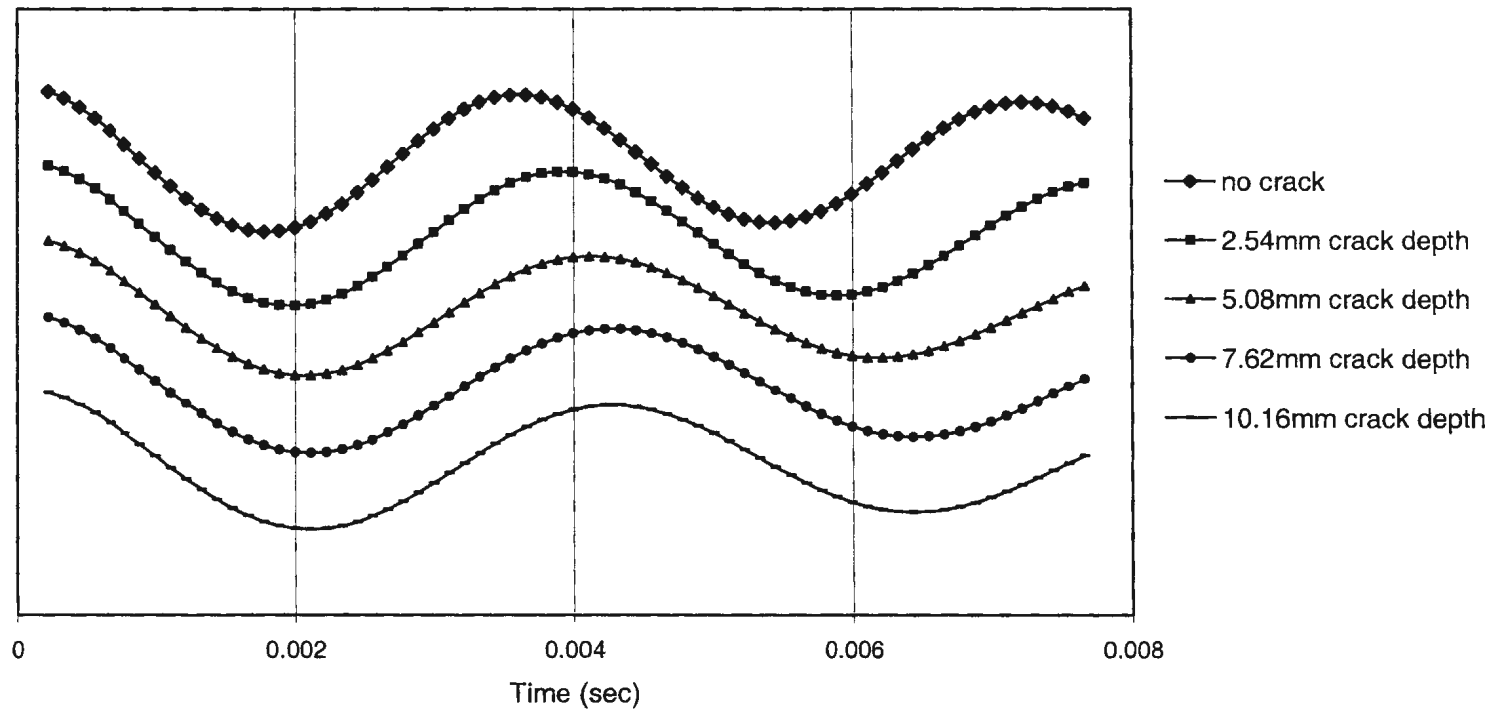


Figure B.7 Auto-correlation functions for simply supported, crack at 1/16 L.

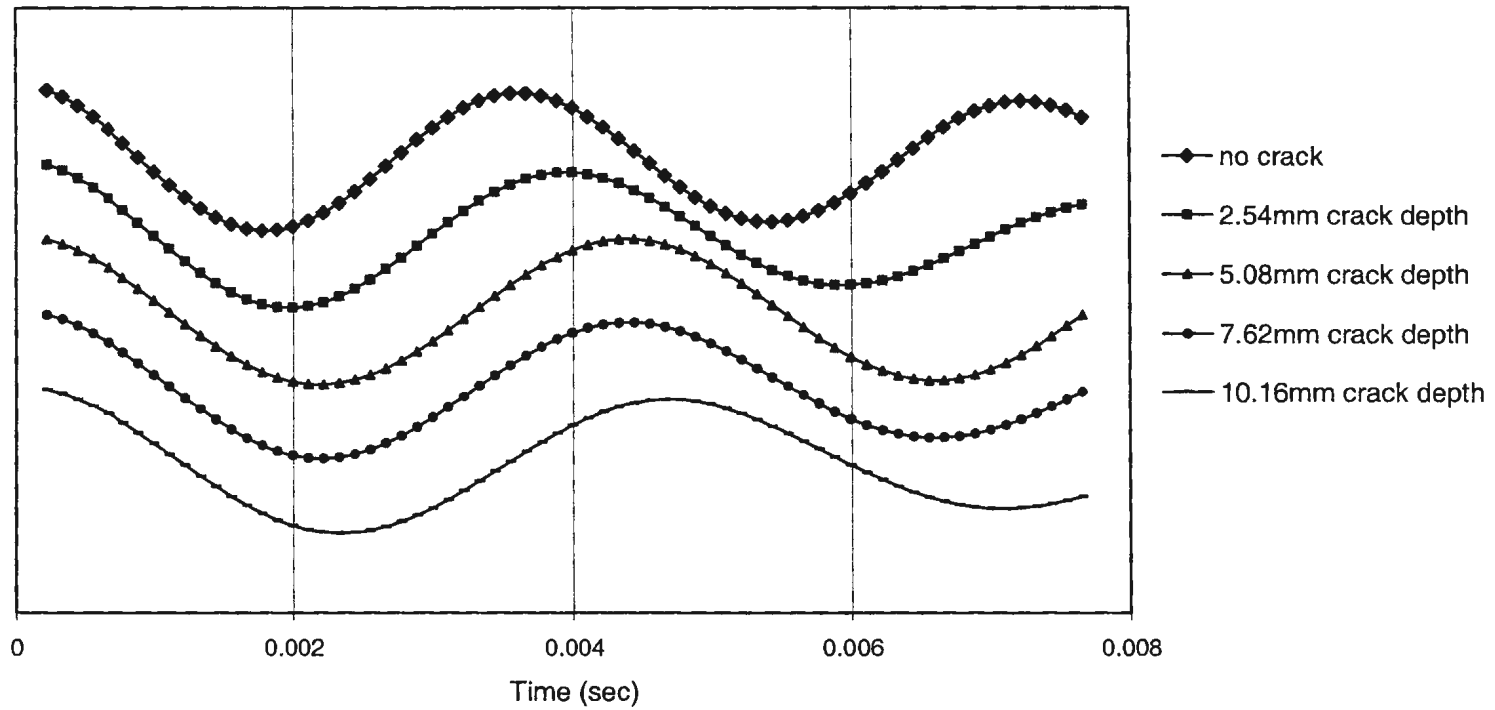


Figure B.8 Auto-correlation functions for simply supported, crack at $3/16 L$.

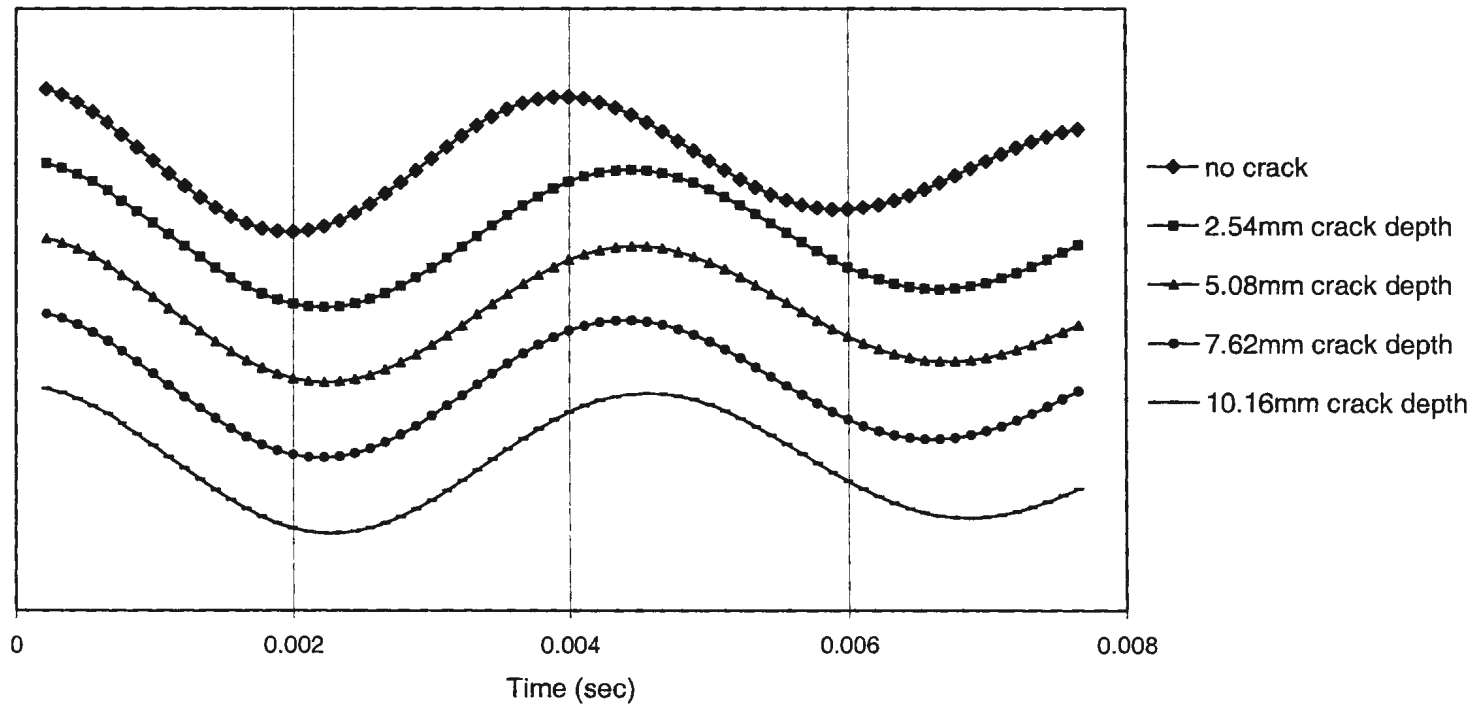


Figure B.9 Auto-correlation functions for simply supported, crack at 5/16 L.

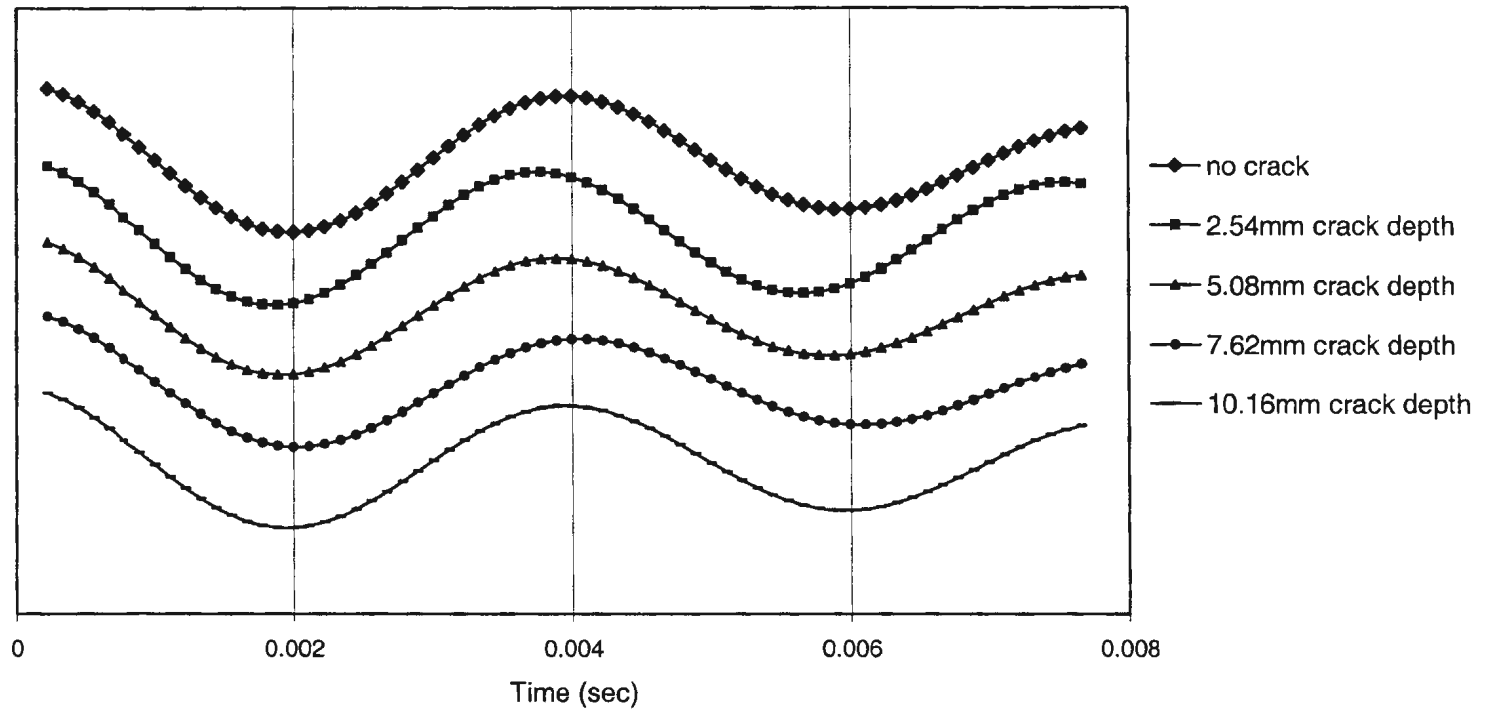


Figure B.10 Auto-correlation functions for simply supported, crack at 7/16 L.

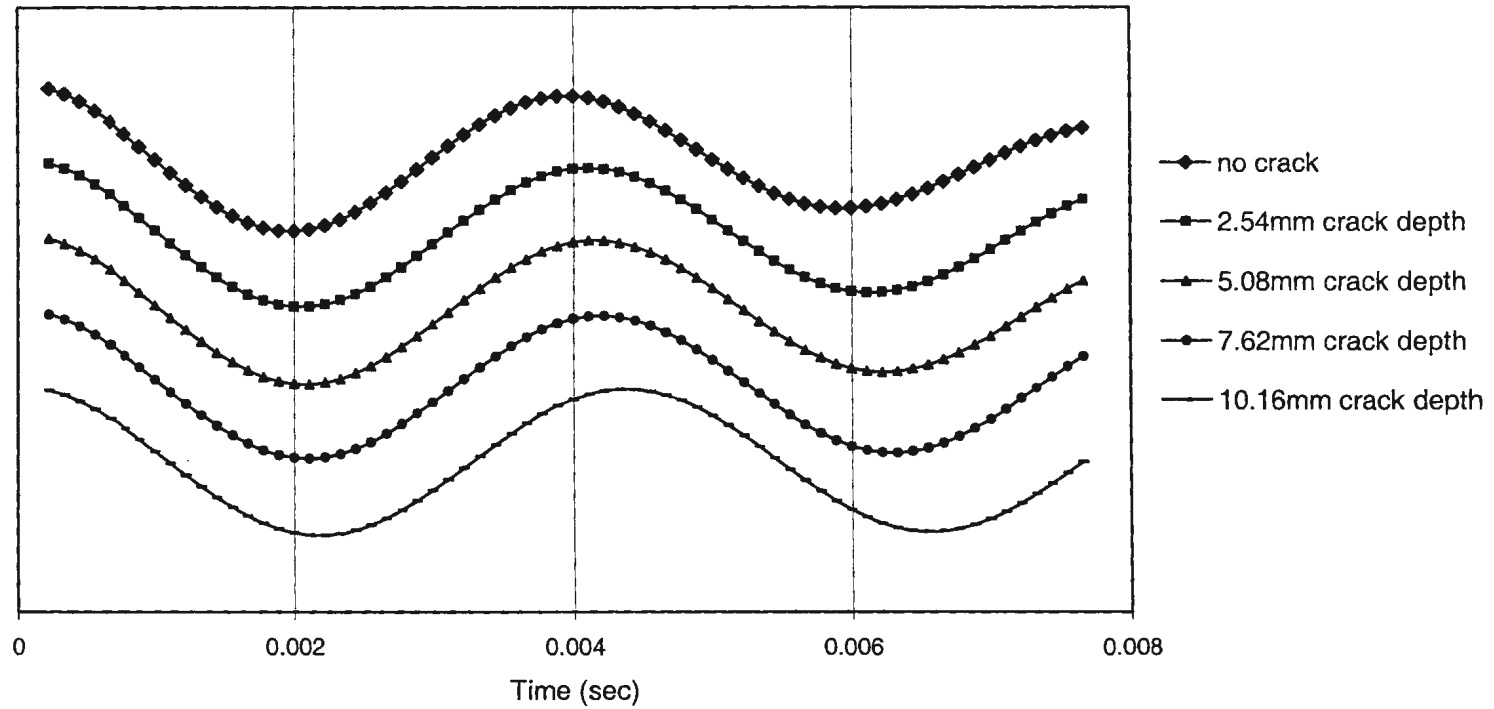


Figure B.11 Auto-correlation functions for simply supported, crack at 8/16 L.

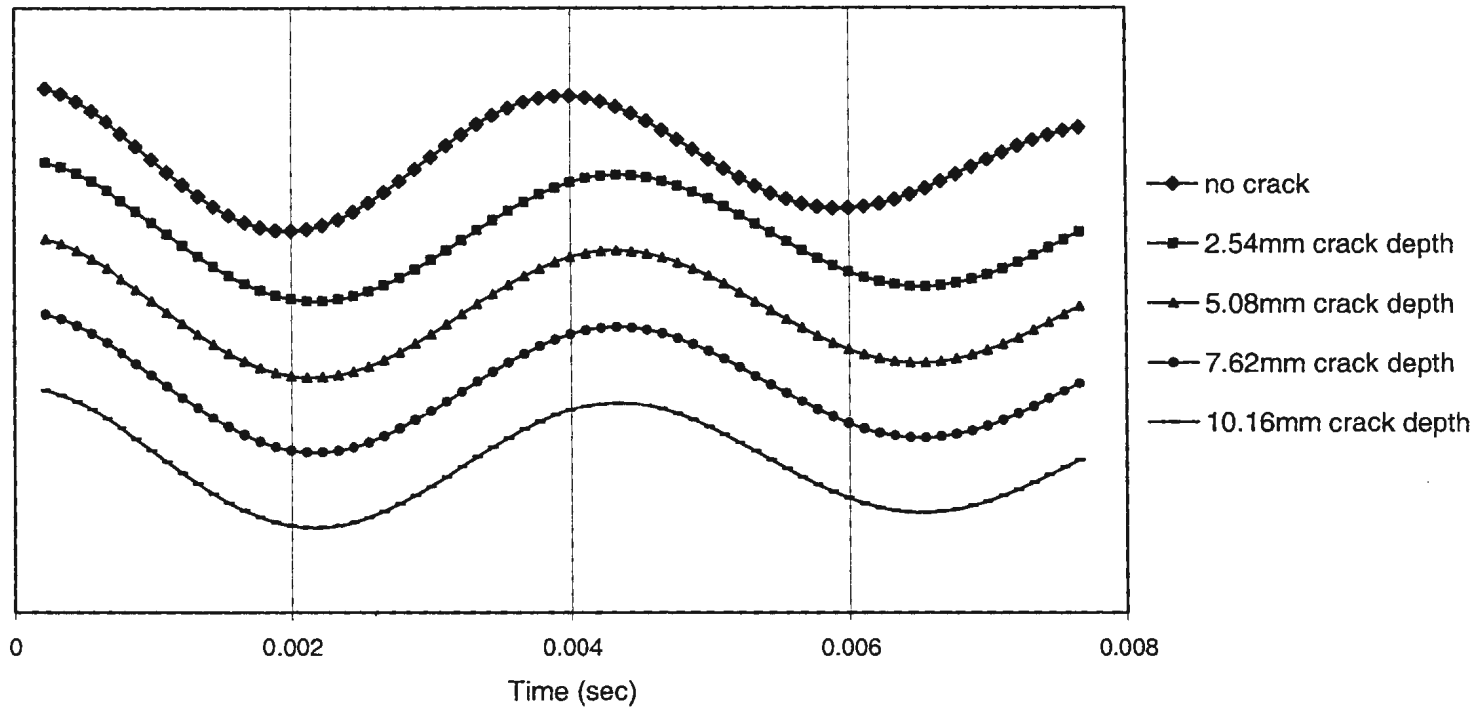


Figure B.12 Auto-correlation functions for simply supported, crack at 11/16 L.

APPENDIX C

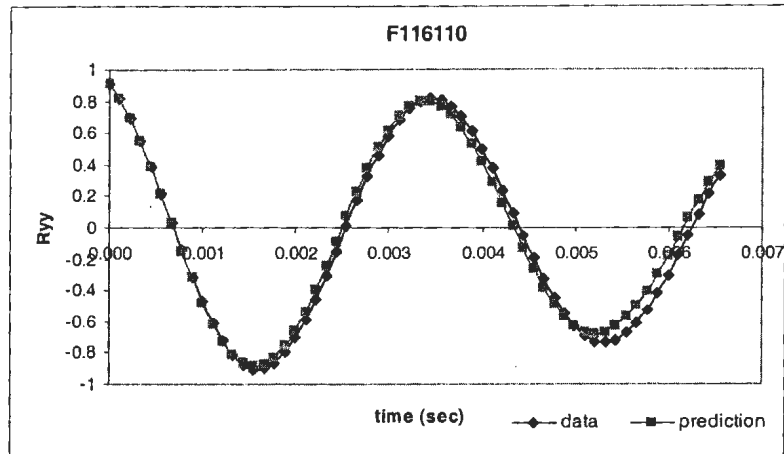


Fig C.1 Auto-correlation function and the neural network prediction for fixed-fixed beam (2.54mm).

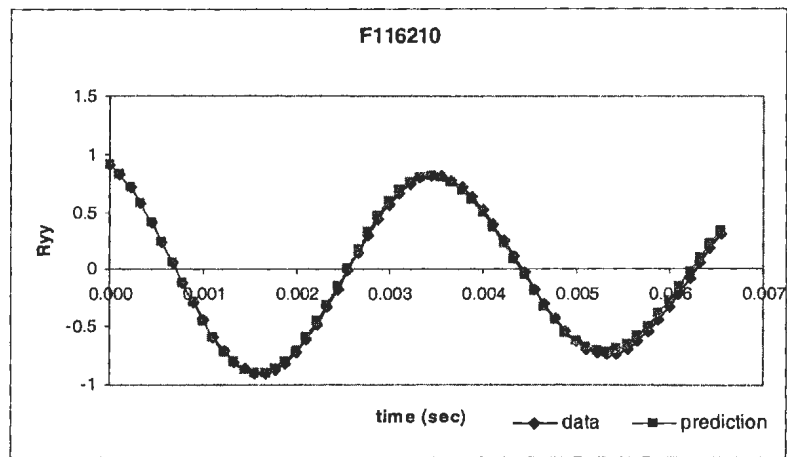


Fig C.2 Auto-correlation function and the neural network prediction for fixed-fixed beam (5.08mm).

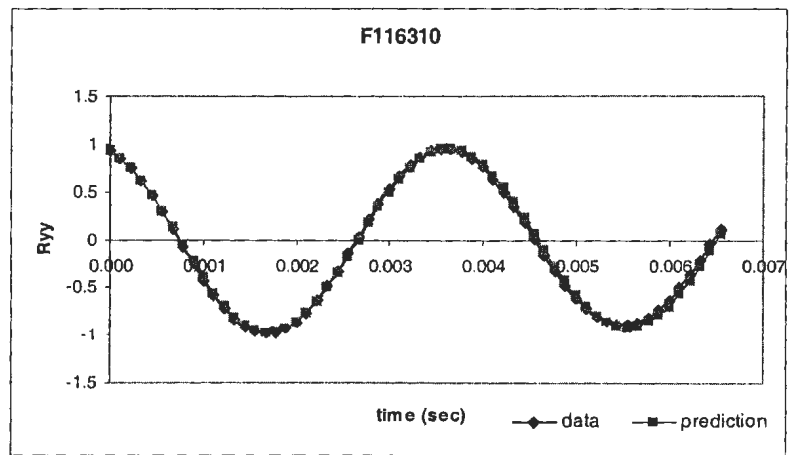


Fig C.3 Auto-correlation function and the neural network prediction for fixed-fixed beam (7.62mm).

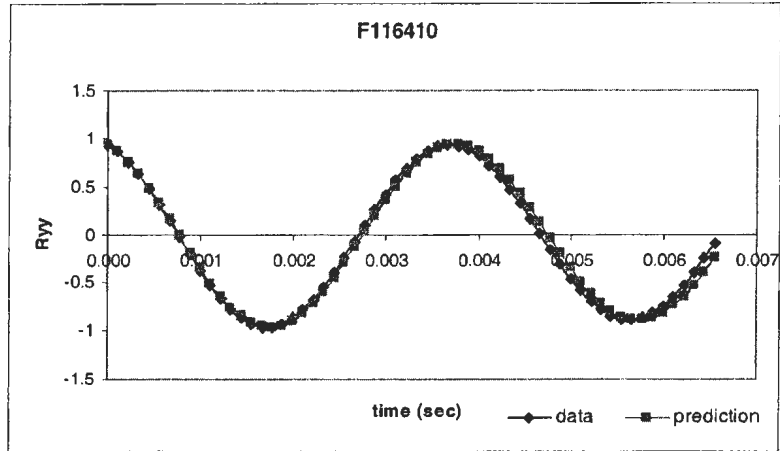


Fig C.4 Auto-correlation function and the neural network prediction for fixed-fixed beam (10.16mm).

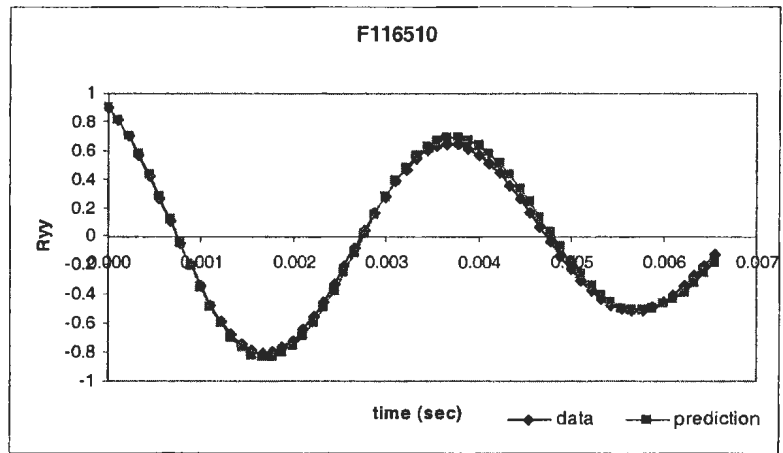


Fig C.5 Auto-correlation function and the neural network prediction for fixed-fixed beam (12.7mm).

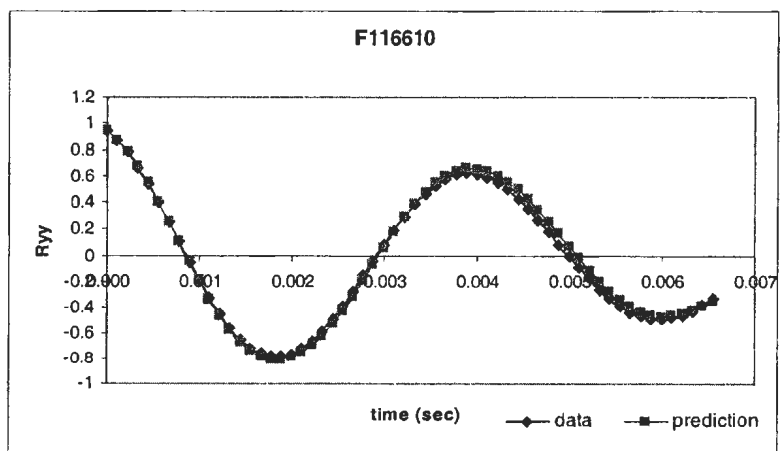


Fig C.6 Auto-correlation function and the neural network prediction for fixed-fixed beam (15.24mm).

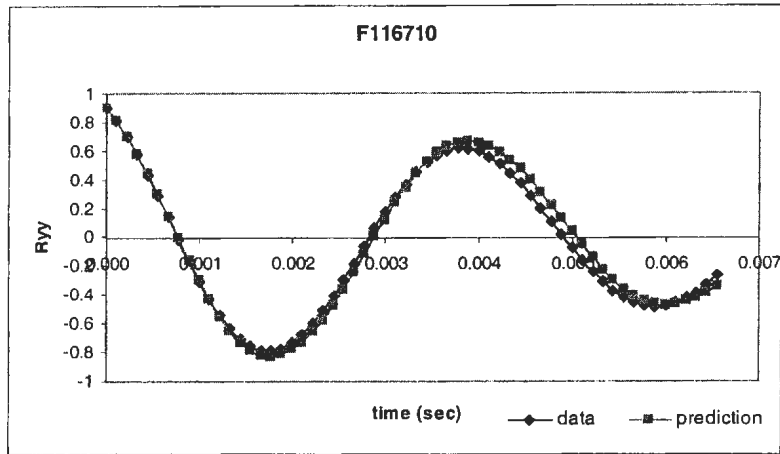


Fig C.7 Auto-correlation function and the neural network prediction for fixed-fixed beam (17.78mm).

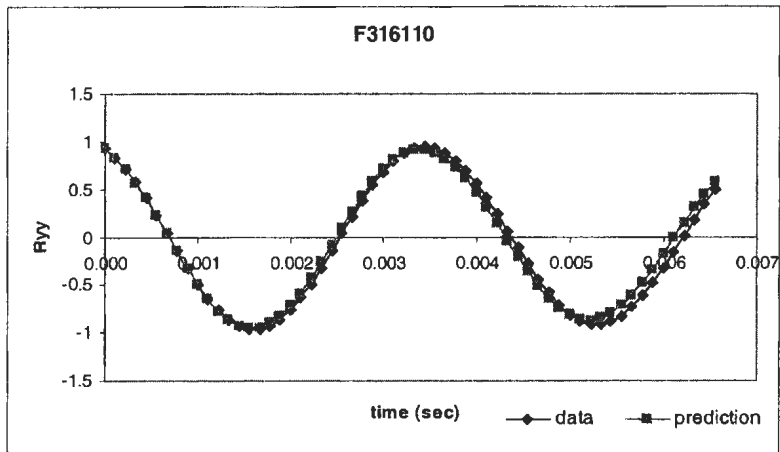


Fig C.8 Auto-correlation function and the neural network prediction for fixed-fixed beam (2.54mm).

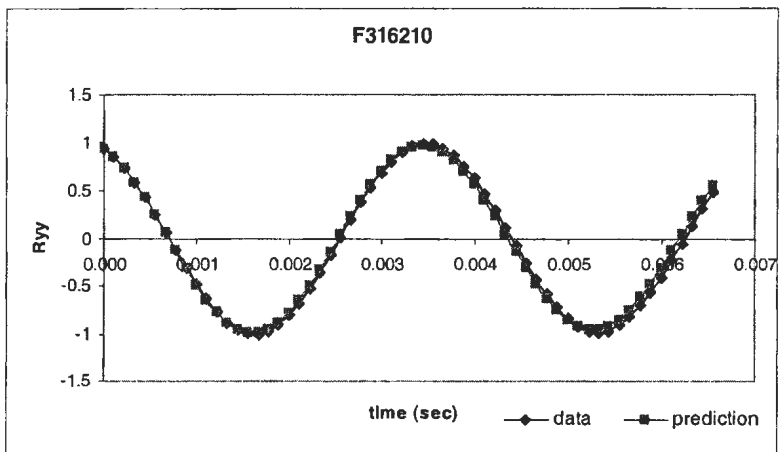


Fig C.9 Auto-correlation function and the neural network prediction for fixed-fixed beam (5.08mm).

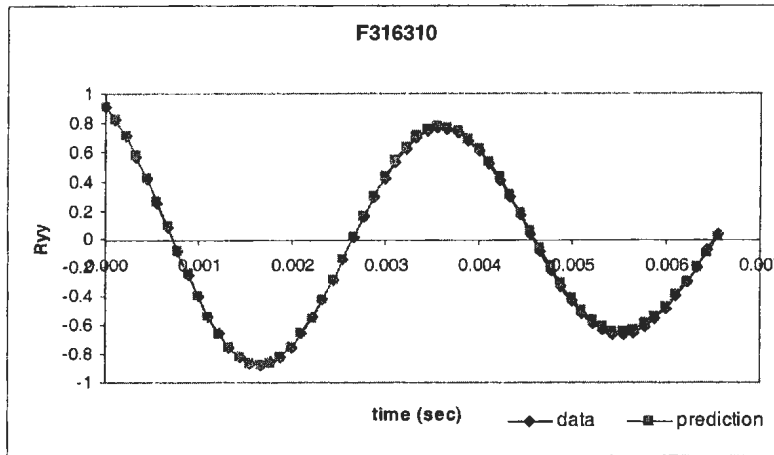


Fig C.10 Auto-correlation function and the neural network prediction for fixed-fixed beam (7.62mm).

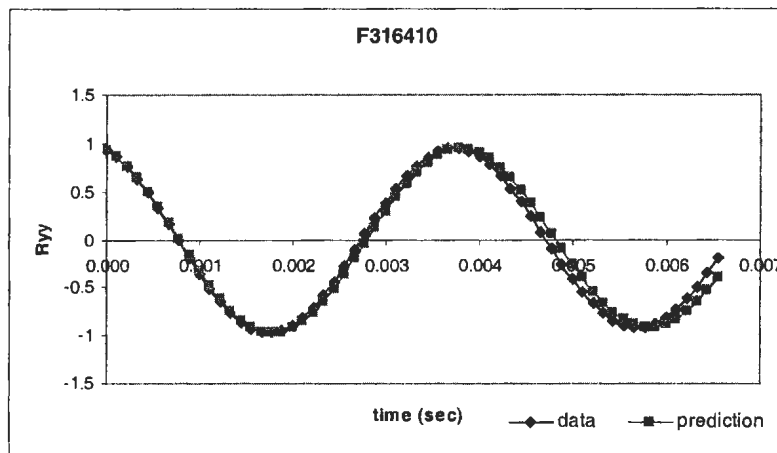


Fig C.11 Auto-correlation function and the neural network prediction for fixed-fixed beam (10.16mm).

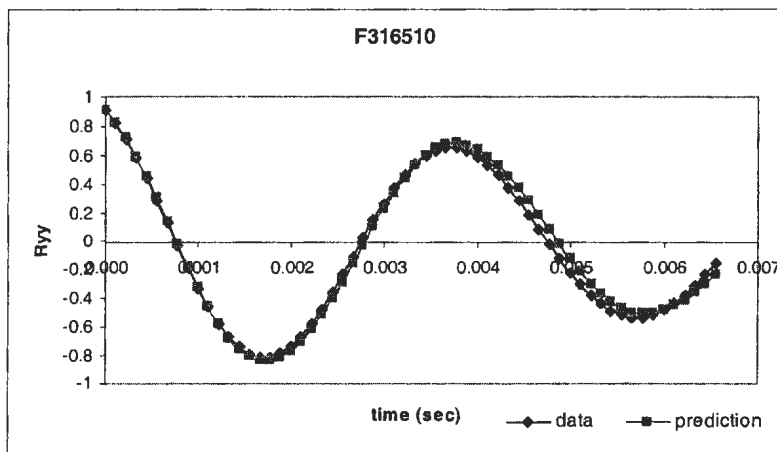


Fig C.12 Auto-correlation function and the neural network prediction for fixed-fixed beam (12.7mm).

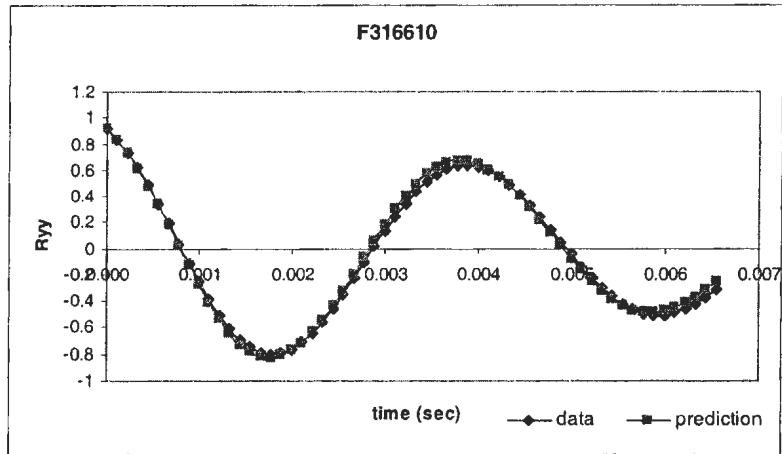


Fig C.13 Auto-correlation function and the neural network prediction for fixed-fixed beam (15.24mm).

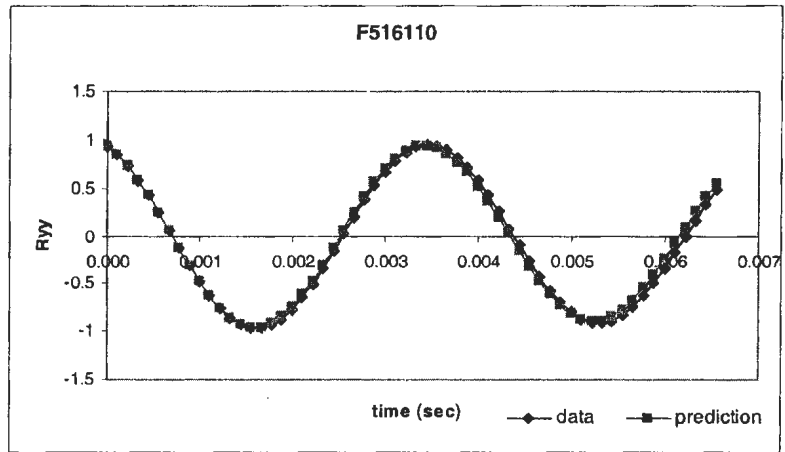


Fig C.14 Auto-correlation function and the neural network prediction for fixed-fixed beam (2.54mm).

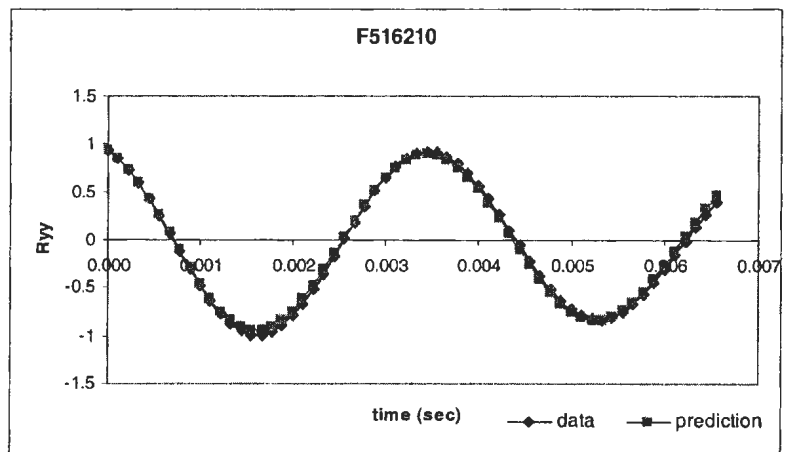


Fig C.15 Auto-correlation function and the neural network prediction for fixed-fixed beam (5.08mm).

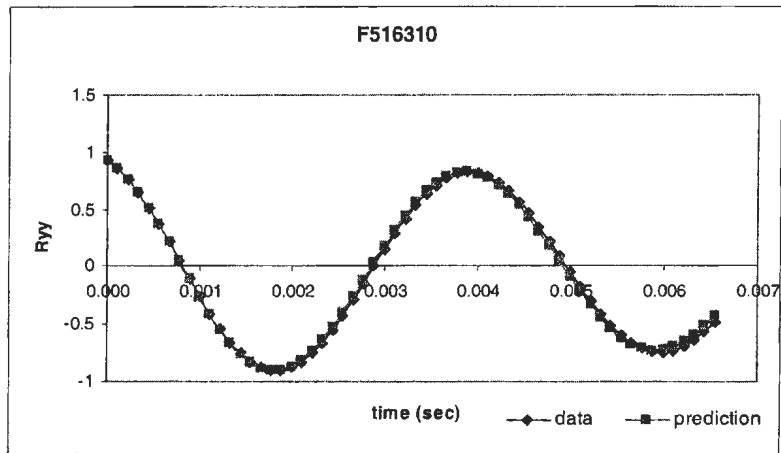


Fig C.16 Auto-correlation function and the neural network prediction for fixed-fixed beam (7.62mm).

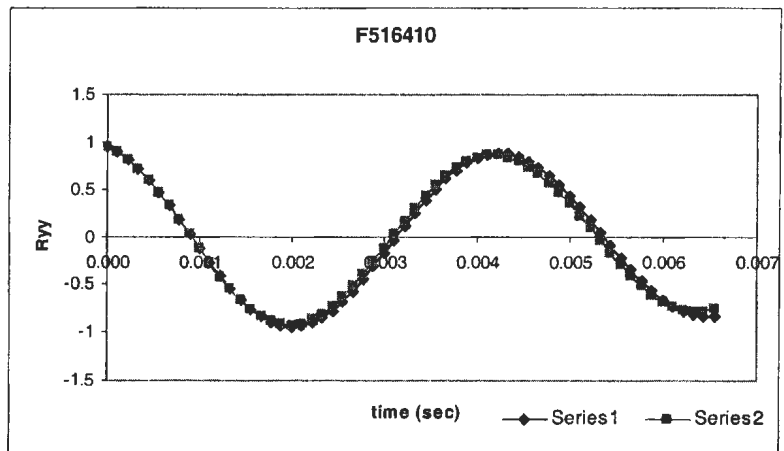


Fig C.17 Auto-correlation function and the neural network prediction for fixed-fixed beam (10.16mm).

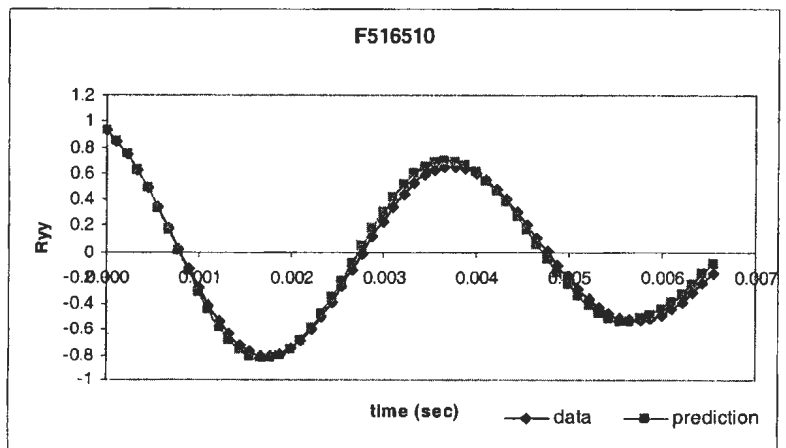


Fig C.18 Auto-correlation function and the neural network prediction for fixed-fixed beam (12.7mm).

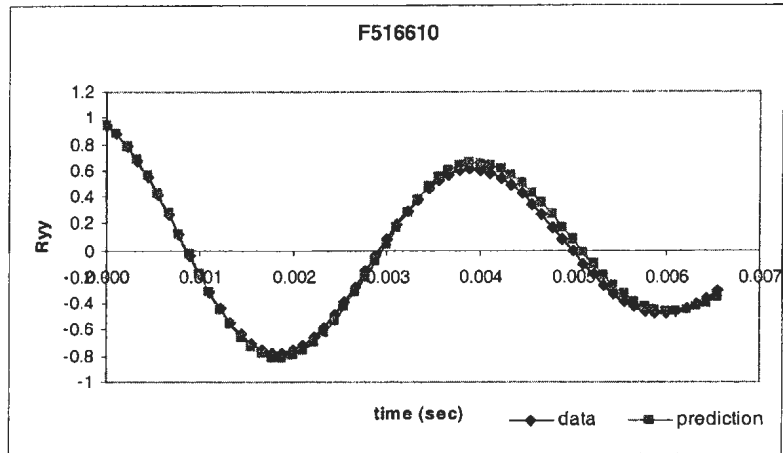


Fig C.19 Auto-correlation function and the neural network prediction for fixed-fixed beam (15.24mm).

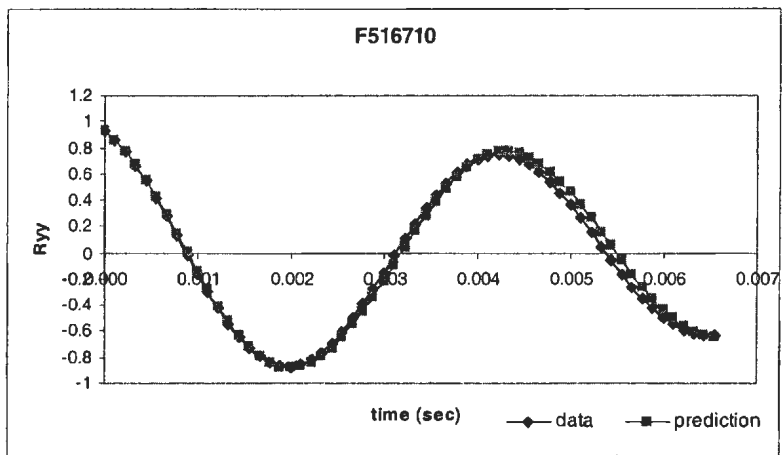


Fig C.20 Auto-correlation function and the neural network prediction for fixed-fixed beam (17.78mm).

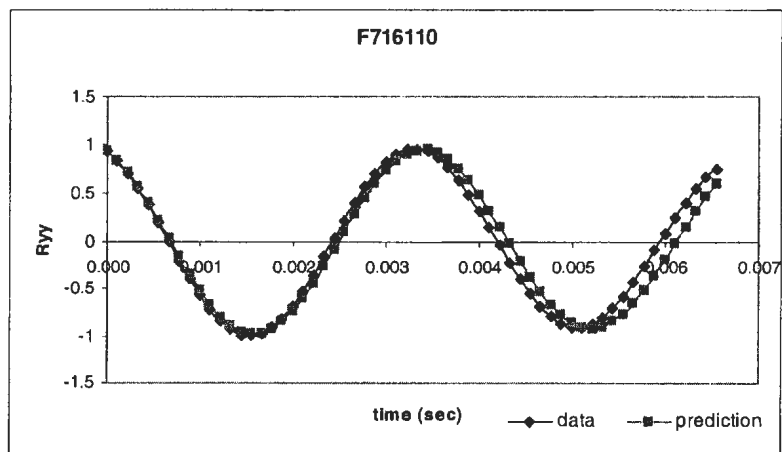


Fig C.21 Auto-correlation function and the neural network prediction for fixed-fixed beam (2.54mm).

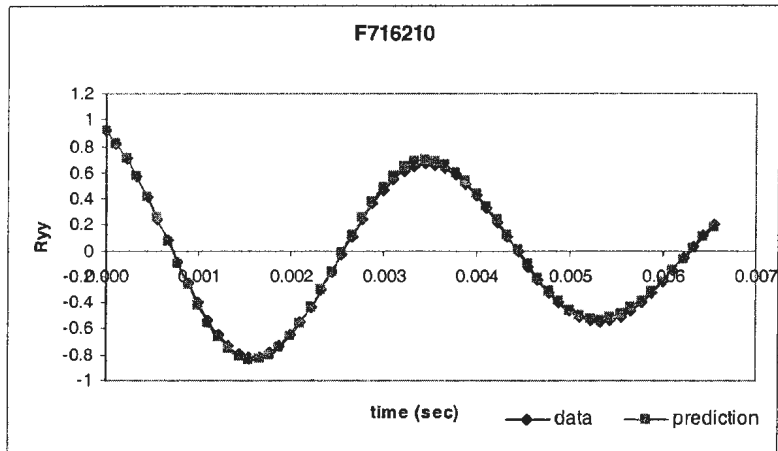


Fig C.22 Auto-correlation function and the neural network prediction for fixed-fixed beam (5.08mm).

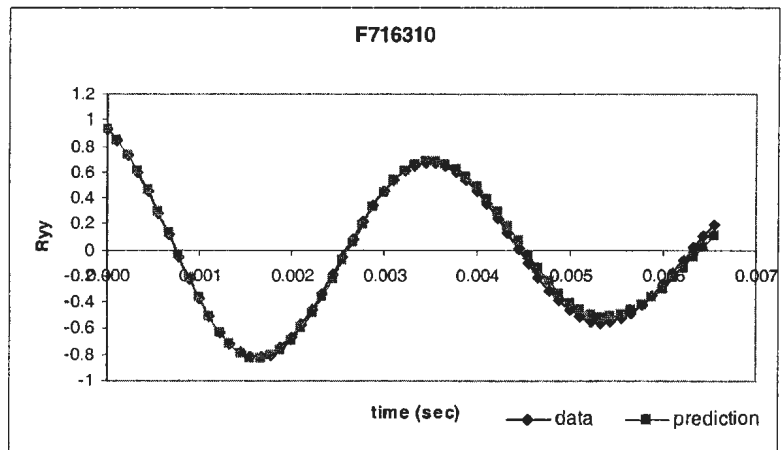


Fig C.23 Auto-correlation function and the neural network prediction for fixed-fixed beam (7.62mm).

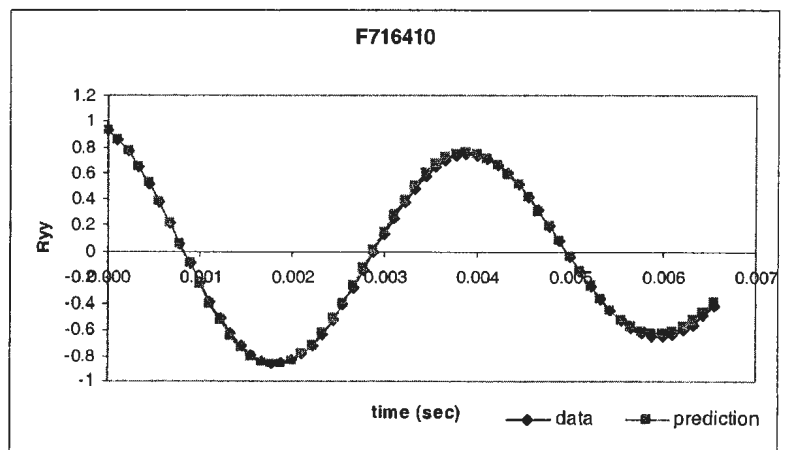


Fig C.24 Auto-correlation function and the neural network prediction for fixed-fixed beam (10.16mm).

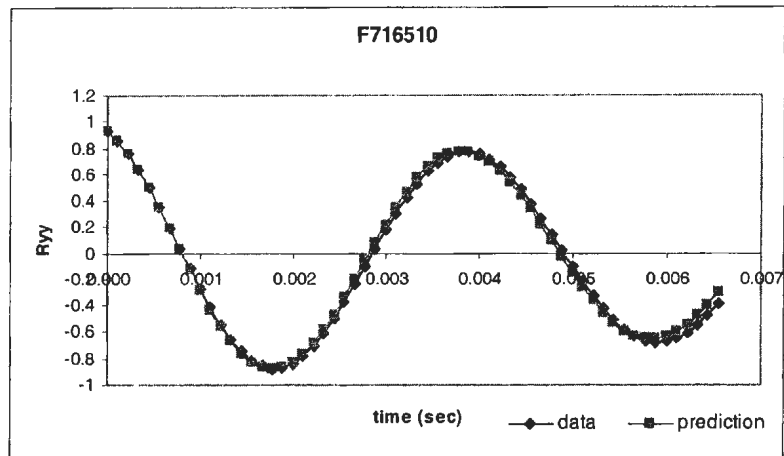


Fig C.25 Auto-correlation function and the neural network prediction for fixed-fixed beam (12.7mm).

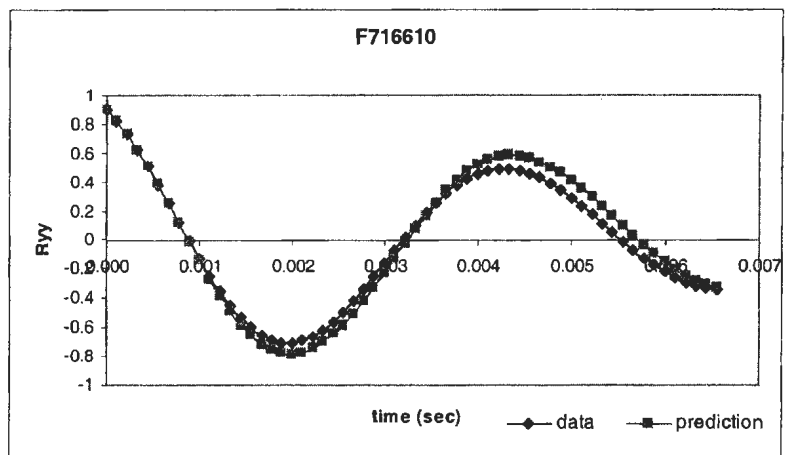


Fig C.26 Auto-correlation function and the neural network prediction for fixed-fixed beam (15.24mm).

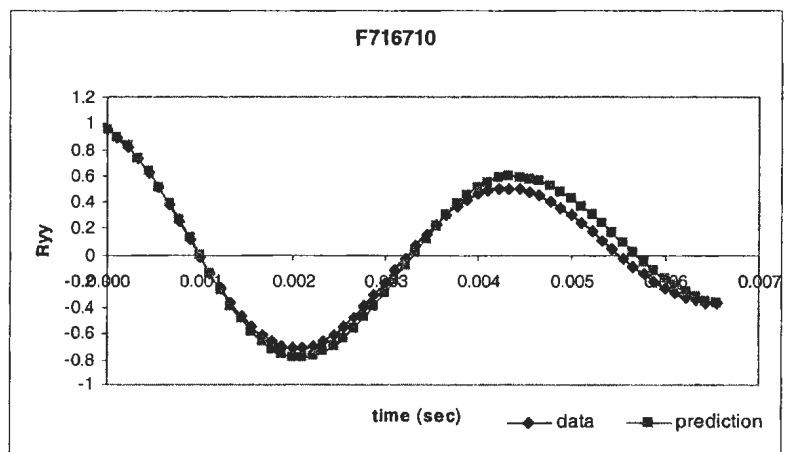


Fig C.27 Auto-correlation function and the neural network prediction for fixed-fixed beam (17.78mm).

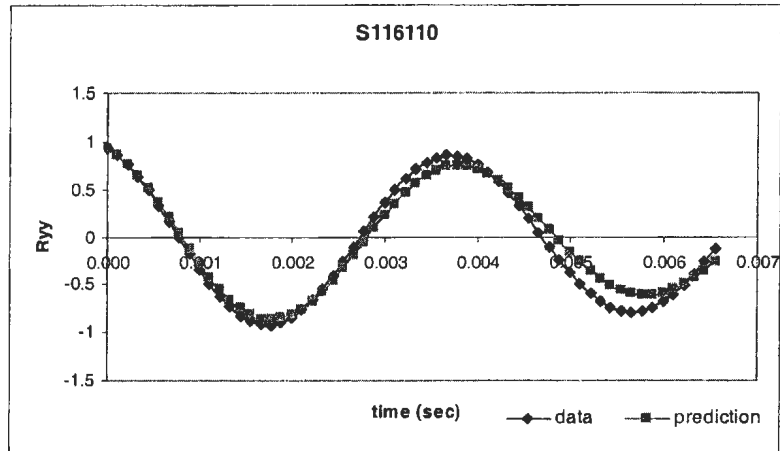


Fig C.28 Auto-correlation function and the neural network prediction for simply supported (2.54mm).

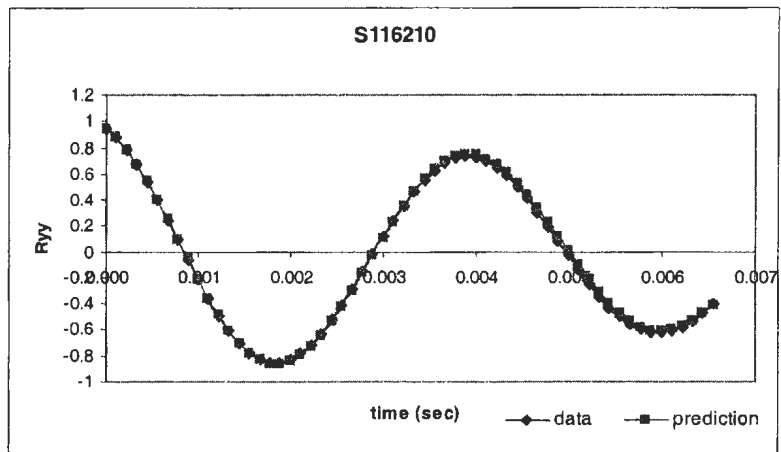


Fig C.29 Auto-correlation function and the neural network prediction for simply supported (5.08mm).

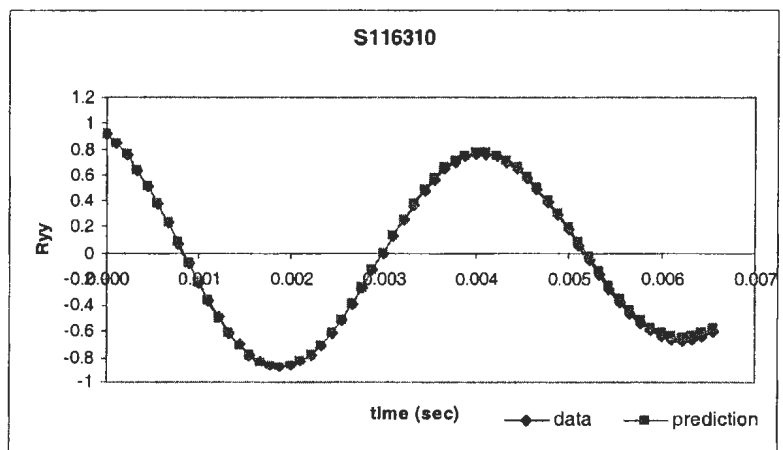


Fig C.30 Auto-correlation function and the neural network prediction for simply supported (7.62mm).

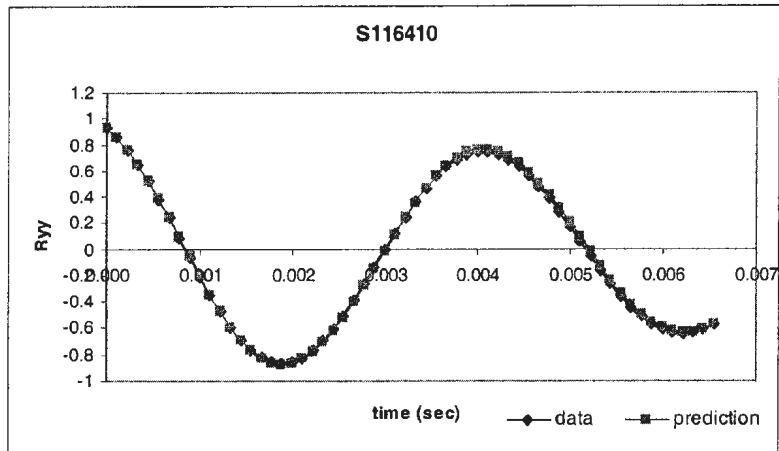


Fig C.31 Auto-correlation function and the neural network prediction for simply supported (10.16mm).

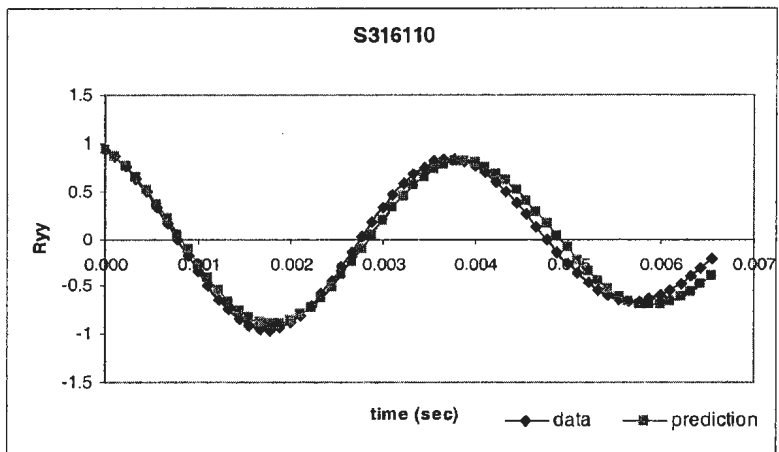


Fig C.32 Auto-correlation function and the neural network prediction for simply supported (2.54mm).

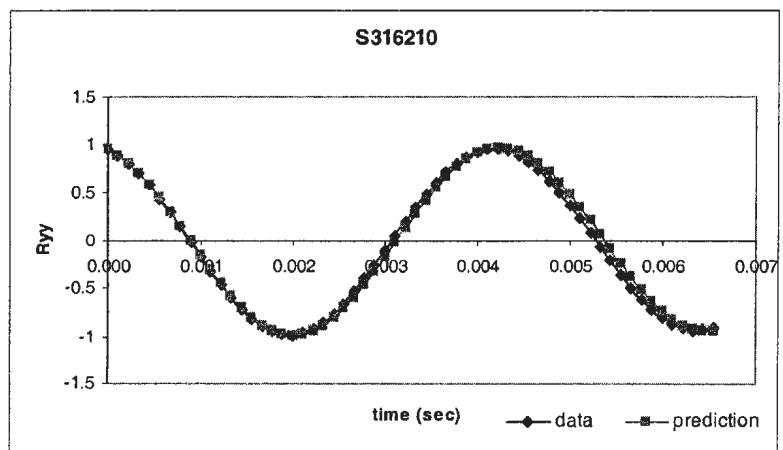


Fig C.33 Auto-correlation function and the neural network prediction for simply supported (5.08mm).

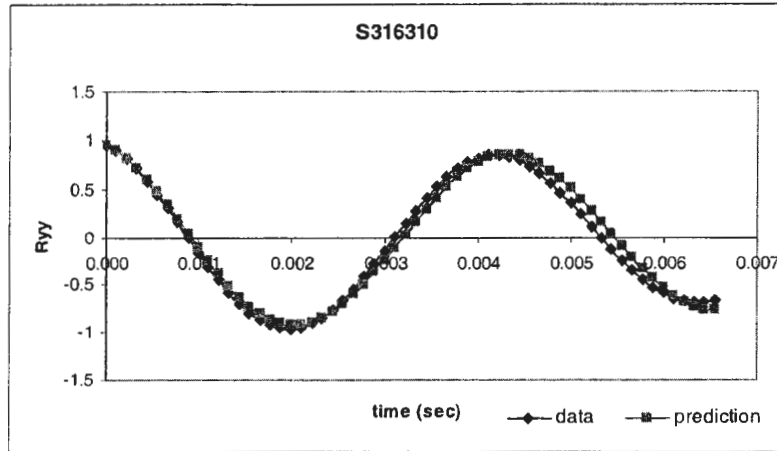


Fig C.34 Auto-correlation function and the neural network prediction for simply supported (7.62mm).

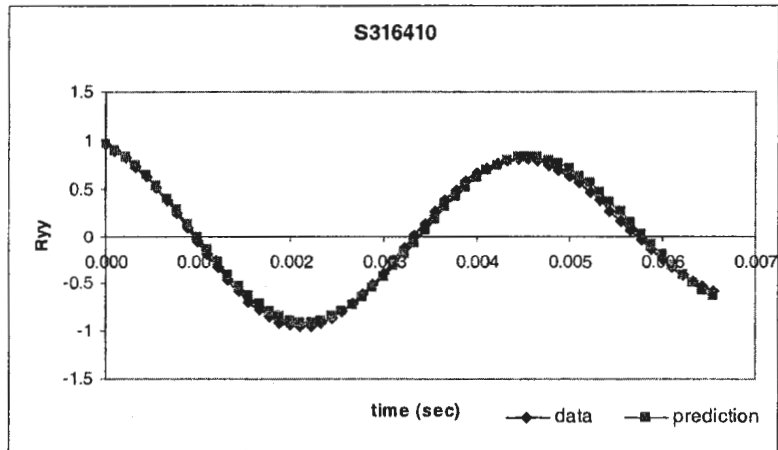


Fig C.35 Auto-correlation function and the neural network prediction for simply supported (10.16mm).

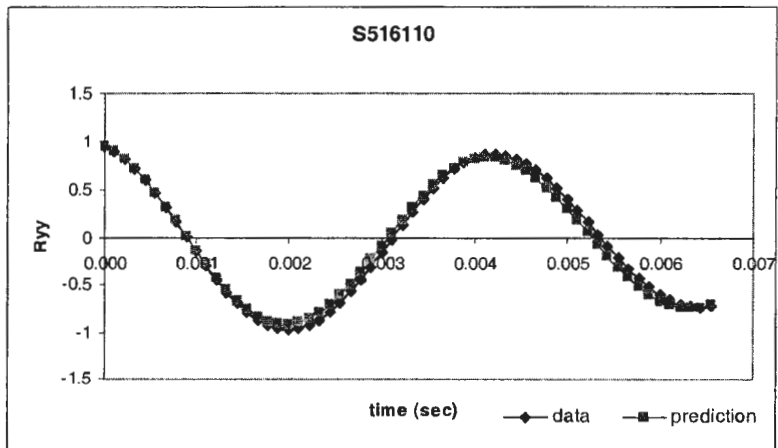


Fig C.36 Auto-correlation function and the neural network prediction for simply supported (2.54mm).

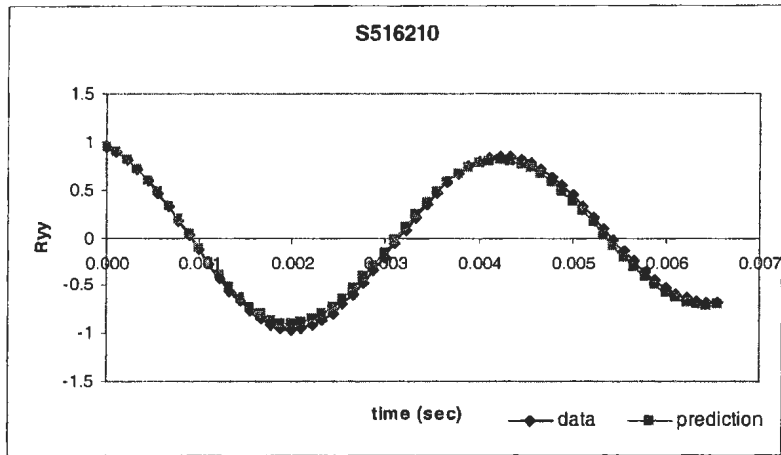


Fig C.37 Auto-correlation function and the neural network prediction for simply supported (5.08mm).

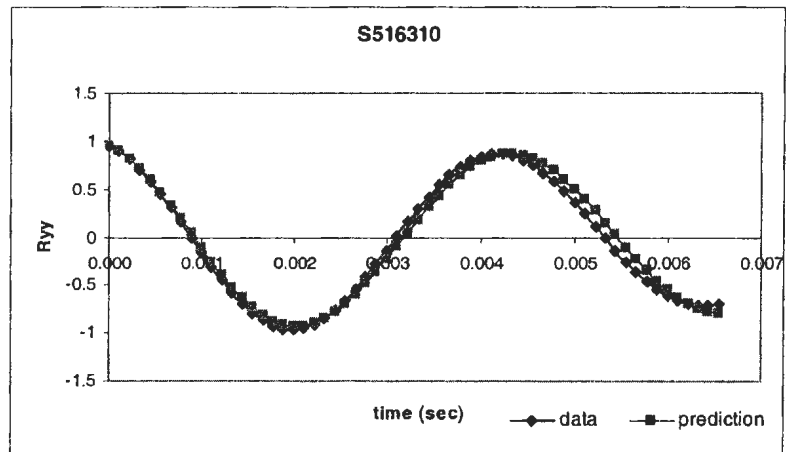


Fig C.38 Auto-correlation function and the neural network prediction for fixed-fixed beam (7.62mm).

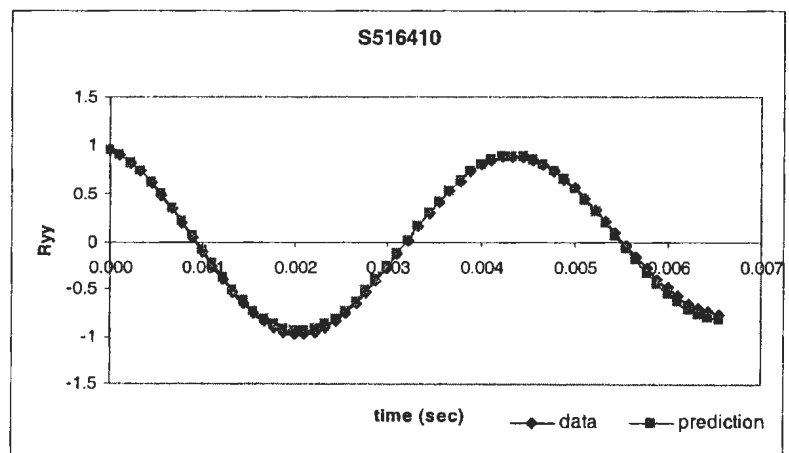


Fig C.39 Auto-correlation function and the neural network prediction for fixed-fixed beam (10.16mm).



